
# NAVAL POSTGRADUATE SCHOOL

**MONTEREY, CALIFORNIA**

# THESIS

**PASSIVE MULTISTATIC DETECTION OF MARITIME TARGETS USING OPPORTUNISTIC RADARS**

by

Chong Sze Sing

March 2014

Thesis Advisor: Herschel H. Loomis
Co-Advisor: David C. Jenn

**Approved for public release; distribution is unlimited**

THIS PAGE INTENTIONALLY LEFT BLANK

# REPORT DOCUMENTATION PAGE

*Form Approved OMB No. 0704–0188*



| **1. AGENCY USE ONLY** *(Leave blank)* | **2. REPORT DATE** March 2014 | **3. REPORT TYPE AND DATES COVERED** Master's Thesis |
|---|---|---|

**4. TITLE AND SUBTITLE**
PASSIVE MULTISTATIC DETECTION OF MARITIME TARGETS USING OPPORTUNISTIC RADARS

**5. FUNDING NUMBERS**

**6. AUTHOR(S)** Chong Sze Sing

**7. PERFORMING ORGANIZATION NAME(S) AND ADDRESS(ES)**
Naval Postgraduate School
Monterey, CA 93943-5000

**8. PERFORMING ORGANIZATION REPORT NUMBER**

**9. SPONSORING /MONITORING AGENCY NAME(S) AND ADDRESS(ES)**
N/A

**10. SPONSORING/MONITORING AGENCY REPORT NUMBER**

**11. SUPPLEMENTARY NOTES** The views expressed in this thesis are those of the author and do not reflect the official policy or position of the Department of Defense or the U.S. Government. IRB Protocol number ____N/A____.

**12a. DISTRIBUTION / AVAILABILITY STATEMENT**
Approved for public release; distribution is unlimited

**12b. DISTRIBUTION CODE**

**13. ABSTRACT (maximum 200 words)**

Passive multistatic radar (PMR) makes use of transmission from opportunistic radars to detect targets. In this thesis, a maritime scenario is created with multiple merchant vessels transmitting at S-band (3 GHz), serving as opportunistic radars and a frigate-size warship acting as the PMR receiver and to detect a low-radar cross-section (RCS) target. The simulations are carried out with actual technical parameters from open sources to best approximate practical performance. To further improve realism, the bistatic RCS simulation of the stealthy Republic of Singapore Navy Formidable-class frigate was included to validate the results.

The simulation results show that the multistatic geometry of four opportunistic transmitters at the same range from the passive receiver with 90-degree separation offers the best coverage. Passive detection of a target of up to a radial range of 30 km with detection coverage of 85% or better is possible. This range coverage is similar to that of the monostatic radar but lacks in the area of detection coverage. The simulations also demonstrated that the detection accuracy is also the highest using this same geometry. The worst-case uncertainty ellipse around the low-RCS target is less than 150 m.

| **14. SUBJECT TERMS** bistatic, multistatic, passive awareness, hitchhiker radar, opportunistic radar, non-cooperative transmitter | **15. NUMBER OF PAGES** 151 |
|---|---|
| | **16. PRICE CODE** |

| **17. SECURITY CLASSIFICATION OF REPORT** | **18. SECURITY CLASSIFICATION OF THIS PAGE** | **19. SECURITY CLASSIFICATION OF ABSTRACT** | **20. LIMITATION OF ABSTRACT** |
|---|---|---|---|
| Unclassified | Unclassified | Unclassified | UU |

NSN 7540–01-280-5500 Standard Form 298 (Rev. 2–89)
Prescribed by ANSI Std. 239–18

THIS PAGE INTENTIONALLY LEFT BLANK

**Approved for public release; distribution is unlimited**

# PASSIVE MULTISTATIC DETECTION OF MARITIME TARGETS USING OPPORTUNISTIC RADARS

Chong Sze Sing
Military Expert 5 (ME5), Republic of Singapore Navy (RSN)
B.Eng. (EE), Nanyang Technological University, Singapore, 2008

Submitted in partial fulfillment of the
requirements for the degree of

**MASTER OF SCIENCE IN ELECTRICAL ENGINEERING**

from the

**NAVAL POSTGRADUATE SCHOOL**
**March 2014**

Author: Chong Sze Sing

Approved by: Herschel H. Loomis
Thesis Advisor

David C. Jenn
Co-Advisor

R. Clark Robertson
Chair, Department of Electrical and Computer Engineering

THIS PAGE INTENTIONALLY LEFT BLANK

# ABSTRACT

Passive multistatic radar (PMR) makes use of transmission from opportunistic radars to detect targets. In this thesis, a maritime scenario is created with multiple merchant vessels transmitting at S-band (3 GHz), serving as opportunistic radars and a frigate-size warship acting as the PMR receiver and to detect a low-radar cross-section (RCS) target. The simulations are carried out with actual technical parameters from open sources to best approximate practical performance. To further improve realism, the bistatic RCS simulation of the stealthy Republic of Singapore Navy Formidable-class frigate was included to validate the results.

The simulation results show that the multistatic geometry of four opportunistic transmitters at the same range from the passive receiver with 90-degree separation offers the best coverage. Passive detection of a target of up to a radial range of 30 km with detection coverage of 85% or better is possible. This range coverage is similar to that of the monostatic radar but lacks in the area of detection coverage. The simulations also demonstrated that the detection accuracy is also the highest using this same geometry. The worst-case uncertainty ellipse around the low-RCS target is less than 150 m.

THIS PAGE INTENTIONALLY LEFT BLANK

# TABLE OF CONTENTS

# LIST OF FIGURES

THIS PAGE INTENTIONALLY LEFT BLANK

# LIST OF TABLES

THIS PAGE INTENTIONALLY LEFT BLANK

# LIST OF ACRONYMS AND ABBREVIATIONS

| | |
|---|---|
| AOA | angle-of-arrival |
| ARMs | anti-radiation missiles |
| AWGN | additive white Gaussian noise |
| CMR | civil-marine radar |
| CMS | combat management system |
| COTS | commercial-off-the-shelf |
| CRLB | Cramér-Rao lower bound |
| DF | direction finding |
| DRFM | digital radio frequency memory |
| ESM | electronic support measures |
| EM | electromagnetic |
| EW | electronic warfare |
| FEKO | field calculations for bodies with arbitrary surface (FEldberechnung für Körper mit beliebiger Oberfläche) |
| FM | frequency modulated |
| GPS | global positioning system |
| HF | high frequency |
| IFF | identification friend or foe |
| IMO | International Maritime Organization |
| IRST | infrared search and track |
| ISAR | Inverse SAR |
| LPI | low probability-of-intercept |
| LOS | line-of-sight |
| NMEA | National Marine Electronics Association |
| MAIS | Marine Automatic Identification System |
| MMSI | Maritime Mobile Service Identity |
| MTI | moving target indicator |
| OODA | observe-orient-decide-act |
| OTH | over-the-horizon |
| PBR | passive bistatic radar |

| | |
|---|---|
| PMR | passive multistatic radar |
| POA | phase-on-arrival |
| PRF | pulse repetitive frequency |
| RAM | radar absorbent material |
| RCS | radar cross section |
| RORO | roll-on roll-off |
| SAR | synthetic aperture radar |
| SNR | signal-to-noise ratio |
| SOLAS | safety of life at sea |
| SOTDMA | self-organizing time division multiple access |
| TOA | time-of-arrival |
| UAV | unmanned aerial vehicle |
| VHF | very high frequency |
| YIG | yttrium iron garnet |

# EXECUTIVE SUMMARY

Using opportunistic transmitters in the form of civil marine radar (S-band and X-band) to detect maritime targets passively is both viable and comparable in performance to monostatic radars. However, in the case of detecting low-RCS (radar cross section) targets, passive multistatic radar (PMR) outperforms monostatic radars. The highly regulated requirements of the International Marine Organization (IMO) ensure that most maritime vessels out-at-sea have the necessary information to support both passive bistatic radar (PBR) and PMR. With the world's trade routed via the sea, there is no shortage of suitable vessels possessing at least one civil marine radar (CMR) and one marine automatic identification system (MAIS) on the main shipping routes. Among all the suitable vessels, larger ships like oil tankers, container ships, etc., have their CMR installed at the highest point, which extends the radar horizon and detection range. The narrow beamwidth and high transmit power of the CMR conveniently lend themselves to exploitation by a PBR system in terms of both detection accuracy and detection range.

The unique geometry formed between the opportunistic transmitter, passive receiver and unsuspecting target provides exceptional military applications not offered by the current military technologies. It offers true passive detection (with zero transmission from the receiving warship) while at the same time supports detection coverage comparable to a monostatic radar. Passive detection means there is no minimum range detection limitation that is unavoidable in a monostatic radar. In the same vein, there is no need for 'blanking' of your electronic support measures (ESM) receiver every time the onboard radar transmits. Passive detection allows for permanent monitoring of the electromagnetic spectrum for intelligence and threat. On the vulnerability front, this removes the risk posed by anti-radiation missiles and, at the same time, enhances mission survivability, allowing the warship to continue tracking targets without a working radar or with a damaged radar.

This same unique geometry also improves the warship's probability of detecting a low-RCS ship that has been treated by shaping and radar absorbent material (RAM) as compared to a monostatic radar. The use of low frequency S-band CMR poses serious

limitations to the use of RAM treatment on a low-RCS ship. It, therefore, restricts the effectiveness of low-RCS ships in the use of shaping. However, it is shown in the bistatic RCS measurement of the model based on the RSS Formidable-class stealthy frigate that shaping alone is capable of reducing the median RCS to values not higher than 200 $m^2$. With all else being equal, with the effect of RCS on detection, the PBR system has an added advantage. The bistatic RCS simulation using FEKO, a commercial RCS modelling software, shows more incidence angles exist that demonstrate a spike in RCS returns. Simply put, there are more degrees-of-freedom created by the transmitter-target-receiver geometry that has a higher probability of directing spikes in the RCS returns toward the receiver. In the case of a monostatic radar, there are limited ways to maximize RCS returns because the shaping of a low-RCS is designed to reduce returns in the direction of the incidence angle.

The simplicity of PMR also lies in the fact that there are no expensive systems to build. Instead, all the information that the PMR system needs is already available on most warships. This information can be extracted and used to carry out tracking.

The passive detection range and coverage is related to many parameters on the transmitter, target and receiver. On the opportunistic transmitter end, the transmit power and antenna gain are the two parameters that determine the maximum detection range. However, it is the relative position of the transmitter in the PBR geometry that determines the detection coverage or detection gaps. On the receiver end, the deciding parameters are the sensitivity and bandwidth of the ESM receiver. These two parameters affect the signal-to-noise ratio and, thereby, change the maximum detection range. Similar to the opportunistic transmitter, it is the geometry of the PBR that affects the detection gaps. Collectively, the factor that is used here to quantify the geometry is the bistatic angle $\beta$ formed between the transmitter and receiver (see Figure 1). Incidentally, the bistatic angle decides the bistatic RCS, which is presented to the receiver depending on the incidence angle of the transmitter's radar emission.

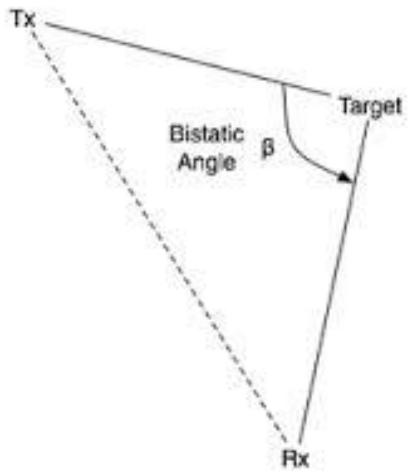


Figure 1. Bistatic Angle - β.

From the simulation plots presented in the thesis, it is shown that when more transmitters are spaced farther apart, they provide better overall coverage with small detection gaps. The minimum number of transmitters is four, placed 90 degrees apart, with one in each quadrant. To achieve maximum coverage with this particular combination of system parameters and transmitter constellation, the baseline distance of 18,000 m is recommended. By rotating the quadrant placement of transmitters, one could direct the detection gaps away from a specific bearing of choice to improve detection.

Using more than four transmitters in the suggested constellation does not significantly extend detection range. However, it is shown in the eight-transmitter simulation that it does improve detection coverage from 80% to 95% through the reduction of detection gaps. This translates to the ability of the PMR to track a target continuously, provided the target offers a strong bistatic return to all eight transmitters. In all likelihood, a low-RCS target would have presented at least two to four strong RCS returns to either the quadrant-based constellation using four transmitters or the two-layered quadrant-based constellation using eight transmitters. If the availability of such a constellation is not possible out-at-sea, one should position oneself to create such a constellation without jeopardizing a passive posture.

There are two dominant factors that affect detection accuracy, namely, the beamwidth of the transmitter and the direction-finding (DF) accuracy of the receiver. It is shown that the worst-case measurement error is approximately $\pm 120$ m for a low-RCS 114 m frigate at a range of 20 km. In most cases, a lower measurement can be achieved using multiple transmitters by overlapping their individual uncertainty ellipses. It is found that the four-transmitter and eight-transmitter constellations recommended for maximum detection coverage are also optimized to reduce the target's uncertainty ellipse. It is shown that with an eight-transmitter constellation, the overlapped area by all the uncertainty ellipses has given rise to a measurement error of 20 m for the same low-RCS target at a range of 6400 m.

In summary, the use of opportunistic transmitters in the form of civil marine radar (S-band and X-band) to detect maritime targets passively is both viable and comparable in performance to monostatic radars. The PMR with four or more transmitters offers a detection range of up to 30 km with detection coverage of 85% or better. The associated worst-case detection error is approximated to be $\pm 120$ m for a low-RCS 114 m frigate at a range of 20 km. On top of that, the PMR offers added capability to defeat low-RCS targets without the need to build extra combat systems. All information required for the PMR to work is available in most modern warships.

# ACKNOWLEDGMENTS

I am very fortunate and grateful to have the opportunity to pursue a topic that generated strong interest in me. After spending the last three years thinking about it, I got the chance to finally do it. There are too many people I would like to express my gratitude to, who, directly or indirectly, gave me strength and support throughout this arduous journey. But here, I would like to focus on those without whom none of this would be possible.

First and foremost, I would like to thank Professor Loomis for his faith in me when I sought his sponsorship to explore this new thesis topic. During the many thesis update sessions, he has offered his steady hand in helping me to navigate through the complex issues that we had to tackle to get to the answer. On more than one occasion, his insightful perspectives helped me to see beyond my blind spots to understand the crux of the matter.

Secondly, I would like to thank Professor Jenn for his advice and for sharing his wealth of experience in RCS prediction on stealth platforms. Without which, the thesis is not complete.

Lastly, but not least, I would like to thank my wife, Belinda, and my two beautiful kids, Cidney and Bradley. I would like to express my sincere gratitude to my wife for taking good care of the family and allowing me to direct my focus on completing my thesis. They are my source of strength and purpose from which I draw my motivation. Without them, this journey would not be possible.

THIS PAGE INTENTIONALLY LEFT BLANK

# I. INTRODUCTION

## A. OVERVIEW

The ability to detect targets passively has been greatly sought after since the development of modern radar. The term 'passive' detection of targets should be interpreted as the ability to detect targets without deliberate or active transmission by the sensor on the target of interest. In this deadly game of cat-and-mouse, the one that gets to 'see' first strikes first. In modern day warships, new technologies and techniques like low probability-of-intercept (LPI) radars, low-radar cross-section (RCS) design, radar absorbent material (RAM) coating and ultra-sensitive electronic warfare (EW) receivers have changed the nature of the game. On the one hand, the risk of being detected by ultra-sensitive EW receivers has forced military ships to go on a strict radar transmission policy and leverage other means of sensing, such as ship-borne unmanned aerial vehicles (UAV) or passive infrared sensor and track (IRST), for target detection. On the other hand, ships equipped with capable LPI radars still have to contend with weak returns from low-RCS designed ships. For both cases, the effective detection range in most maritime missions is generally reduced to slightly beyond the visual range with the exception of over-the-horizon (OTH) radar.

A proposed solution to resolve this deadlock, which is investigated in this thesis, is the use of multiple pairs of passive bistatic radar (PBR) to detect targets using common radar transmission by opportunistic transmitters. This approach offers many advantages. Firstly, there is no radar transmission by a source eliminating the risk of being intercepted by the target's EW receiver, or worse, by anti-radiation missiles (ARMs). Detection occurs passively, thus advancing one's observe-orient-decide-act (OODA) loop while denying the target's own OODA loop. Secondly, the unique geometry formed by separating transmitter and receiver reduces the effectiveness of low-RCS design, which to date has only been optimized to reduce monostatic returns. Simulations have shown that the RCS of stealth ships changes with different bistatic angles $\beta$, and some of these angles have considerably larger RCS returns. This unique effect may support detection of targets that are not in the line-of-sight (LOS) of one's radar. In the maritime environment, the

opportunistic transmitters are civil marine radars (CMR) operating in S-band (2.9 GHz – 3.1 GHz) and X-band (9.2 GHz – 9.5 GHz) installed on all seagoing vessels regulated by the International Maritime Organization (IMO) under Regulation 19 in safety of life at sea (SOLAS), Chapter V. The use of S-band transmission as a source also improves the chance of detection as most RAM treatment is frequency specific and wavelength dependent. As the wavelength increases, the thickness of the corresponding RAM material increases; however, the RAM treatment is not effective at lower frequencies. In addition, the abundance of opportunistic transmitters out-at-sea allows one to choose from different combinations of bistatic pairs to optimize detection coverage, probability of detection and range accuracy. Next, all hardware required for the PBR to work is currently available on most warships. There is no requirement for additional equipment. Lastly, it enhances the mission capability of warships by allowing target detection with a defective or damaged radar.

In Figure 1, a typical bistatic radar geometry is presented with the transmitter (Tx) and receiver (Rx) separated by the baseline distance, also known as the direct path or line-of-sight (LOS) of transmission, denoted by *L*. The distance from the transmitter to the target is denoted as $R_T$, while the distance from the target (Tgt) to the receiver is denoted as $R_R$. The angle formed between $R_T$ and $R_R$ is known as the bistatic angle $\beta$.

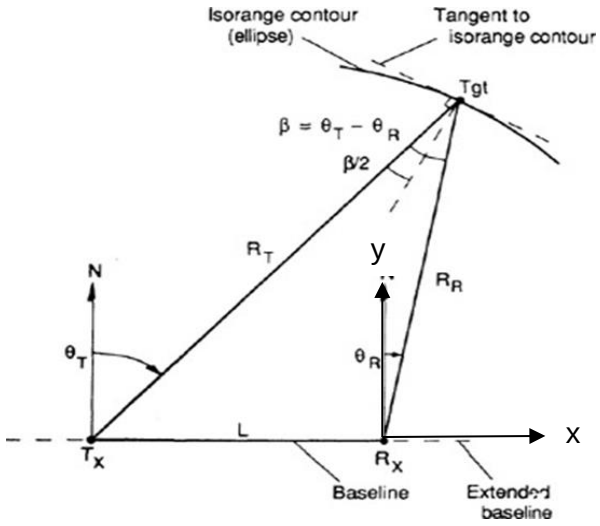


Figure 1. Bistatic geometry showing the Tx, Tgt and Rx. From [1].

## 1. History

The concept of bistatic radar is not new. In fact, the oldest form of radar is of the bistatic kind, which operated in the forward scattering configuration for aircraft detection in the 1930s [1]. The operation of this forward scatter radar ($\beta$ = 180°) is based on Babinet's principle that states that a target's RCS is greatly enhanced when observed by the receiver in a bistatic configuration with the transmitter, target and receiver on the same baseline, arranged in the order stated earlier [2]. Although the forward scatter radar supports extended detection, it is restricted in practical applications, serving more like a 'trip-wire'. Initially, little was known about the benefits that bistatic radar brings. Concurrently, the monostatic radar technology was gaining momentum with the invention of the magnetron during World War II. This technology gradually matured and ushered in the birth of pulsed radar, moving target indicator (MTI) radar, phased array radar and synthetic aperture radar (SAR) [3].

Thirty years later, in the 1960s, a bistatic radar exploiting a transmitter of opportunity, fitting the definition of a PBR, was mentioned in a paper by Rittenbach and Fishbein [4] and demonstrated a more advanced application of the bistatic radar. The most famous bistatic system built in the 1960s was the Sugar Tree system, a high frequency (HF) OTH bistatic receiver that exploited the Soviets' international broadcast transmitter to detect missile launches [4]. By then, the mainstream use of radar was dominated by monostatic radar, closely followed by counter-detection techniques known as EW. Concepts like LPI radars, low-RCS designs, and RAM were explored and pursued, leaving bistatic radar concepts relatively untouched.

In the 1990s, a renewed interest in bistatic radar occurred as a possible solution to defeat anti-radiation missiles and low-RCS designed platforms. With better technologies and computing capabilities, many possible applications of bistatic radars were re-examined. The most notable systems developed during the period are summarized in Table 1.

## 2. Bistatic Radar Research Areas

The current research interest in bistatic radar and multistatic radars can be broadly classified into three areas: (1) target detection and parameter extraction, (2) multistatic radar systems and configuration, and (3) target tracking and accuracy.

Under category (1), the forward scattering configuration of bistatic radar is combined with inverse SAR (ISAR) techniques. The bistatic radar, particularly in the forward scatter region, is used to detect crossing maritime targets cutting through the baseline formed by the transmitter and receiver. Target detection is accomplished through differentiating the target's Doppler frequency from the sea clutter. Using the rate of change of the Doppler frequency, we can approximate the target's speed and length with an error of 20% and an associated probability of detection of 80% based on the 70 maritime targets tracked [5]. This system allows for autonomous extraction of target parameters in support of target identification and classification. A separate paper went further to investigate the differences between ISAR returns from forward scatter and backscatter [6]. In that experiment, an additional transmitter, operating at a slightly different frequency, is collocated near the receiver to allow simultaneous capturing of both the forward scatter and backscatter when the ship crosses the baseline. The results confirmed that the Doppler frequency returns collected from the forward scatter and backscatter have distinctly different profiles in the Doppler versus time plot.

The forward scatter returns have a better reproduction of the ship's silhouette, most likely due to the diffraction of electromagnetic (EM) waves around the ship's superstructure. As for the case of the backscatter returns, the Doppler frequency is almost uniformly spread out across the ship structure. In summary, there is great potential in combining these two returns to enhance the capability to detect, classify and identify targets.

Table 1. Parameters of significant passive bistatic radar programs designed and tested for air surveillance. From [4].

| System | Silent Sentry™ | TV-Based Bistatic Radar (I) | TV-Based Bistatic Radar (I) | FM Radio-based Bistatic Radar | Multistatic HDTV-based Radar |
|---|---|---|---|---|---|
| **Developer** | IBM, now Lockheed Martin | University College London | DERA United Kingdom | NATO | SAIC, U.S. Army |
| **Decade** | 1980 - 2000 | 1980 | 1980 | 2000 | 2000 |
| **Configuration** | Multistatic Rx -1, Tx – Up to 6 | Bistatic | Bistatic, Near forward scatter | Bistatic | Multistatic Rx -4, Tx – 1 |
| **Transmitter Operation** | FM – realtime TV – Non-realtime | TV – Non-realtime (543 MHz) | TV – Near realtime (543 MHz) | FM – realtime | HDTV - realtime |
| **Baseline** | 100 km typical | 12 km | 150 km | 50 km | 10 km typical |
| **Target** | Aircraft, Missile Launch | Aircraft | Aircraft | Aircraft | Aircraft below 5000ft |
| **Target Data** | Range, Doppler bearing | Range, Bearing | Doppler, Bearing | Range, Doppler, Bearing | Range, Doppler |
| **Measured Performance** | $R_M$ = 100km – 150km 2D track on Aircraft 3D track on missile launch | $R_M \sim$ 25km Occasional A/C detections, but mostly negative | $R_M \sim$ 160 km Detections on high and medium altitude A/C but only 1/3 tracked | $R_M \sim$ 175 km. Achieved with innovative direct path excision | $R_M \sim$ 30 km Target location via range multi-lateration Ghost excision via doppler |

A PBR system is an attractive and low-cost choice when it comes to detection of low-flying aircraft traversing a terrestrial region. Many terrestrial transmitters such as frequency modulated (FM) radio antennas, cellphone base-stations and digital radio antennas provide the transmission source for PBR to detect these aircraft. The paper by Griffiths and Baker [7] evaluates each of the opportunistic transmitters and their detection ranges. The result shows the FM radio station at Wrotham in England has a detection range of up to 27 km with a minimum signal-to-noise ratio (SNR) of 15 dB using a coherent integration period of 0.1 s. In the case of a low-power digital radio transmitter, the detection range is reduced to 9 km with the same parameters. The cellphone base

station reduced the detection range to 1.2 km, the shortest of the three. However, the extensive network of cellphone base-stations makes up for the short detection range with good detection coverage. Delving into how the transmission waveforms affect detection, the paper found that wideband signals like FM and digital radio introduced added complexity in the bistatic and multistatic ambiguity function and concluded that the narrowband signal is more suitable for PBR system. In effect, the varying bandwidth and dynamic amplitude range of the broadcast music makes detection and tracking accuracy extremely difficult to quantify.

Data fusion is the combination of information on the same target from different sources (multiple radars) to improve probability of detection and tracking accuracy. Even in network-centric warfare concepts, it is applied almost exclusively to monostatic radar sources where system parameters such as range bin, tracking errors, and SNR are known and linear. In bistatic and multistatic radar systems, these parameters change in a non-linear fashion with respect to the geometry of the transmitter, receiver and target. In an attempt to better understand whether data fusion yields a similar advantage in a multistatic netted radar system, two sets of commercial-off-the-shelf (COTS) transmitter and receiver pairs operating at 2.4 GHz were set up to form a bistatic angle of 20° with the target [8]. The results showed that SNR improved by 3 dB with data fusion of both monostatic and bistatic returns as compared to only monostatic returns. The experiment also showed that the fusion of non-coherent returns does not improve the SNR.

The greatest advantage offered by the PBR configuration lies in its ability to leverage the EM emission of opportunistic transmitters to detect targets. This allows the receiver to detect and track targets without the target being aware of the radar's presence. One of the key challenges of this approach is to ensure consistent detection coverage and good tracking accuracy. One of the solutions proposed is to derive a method to identify the suitable transmitter-receiver geometry pair to achieve good coverage. By applying the Cramer-Rao lower-bound (CRLB) to the bistatic ambiguity function, we find that the results show that regardless of the transmitter-receiver pair chosen, the range and velocity error is lowest when the target is close to and within the vicinity of the transmitter and receiver [9]. The error increases in a radially outwards manner as the target moves

farther. In summary, to achieve good detection coverage and accuracy, there should be a transmitter or receiver in each sector-of-interest centered at the receiver. In one particular configuration, an array of transmitters can be chosen to form range rings around the receiver.

The ambiguity function of the radar waveform determines the accuracy of target tracking performance in both range and velocity. In the case of the bistatic radar (multistatic included), the ambiguity function incorporates many non-linear variables created by the spatial separation of the transmitter and receiver. Based on simulation, it was found that range resolution worsens with the increase of the bistatic angle. In the Doppler frequency domain, larger detection gaps and tracking errors are also created due to the geometry of transmitter-target-receiver [10]. In a later paper [11], the authors extend the investigation of the ambiguity function to cover coherent and non-coherent multistatic radars. The results agreed with the earlier findings and went further to emphasize the importance of time synchronization and positional accuracy of the transmitter and receiver to achieve good range accuracy. It also states that coherence between the transmitter and receiver improves the range resolution and accuracy.

From [12], improvement in detection and tracking accuracy can be achieved by fusion of data from multiple domains, e.g., time-of-arrival (TOA), phase-on-arrival (POA) and angle-of-arrival (AOA). This approach reduces the tracking error by overlapping the area of uncertainty of the target and taking the overlap area (smallest) of the three as the final range resolution. It also adds frequency diversity by transmitting a range of frequencies with multiple transmitters to further enhance performance against targets of different dimensions that are moving at different speeds. The results also show that further improvement in tracking accuracy can be achieved with a larger separation between transmitters.

In summary, there is a strong interest in a PBR system working with opportunistic transmitters. Experimental systems of this type are almost always used exclusively to detect aircraft in a terrestrial environment. The choice of transmitter waveform is almost always broadband, continuous transmission with or without FM chirp. In the maritime domain, the use of bistatic systems is almost always in the forward scatter mode with a

configurable transmitter. The focus lies in target parameter extraction and classification using ISAR techniques. Multistatic systems with good detection range and accuracy almost always maintain coherency between transmitter and receiver. It was also found that a narrowband transmitter waveform performs better in PBR. Good spatial placement of the transmitters by sector with sufficient distance improves detection coverage. In the case of tracking accuracy, the importance of having good transmitter and receiver position information and good time synchronization cannot be understated. One could improve range accuracy by choosing transmitters near to intended targets and keeping the bistatic angle between transmitter-receiver to between 30° and 160°.

## B. THESIS OBJECTIVES

The goals of this thesis are to 1) evaluate the suitability of using passive multistatic radar to detect low-RCS marine targets using civil marine radar, 2) propose the optimal multistatic radar system configuration for best detection coverage, and 3) quantify the detection accuracy of the optimal configuration using MATLAB simulation. The simulation results are obtained using actual system parameters extracted from civil marine radar equipment manuals or open sources materials.

The proposed multistatic radar system configuration is a single receiver (warship) and multiple transmitters (merchant ships) configurations. The scenario assumes a single warship is tasked to carry out comprehensive surveillance of a sector out-at-sea to enhance maritime domain awareness. Presumably, the warship is positioned somewhere in the South China Sea to monitor ships going into and out of the Singapore Straits. The targets are assumed to have low-RCS design, operating with either LPI radars or search radars with infrequent and irregular scans. The own-force warship is equipped with a broadband EW receiver with direction-finding (DF) capability. The merchant ships and the warship are equipped with class-A maritime automatic identification system (MAIS) regulated under SOLAS, which functions like identification friend or foe (IFF) on aircraft, sending out information such as identity, global positioning system (GPS) position, course and speed at short intervals on a very high (VHF) frequency. The pictorial representation of the scenario is illustrated in Figure 2.

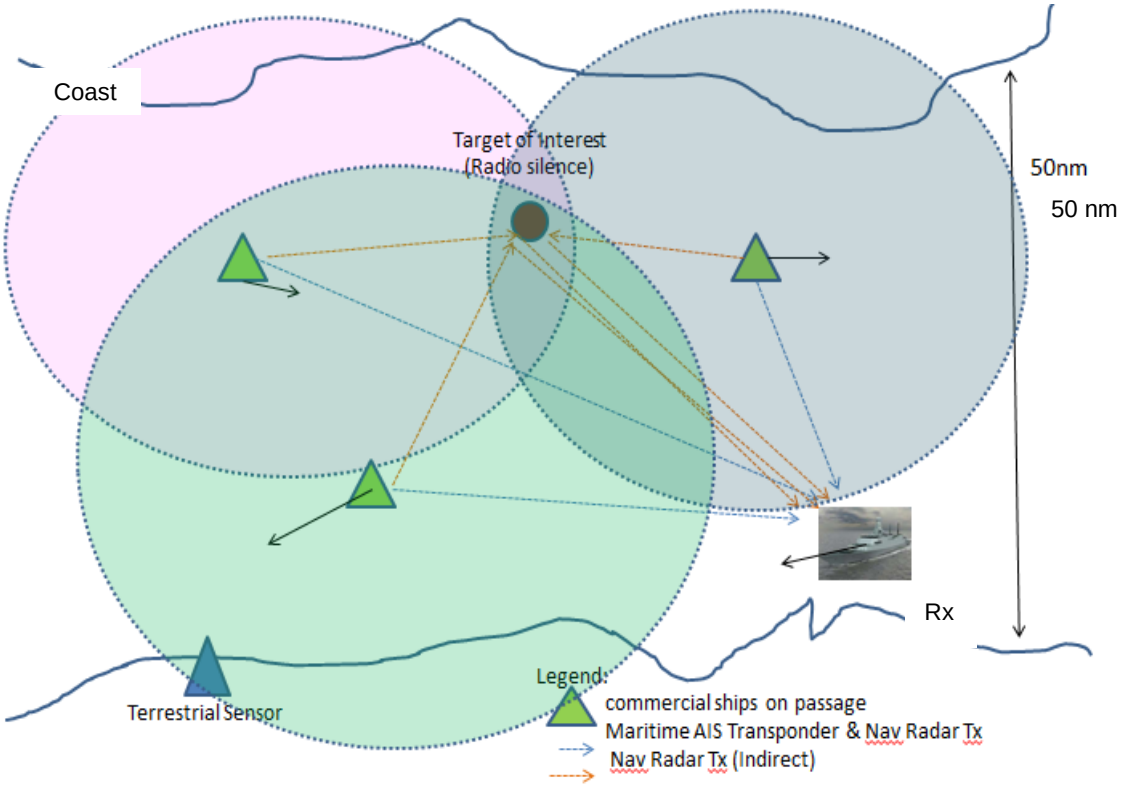


Figure 2. Pictorial representation of the PBR setup.

Typically, the process of target detection begins with the warship receiving all merchant ships' MAIS transmissions on its own transponder. The warship forms a tactical picture of all known targets on its combat management system (CMS) console screen. Using the onboard EW and DF receiver, each of the CMR's transmissions in both S-band and X-band can be correlated with the individual merchant ships. With these two sets of information, the EW DF receiver is now able to discern the same civic marine radar's transmission parameter coming from two different bearings due to the direct path and reflection off an unknown target. The difference in the time-of-arrival of the direct and indirect signals is used to compute the range of the unknown target from the warship. This set of range and bearing information has inherent errors due to DF error, data age and uncertainty in the positional information of the opportunistic transmitter. The error can be minimized by averaging and combining multiple range computations of the same target using another bistatic pair.

The first step is to determine the maximum possible detection range based the radar horizon and the maximum detection range using the bistatic radar equation. The latter takes into consideration system and physical parameters like antenna gains, transmission losses, frequency, bistatic RCS, antenna beamwidth, bistatic geometry of transmitter-target-receiver, receiver sensitivity for detection, etc.

Next, evaluation of the combined detection range for different bistatic geometries, based on the SNR at the receiver, is presented. Based on the coverage characteristics of individual bistatic geometry, combinations of multiple bistatic pairs at different angles and ranges are simulated to determine the optimal detection coverage. The simulations are run by varying frequency between S-band and X-band while combining them with different bistatic pairs.

Finally, the range accuracy is determined for each of the previously mentioned simulation runs. The objective is to evaluate the worst-case position uncertainty of the target and assess how choices of different bistatic pairs are affecting the results. The combination of these two results provides the basis by which the receiver can choose different combinations of bistatic pairs for optimal detection coverage and detection accuracy.

## C. THESIS OUTLINE

The remaining parts of the thesis are organized as follows. The background theoretical concepts needed to understand and carry out the analysis are covered in Chapter II. Starting with Chapter III, we present simulation results in a progressive order with the detection coverage of a single bistatic pair. Different combinations of multistatic geometry are presented in Chapter IV with analysis on the optimal detection coverage. The expected detection accuracy of different multistatic geometries and possible improvements are presented in Chapter V. Finally, the conclusions drawn based on the results obtained and suggestions for future work are found in Chapter VI.

# II. BACKGROUND

## A. CIVIC MARINE RADAR AND MAIS

Probability of target detection by radar is determined by the SNR. A higher SNR increases the probability of detection. This is also true in the case of a PBR; the only difference is that the CMR's signal comes in many forms and may not be designed to optimize detection. Therefore, the first step is to determine the availability of the said opportunistic transmitters, their performance specifications and operational characteristics.

The purpose of CMR, as defined by the IMO, is to "assist in safe navigation and in avoiding collision by providing an indication, in relation to one's ship, of the position of other surface craft." The technology of the CMR is heavily influenced by the regulations issued by the UN-based IMO. CMR is restricted to operate in the 3 GHz range (for good range performance) and the 9 GHz range (for enhanced detection performance in rain and fog). Since 2004, IMO has encouraged the use of coherent radars in place of the simple pulsed-radar CMR for improved detection performance against heavy sea clutter conditions [13]. The New Technology Radars, as they are known, do not have restrictions on the type of waveforms that can be used. Some companies have developed LPI CMR that is marketed for its low power requirement and improved reliability [14].

According to IMO regulations, any vessel exceeding 300 gross metric tonnage is to be fitted with a CMR. This translates to more than 50,000 ships sailing in international waters, and many of them are fitted with two radars operating in different frequency bands to enhance navigation safety. This same regulation also applies in the carriage of MAIS but with the coverage expanded to include ships exceeding 500 gross metric tonnage not on international voyage and all passenger ships irrespective of size [15]. A good estimate of the number of ships installed with CMR and MAIS, passing through the Singapore and Malacca Straits is shown in the Figures 3 and 4. Notice that in both scenes,

there are over 500 vessels that are within the reception range of the shore-based MAIS system as captured by a free online resource, www.marinetraffic.com.


Figure 3. Snapshot of MAIS targets along Malacca Straits dated Feb. 20, 2014.

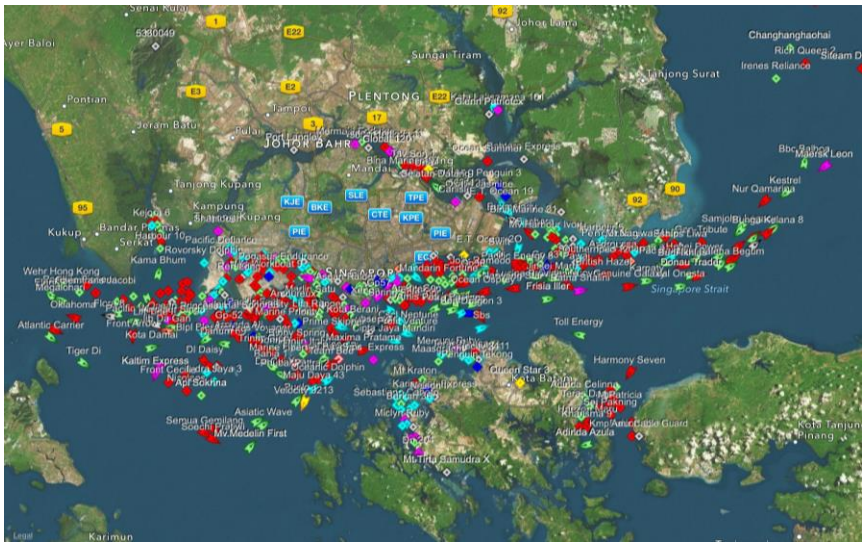


Figure 4. Snapshot of MAIS targets along Singapore Straits dated Feb. 20, 2014.

According to a report by the U.S. Energy Information Administration, over 60,000 seagoing vessels transit through the Malacca Straits (passing through the Singapore Straits) every year [16]. Assuming even distribution, one expects a daily

average of approximately 150 vessels transiting though the Singapore Straits on the Indian Ocean-South China Sea shipping route. To further narrow this down, the assumption made in the simulation is the use of frigate-class warship as own ship and the largest merchant vessels that conform to the MALACCAMAX to determine the radar horizon. MALACCAMAX is the term used in Naval Architecture to denote the largest seagoing vessel with a maximum draft of 25 m that can fit through the Malacca Straits. According to [17], the numbers of conventional cargo ship, tanker, container ships and roll-on roll-off (RORO) ships passing through the Malacca Straits in 1994 was 11620, 9688, 5244 and 1130, respectively. That translates to an average of 76 vessels on any given day.

To compute the radar horizon, two parameters are needed according to the radar horizon formula (standard atmosphere) [14]:

$$R_{\max} = 2.21\sqrt{h_{tx}} + 2.21\sqrt{h_{tx}} \tag{1}$$

where $R_{\max}$ is the range in nautical miles, $h_{tx}$ is the height of the transmitter antenna in meters and $h_{rx}$ is the height of the receiver antenna in meters.

For seagoing vessels, their dimensions are defined in length, breadth, draught and tonnage. The height above sea level or air draught, as defined in Naval Architecture terms, is seldom specified. To approximate the height of the CMR above sea level, the new PANAMAX standard states that all ships passing through the Suez Canal must not have an air draught of more than 68 m, with the restriction set by the Suez Canal bridge. It is reasonable to assume the likes of oil tankers and containers ship on international voyage are designed to conform to this requirement. For a commercial vessel, the CMR is normally installed at the highest point. On the other end, the height of the EW receiver on the frigate is approximated to be at 20 m above sea level. Therefore, $R_{\max}$ is calculated from (1) to be 52 km.

There are many international companies like the UK-based Kelvin Hughes and Japanese-based Furuno that supply the world's shipping industry with integrated bridge control systems along with CMR and MAIS. CMR such as Kelvin Hughes's MantaDigital Radar (See Appendix A for data sheet) and Furuno's FAR28x7 series (See Appendix B for data sheet) are the most commonly installed onboard larger class vessels. Out of all the technical specifications, a few parameters are needed for the computation of the SNR for detection. The specifications and comparison between the two CMRs are presented in Table 2.

Table 2. Comparison of two of most commonly installed CMR.

| **Technical Specifications** | **MantaDigital** | | **FAR28x7 series** | |
|---|---|---|---|---|
| | S-Band | X-band | S-band | X-band |
| **Pulse Width** | 55 ns (Short), 250 ns (Med), 950 ns (Long) | 70 ns (Short), 250 ns (Med), 900 ns (Long) | 0.5 µs (Short), 0.7 µs (Med), 1.2 µs (Long) | 0.5 µs (Short), 0.7 µs (Med), 1.2 µs (Long) |
| **Beamwidth (Vertical)** | 26° | - | 25° | 20° |
| **Beamwidth (Horizontal)** | 1.9° | 1.25° | 1.8° | 1.23° |
| **Pulse Repetitive Frequency** | 3000 Hz (Short), 750 Hz (Med), 750 Hz (Long) | 3000 Hz (Short), 1500 Hz (Med), 750 Hz (Long) | 1000 Hz (Short), 600 Hz (Med), 600 Hz (Long) | 1000 Hz (Short), 600 Hz (Med), 600 Hz (Long) |
| **Receiver Noise Figure** | < 6 dB | < 6 dB | - | - |
| **Antenna Gain** | 28 dB | 30 dB | - | - |
| **Transmitter Power** | 30 kW | 25 kW | 30 kW | 30 kW |
| **Frequency** | 3050 MHz +/- 10 MHz | 9410 MHz +/- 30 MHz | 3050 MHz +/- 30 MHz | 9410 MHz +/- 30 MHz |
| **Scan Rate** | 24 rpm/ 45 rpm | 24 rpm/ 45 rpm | 24 rpm/ 42 rpm | 21 rpm/ 26 rpm/ 45 rpm |

In reference to the technical specifications shown in Table 2, both CMRs share similar parameters, but not all parameters of the FAR-28x7 series are available in its product catalog. For the purpose of this thesis, the technical specifications of the

MantaDigital Radar are used to compute the SNR and maximum detection range of the PBR.

After selecting the technical specifications of the opportunistic radar, the next step is to obtain an accurate position of all available opportunistic radars so as to calculate the baseline distance between the transmitter and EW receiver on the warship. Furthermore, the receiver needs to be able to uniquely classify each CMR transmission and associate it with the source vessel on the CMS. From the operating specifications requirement stated by the IMO, the MAIS's function is to support automated tracking and identification among vessels and port authorities. It operates autonomously and continuously to exchange ship identity and GPS locations using the VHF transceiver. There are two types of MAIS: Class A installed onboard a majority of seagoing commercial vessel, and the more economical Class B used typically by leisure and smaller crafts. The MAIS communication network uses self-organizing time division multiple access (SOTDMA) to allow for at least 4500 communication timeslots for vessels to exchange up to 27 different National Marine Electronics Association (NMEA) – 0183 messages, sorted into different level of priorities. The highest priority message is the GPS positional information accompanied by a unique nine-digit identification number assigned to each vessel known as the maritime mobile service identity (MMSI). This information allows the warship to discern targets of interest from neutrals on its CMS display. Extracted from the U.S. Coast Guard website, the key difference in specifications between Class A and Class B MAIS are summarized in Table 3.

Table 3. Comparison of specifications between Class A and Class B MAIS.

| Shipboard AIS | Class A | Class B/Self-Organizing | Class B/Carrier Sense |
|---|---|---|---|
| **Transmit Power (Watts)** | 12.5 W / 2 W | 5 W / 2 W | 2 W |
| **Primary Access Scheme** | SOTDMA | SOTDMA Carrier-sense | TDMA non-competing with SOTDMA units |
| **Position Reporting Rate** | Either every 2, 3 ½, 6 or 10 s based on speed and course change. Every 3 min when < 3 kts | Either every 5, 15 or 30 s based on speed Every 3 min when < 2 kts | Every 30 s Every 3 min. when < 2 kts. |
| **Static Data Reporting Rate** | Every 6 min | Every 6 min | Every 6 min |
| **Transmit Data** | All | No Rate of Turn, Navigation Status, Destination, ETA, | No Rate of Turn, Navigation Status, Destination, ETA, |

From the U.S. Coast Guard website, the worst-case GPS positional accuracy of the MAIS is 0.001 minute in both latitude and longitude with an update rate of no longer than 10 s for a Class A MAIS. That translates to a positional error of not more than 2 m all round. With reference to the MantaDigital Radar chosen earlier, the same class of vessel is equipped with a Class A MAIS. For the purpose of this thesis, the information provided by Class A MAIS is used to calculate the baseline distance and the detection accuracy of the target.

## B. EW AND DF RECEIVERS

Onboard a warship, the EW receiver is responsible for the extraction of key parameters from the intercepted transmission for follow-on classification and identification typically through digital radio frequency memory (DRFM). The EW receiver is capable of measuring the intercepted transmission's center frequency, pulse width, pulse repetitive frequency (PRF), antenna scan rate, type of radar, transmission mode, etc. Integrated with the DF receiver, the angle-of-arrival can be determined and used to point to the source of transmission with the aid of a bearing line. Parameters like these are saved in the DRFM to help with future identifications.

The important parameters to quantify on the EW and DF receiver are the lowest received power that can be detected, known as sensitivity, bandwidth of the receiver, detection bandwidth and DF accuracy. Due to the classified nature of these parameters, they are seldom available in open source literature. As such, the parameters are based on systems with published specifications that best matched our scenario and as practical as reasonable.

The EW receiver specifications are based on UK-based Teledyne Defense Ltd.'s high performance receiver model QR026 (See Appendix C for data sheet). This wideband receiver operates from 0.2 GHz to 18 GHz and is expandable to frequencies up to 40 GHz. It has a sensitivity of approximately $-70$ dBm, a typical noise figure of 13.5 dB, and a receiver gain of 20 dB if operating with a scanning bandwidth of 500 MHz. Most EW receivers support tuning of bandwidth to enhance detection of specific frequency band and the use of a notch or Yttrium iron garnet (YIG) filter to carry out narrowband detection and classification. For our case, the bandwidth of the receiver can tuned to coincide with the frequency band of interest, thus reducing additive white gaussian noise (AWGN), thereby, improving the sensitivity and SNR.

The DF receiver specifications are based on South Africa's Poynting Defense's land-based DF Antenna model DF-A0062 (See Appendix D for data sheet), which has an effective DF range from 20 MHz to 6 GHz and U.S.-based DRS Defense Solutions shipboard DF Antenna array model ZA-4501. Both DF antenna systems work on a five-element phase interferometer concept with an azimuth DF accuracy of between 1° to 2°. For the purpose of this thesis, the average DF accuracy of 1.5° is used.

## C. BISTATIC RCS

Bistatic RCS of a target is dependent on the angle formed between the direction of incidence and the direction of reception, known as the bistatic angle $\beta$. Unlike the monostatic RCS, which is a measure of the amount of EM energy re-radiated back in the direction of incidence, the bistatic RCS is the measure of the amount of EM energy returned in the direction of the receiver that is not co-located with the transmitter. Putting everything in perspective, there is only one set of 360 values in monostatic RCS

corresponding to 360 degrees in azimuth for each target. However, in the case of the bistatic RCS, each direction of incidence has its own set of RCS values for 360 degrees. So to completely map out the bistatic RCS of a target, there are 360 sets of values per target.

The definition of RCS can be stated [2] as

$$\sigma = \lim_{R \to \infty} 4\pi R^2 \frac{\left|\vec{E}_s\right|^2}{\left|\vec{E}_i\right|^2}. \tag{2}$$

For simple geometrical shapes, the RCS can be easily calculated using

$$\sigma = \frac{4\pi A_{ea}^2}{\lambda^2} \tag{3}$$

where $A_{ea}^2$ is the equivalent area in $m^2$ and $\lambda$ is the wavelength in meters. In the case of a complex-shaped low-RCS warship, the approximation of the RCS has to take into consideration the 'electrical size' of the target, which is defined by the largest relative dimension of the target in terms of the incident wavelength. There are three frequency regions in which the RCS of a target can vary significantly, namely the Rayleigh region (low frequency), Mie region (resonance) and Optical region (high frequency). The three regions are classified based on the magnitude of the 'electrical size.' The graph (Figure 5) presents the effect on the monostatic RCS by varying the wavelength on the same sphere.

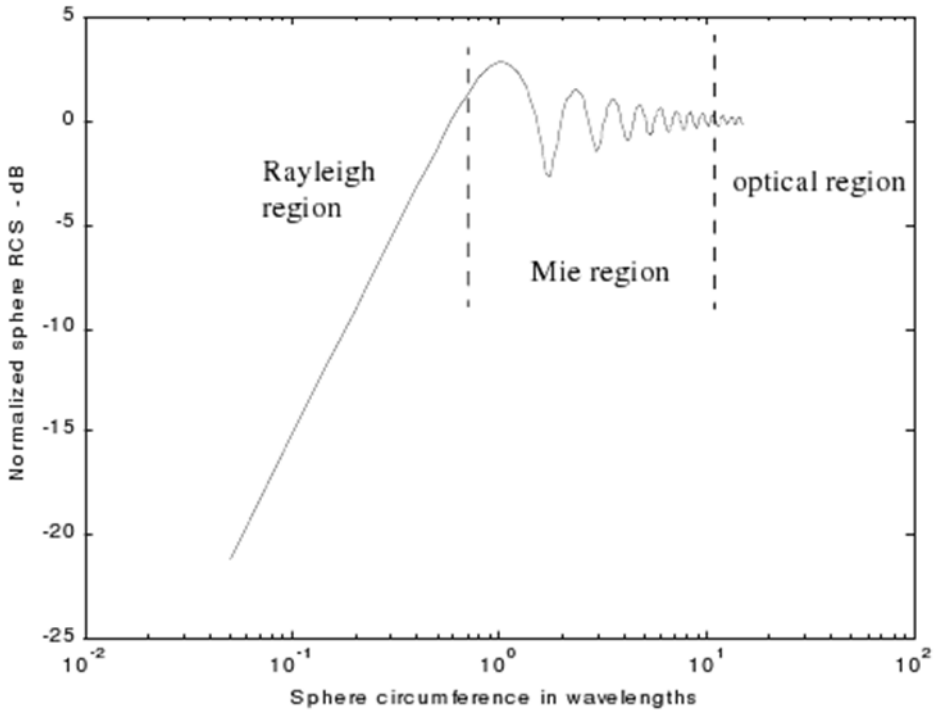


Figure 5. Effects on monostatic RCS of a sphere with changes to the wavelength. From [1].

Due to the profound effect of the ratio of the target length versus the input transmission wavelength, different methods of RCS prediction are used in response to the dominant scattering mechanism that is present. The RCS prediction methods most commonly used are physical optics, microwave optics, method of moments, the finite element method and the finite difference method. For our case, the low-RCS warship is chosen to be the Republic of Singapore Navy's (RSN) Formidable-class frigates. A three-dimensional model (Figure 6 and 7) of the Formidable-class frigate is created in CST Studio and ported over to FEKO, a commercial RCS modeling software, to calculate the free space monostatic and bistatic RCS at S-band and X-band using physical optics. The physical optics method is suited for use to predict the RCS for targets that are in the optical frequency region.

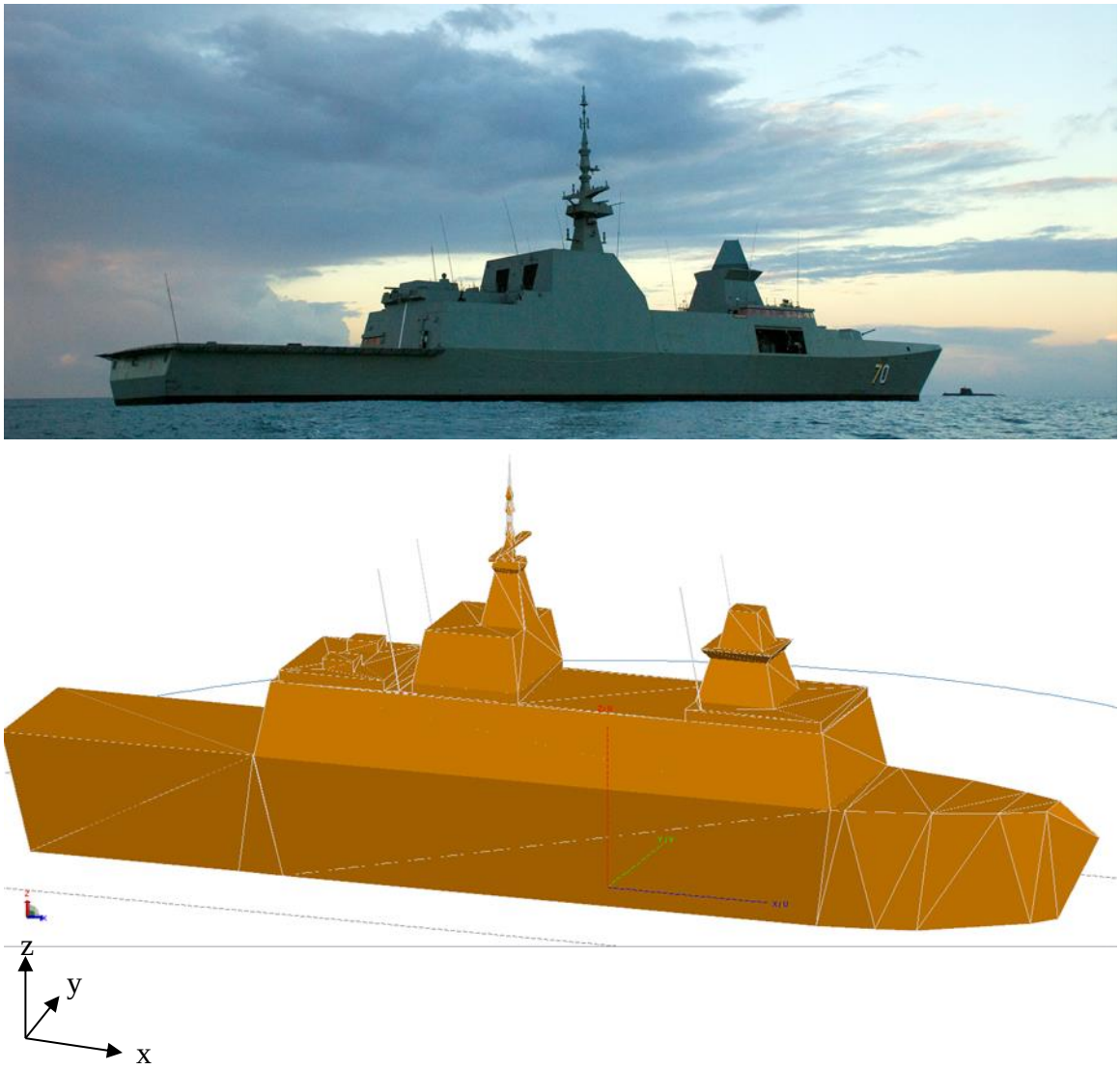


Figure 6. Actual photo of RSN's Formidable-class stealth frigate (top, from [18]) versus its model (side profile).

A quick comparison between the monostatic RCS and bistatic RCS shows that the RCS differences can fluctuate up to a factor of 30 dB over an aspect change of a few degrees as illustrated in Figure 8. A sample set of bistatic RCS plots are attached as Appendix E, and the values are added to the MATLAB simulation in the area of detection coverage.

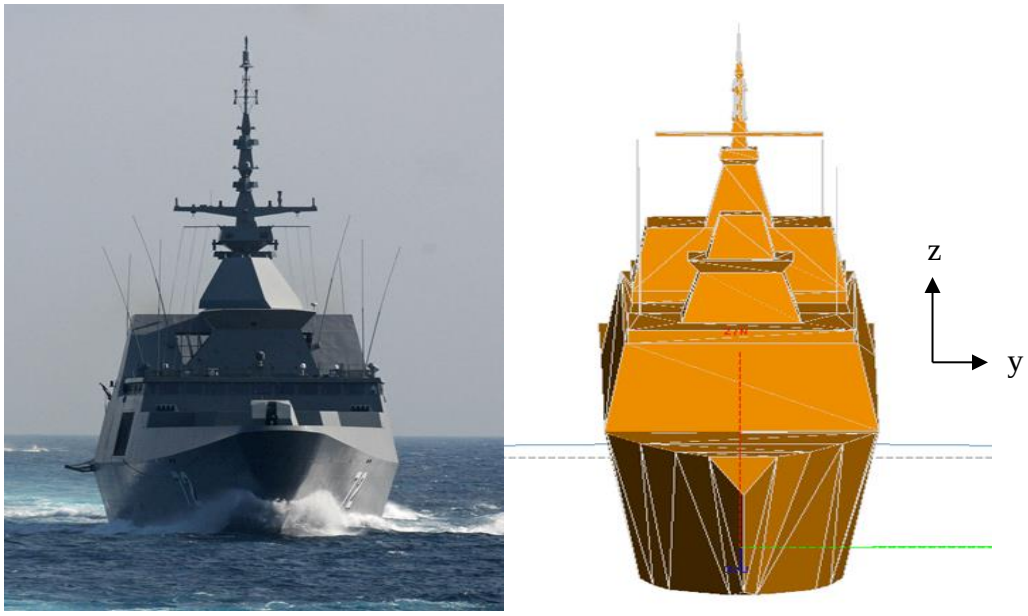


Figure 7. Actual photo of RSN's Formidable-class stealth frigate (top, from [19]) versus its model (front profile).

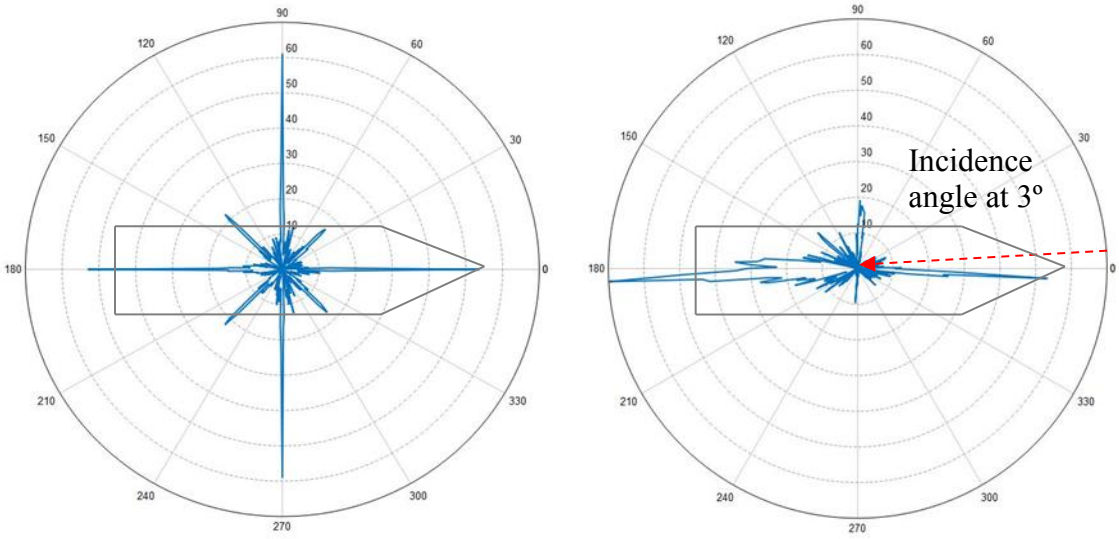


Figure 8. Comparison of monsotatic RCS (dBsm) of the model measured at 3 GHz (left) and bistatic RCS with incidence angle at 3 degrees (right).

## D. BISTATIC RADAR RANGE EQUATION

In reference [1], the bistatic radar range equation is derived. The single range in the monostatic case is now split into two range variables $R_T$ and $R_R$, and the monostatic RCS is replaced with the bistatic RCS denoted by $\sigma_B$ as

$$(R_T R_R)_{\max} = \left[ \frac{P_T G_T G_R \lambda^2 \sigma_B F_T^2 F_R^2}{(4\pi)^3 k T_s B_n (S/N)_{\min} L_T L_R} \right]^2 = \kappa \tag{4}$$

where

$R_T$ = transmitter-to-target range,
$R_R$ = target-to-receiver range,
$P_T$ = transmitter power output,
$G_T$ = transmitter antenna power gain,
$G_R$ = receiving antenna power gain,
$\lambda$ = wavelength,
$\sigma_B$ = bistatic RCS,
$F_T$ = pattern propagation factor for transmitter-to-target path,
$F_R$ = pattern propagation factor for target-to-receiver path,
$k$ = Boltzmann's constant,
$T_s$ = receiving system noise temperature,
$B_n$ = noise bandwidth of receiver's pre-detection filter, sufficient to pass all spectral components of the transmitted signal,
$(S/N)_{\min}$ = signal-to-noise power ratio required for detection,
$L_T$ = transmitting system losses (> 1) not included in other parameters,
$L_R$ = receiving system losses (> 1) not included in other parameters, and
$\kappa$ = bistatic maximum range product.

By grouping some of the terms listed, Eq. (4) can be presented in a more compact and generalized form for any SNR value. Defining

$$\mathrm{K} = \frac{P_T G_T G_R \lambda^2 \sigma_B F_T^2 F_R^2}{(4\pi)^3 k T_s B_n L_T L_R}, \tag{5}$$

we can write, in general,

$$S/N = \frac{\mathrm{K}}{R_T^2 R_R^2}. \tag{6}$$

The SNR value is only sensitive to parameters associated with the CMR and EW receiver. It is not grounded in any coordinate system or locations of the transmitter, receiver and target.

From geometry (refer to Figure 1),

$$R_R = \frac{(R_T + R_R)^2 - L^2}{2(R_T + R_R + L\sin\theta_R)} \tag{7}$$

where $L$ is the baseline distance between the transmitter and receiver, and $\theta_R$ is the angle between North (*y*-axis) and the target.

In the real world, target detection begins with the measurement of $(R_T + R_R)$ using one of two methods, namely the direct method which requires a line-of-sight between the transmitter and receiver or the indirect method which requires synchronization of stable clocks between the transmitter and receiver. Given the use of opportunistic transmitters, the direct timing method is used here and

$$(R_T + R_R) = c\Delta T_n + L \tag{8}$$

where

$c$ = speed of light, and
$\Delta T_n$ = time interval between the reception of the transmitted pulse and reception of the target echo.

In this case, the EW receiver is the one providing this information. The EW receiver must first characterize the transmission of each CMR for quick recognition. Upon receiving the direct transmission from the CMR as verified by the DF receiver, the timer starts counting until it receives the same CMR transmission from a different bearing. This time difference is $\Delta T_n$. The measured difference in bearing is then used to determine $\theta_R$. With that, the detection coverage based on SNR can be plotted. The plot is

then normalized using the $SNR_{\min}$ to display the detection coverage supportable by the EW receiver. The $SNR_{\min}$ (in dB) is calculated from

$$Sensitivity = SNR_{\min} + 10\log(B_n) + NF_{rec} - 174 \tag{9}$$

As shown in Eqs. (6) through (8), the SNR value corresponding to a specific combination of Tx-Tgt-Rx can be calculated given all the parameter values. Putting all these individual SNR contours together on a Cartesian coordinate plot, we find the detection coverage for a particular combination of PBR. Given the high availability of opportunistic transmitters out-at-sea, multiple combinations of PBR can be used for optimum coverage in real-time to allow for the highest probability of detection.

## E. MEASUREMENT AND LOCATION ERROR

From [1], there are three geometry-dependent measurement and location errors in a PBR system, namely the receiver-to-target error due to measurement of $(R_T + R_R)$, baseline measurement error of $L$ and receiver look angle error due to DF error by the DF receiver. The receiver-to-target error is the result of transmitter beamwidth spread at the target at $R_T$ where the edge of azimuth beamwidth is strong enough to create returns back to the receiver. The baseline measurement error is dependent on the means by which the measurement of the baseline is obtained. In our case, the baseline $L$ is computed as the difference between the differential GPS locations of the transmitter and receiver. As such, the measurement error is a function of the accuracy of the GPS position fix. The root-sum-squared (rss) of the three errors in [1] is expressed as

$$dR_R = \left\{ \left[ \frac{\partial R_R}{\partial (R_T + R_R)} d(R_T + R_R) \right]^2 + \left( \frac{\partial R_R}{\partial L} dL \right)^2 + \left( \frac{\partial R_R}{\partial \theta_R} d\theta_R \right)^2 \right\}^{1/2} . \tag{10}$$

Depending on the geometry of Tx-Tgt-Rx, the three errors are still additive but with components on different planes, as shown in Figures 9 through 11. With changing geometry, the combined error forms an ellipse with a different major and minor axis.

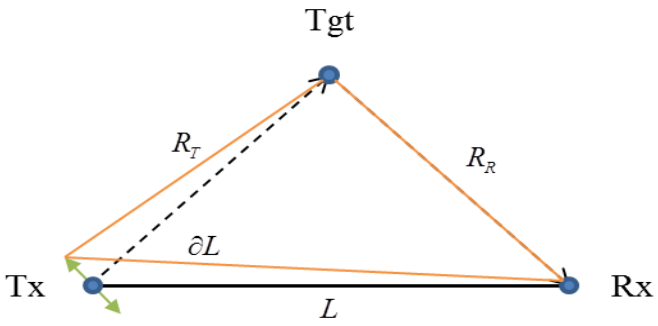


Figure 9. Illustration of measurement error due to variation of $L$.

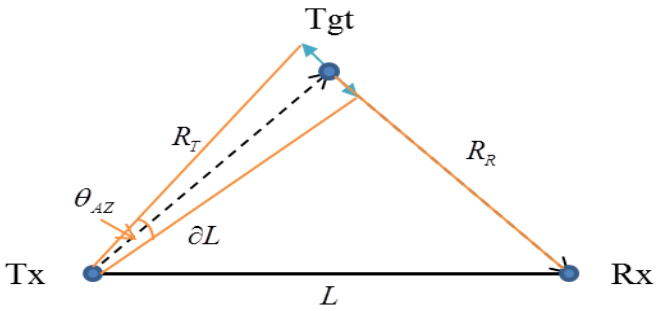


Figure 10. Illustration of measurement error due to transmitter's $\theta_{AZ}$ .

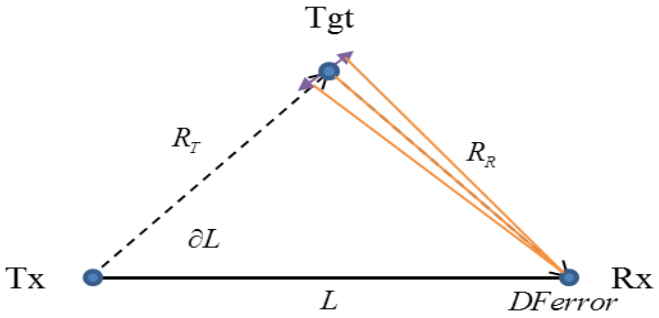


Figure 11. Illustration of measurement errors due to receiver's DF error.

The three components of error contributing to the rss in Eq. (10) are

$$\frac{\partial R_R}{\partial (R_T + R_R)} = \frac{(R_T + R_R)^2 + L^2 + 2L(R_T + R_R)\sin\theta_R}{2(R_T + R_R + L\sin\theta_R)^2}$$
$$= \frac{1 + e^2 + 2e\sin\theta_R}{2(1 + e\sin\theta_R)^2}, \qquad (11)$$

$$\frac{\partial R_R}{\partial L} = \frac{[L^2 + (R_T + R_R)^2]\sin\theta_R + 2L(R_T + R_R)}{2(R_T + R_R + L\sin\theta_R)^2}$$
$$= -\frac{(e^2 + 1)\sin\theta_R + 2e}{2(1 + e\sin\theta_R)^2}, \tag{12}$$

and

$$\frac{\partial R_R}{\partial \theta_R} = -\frac{L[(R_T + R_R)^2 - L^2]\cos\theta_R}{2(R_T + R_R + L\sin\theta_R)^2}$$
$$= -\frac{L(1 - e^2)\cos\theta_R}{2(1 + e\sin\theta_R)^2} \tag{13}$$

where $e$ = eccentricity given by $L/(R_T + R_R)$.

To begin using this PBR system in a real-world scenario, one has to first determine what CMRs (opportunistic radars) are within range and what combination of them offers the best overall detection coverage and, if not, at a minimum, optimize coverage within their operating areas.

With the warship's MAIS in the receive-only mode, all merchant ships that are within the VHF reception range are displayed on the CMS screen. Based on the returns from the MAIS, the merchant ships that operate with Class-A MAIS are selected, and their S-band and/or X-band CMRs' parameters are collected and analyzed using the EW receiver. The parameters are then saved into the DRFM and associated with the bearing relative to the warship (receiver) given by the DF receiver. The Class-A MAIS of all selected merchant ships are constantly updating their GPS positions at an update rate of no greater than 10 s. With the unique identifier provided by the MAIS, the specifications of the CMR can be determined. Putting all this information together, the crews onboard the warship have all the necessary information for Eqs. (5) and (8) to plot the detection coverage for a single PBR system. All the involved parameters tagged to their individual sources are summarized in Table 4. A further extension of this is to establish the relationship between different Tx-Rx PBR pairs and their associated detection coverage. The warship can choose multiple PBR pairs and combine their individual detection coverage plots to form a more comprehensive coverage in the area of interest. Different constellations of Tx-Rx pairs offer different advantages and disadvantages. Knowing this

in advance, along with practice, allows the warship operators to pick the best constellations from the prevailing availability of opportunistic transmitters in a minimum time.

Table 4. Parameters summary for Eqs. (5) and (8).

| Systems | MantaDigital (CMR) | Class-A (MAIS) | QR026 (EW Receiver) | DF-A0062 (DF Receiver) | FEKO RCS Modeling Software | Remarks |
|---|---|---|---|---|---|---|
| $P_T$ | 30 kW (S-band) 25 kW (X-band) | - | - | - | - | - |
| $G_T$ | 28 dB (S-band) 31 dB X-band) | - | - | - | - | - |
| $G_R$ | - | - | 2 dB | - | - | - |
| $\lambda$ | - | - | 0.0984 m (S-band) 0.0319 m (X-band) | - | - | - |
| $\sigma_B$ | - | - | - | - | See Appendix E | - |
| $F_T$ $F_R$ | - | - | - | - | - | 1 See reference [4] |
| $T_s$ | - | - | 3915 K (based on noise figure of 13.5 dB) | - | - | - |
| $B_n$ | - | - | 500 MHz | - | - | - |
| $L_T$ $L_R$ | - | - | - | - | - | 2 See reference [4] |
| $L$ | - | Based on GPS location of Tx and Rx | - | - | - | - |
| $\Delta T_n$ | - | - | Based on GPS location of Tx and Rx | - | - | - |
| $\theta_R$ | - | - | - | Bearing Line | - | - |

To plot an operationally usable detection plot, the minimum SNR with reference to the sensitivity of the EW receiver has to be determined using Eq. (9). This defines the value of SNR beyond which reception of the returns from the target is possible. Based on a sensitivity value of $-70$ dBm, the $SNR_{min}$ required in our scenario is more than 3.5 dB for single pulse. To allow for unaccounted losses or unforeseen variations, an additional buffer is added to increase the $SNR_{min}$ to 10 dB in our simulation.

In situations where signal strength of the returned signal is weak, non-coherent pulse integration across multiple pulses can improve the chance of detection by approximately $\sqrt{N}$ dB, where $N$ is the number of pulses used in the integration [19]. This approximation is heavily dependent on the type of receiver architecture used and is more applicable for envelope detector receiver types. The number of pulses transmitted downrange can be calculated using

$$N = \frac{\theta_{AZ}}{360(scanrate)}(PRF) \tag{14}$$

where

$\theta_{AZ}$ = Azimuth beamwidth of the CMR in degrees,
*scanrate* = CMR Antenna scan rate in revolution per second (rps),
*PRF* = CMR's antenna PRF in Hz.

In the case of the S-band KH MantaDigital radar, the number of pulses that are available for integration per second is five pulses with $\theta_{AZ}$ of 1.9°, *scanrate* of 45 rpm and *PRF* of 750 Hz. This translates to a gain of 2.2 dB. Thus, by allowing for more integration time, it is possible to increase detection range. The low SNR of each pulse and the long integration time also bring with them increased measurement errors, specifically, in the TDOA measurements of the leading edge of the returned pulse. The increase in error is discussed in [20] for a monostatic radar, but the application to PBR adopting the discussed form of TDOA is not well-defined.

## F. DETECTION ACCURACY

As the PBR system detects targets passively and displays them on the CMS screen, a problem of detection accuracy arises. As shown in Eqs. (13) through (15), there are measurement and location errors that form an uncertainty ellipse around the target. On top of these baseline errors, there are three sources of errors that add to the growing uncertainty ellipse. They are: (1) azimuth beam spread of the CMR with target range, (2) accuracy of the DF receiver and (3) positional errors due to data age and moving targets. These sources of errors are added in their respective planes and determine the uncertainty ellipse for each Tx-Rx pair. By knowing the passively-detected target range and azimuth with respect to the warship, one can compute the worst-case location errors in Cartesian coordinates. The location errors can be reduced by using more Tx-Rx pairs to narrow down the overlapped area.

In the next chapter, the simulation of PBR and PMR are presented. Different opportunistic transmitter placements are simulated to understand their effects on detection coverage and detection accuracy.

THIS PAGE INTENTIONALLY LEFT BLANK

# III. SIMULATION RESULTS FOR DETECTION COVERAGE

In this chapter, the detection coverage of the PBR is investigated with different combinations of Tx-Rx constellations. The chapter begins with a single transmitter and receiver pair and demonstrates how a PBR system has a higher probability of detecting a low-RCS target. The simulation results also show the limited detection coverage of a single PBR system. The investigation goes on to explore a multiple PBR system and evaluates the detection performance of the combined system using different Tx-Rx constellations. All simulation results are generated using MATLAB with the source codes included in Appendix F.

## A. SINGLE TX-RX PAIR

To appreciate the benefits brought about by combining multiple PBRs into a multistatic radar system, one first needs to understand the capabilities and limitations of a PBR system operating with S-band and X-band CMR.

### 1. Monostatic RCS with S-Band CMR

According Skolnik [14], at low grazing angle, the median RCS of a ship can be estimated using the empirical formula

$$\sigma = 52\sqrt{f}D^{3/2} \tag{15}$$

with the $f$ in MHz and ship's displacement $D$ in kilotons. Substituting $f$ as 3050 MHz and $D$ as 3.2 kilotons, the displacement of RSS Formidable-class frigate, we find the RCS of a non-RCS treated frigate to be 5137 $m^2$. A separate simulation using FEKO on the model based on RSN's Formidable-class frigate yields a more representative monostatic RCS plot (Figure 12). The monostatic RCS fluctuates from 0 dBsm to 72 dBsm dependent on the incidence angle. Using the results shown in Figure 12, we estimated the simulated median RCS as 18 dBsm (63 $m^2$) for S-band.

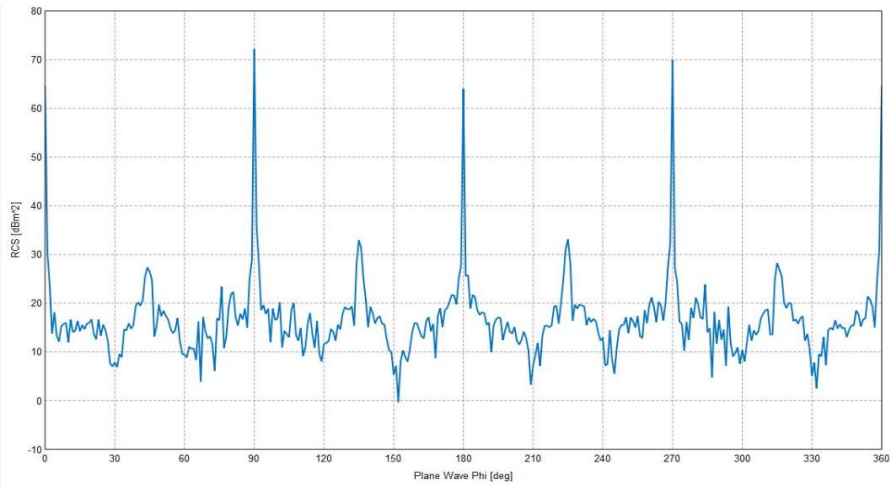


Figure 12. Monostatic RCS of RSN's Formidable-class frigate simulated at 3050 MHz using FEKO.

Putting both median monostatic RCS values into simulations, we found the resulting detection coverage of a PBR with a S-band CMR at $(-5000,0)$ as shown in Figures 13 and 14. These plots are generated using Matlab scatter plot function. Each data point is shown as a colored dot. The density of the data changes from plot to plot. Note that gaps between the individual dots on the low density plots are not areas of low SNR, which has been set at 10 dB.

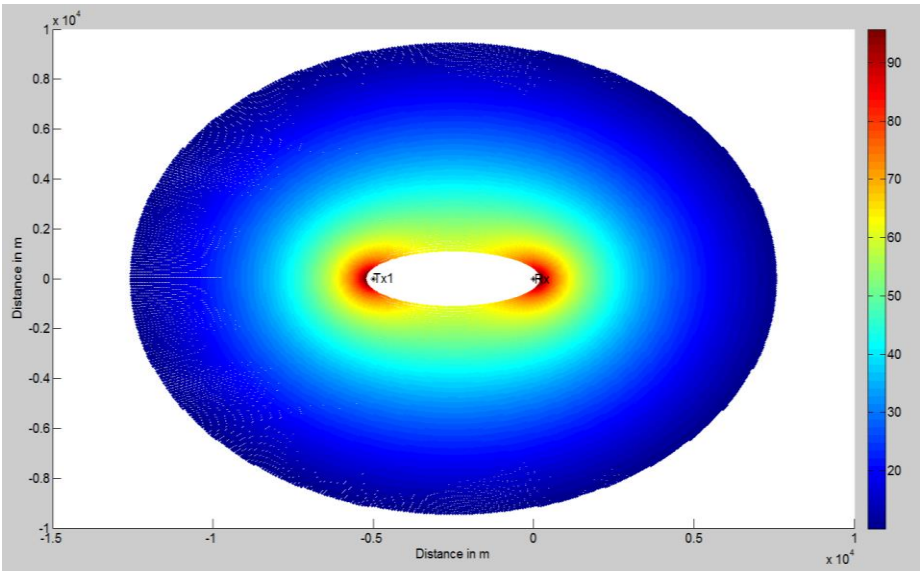


Figure 13. SNR detection plot (dB) using empirical median RCS at S-band CMR with Rx at the origin and single Tx at $(-5000,0)$.

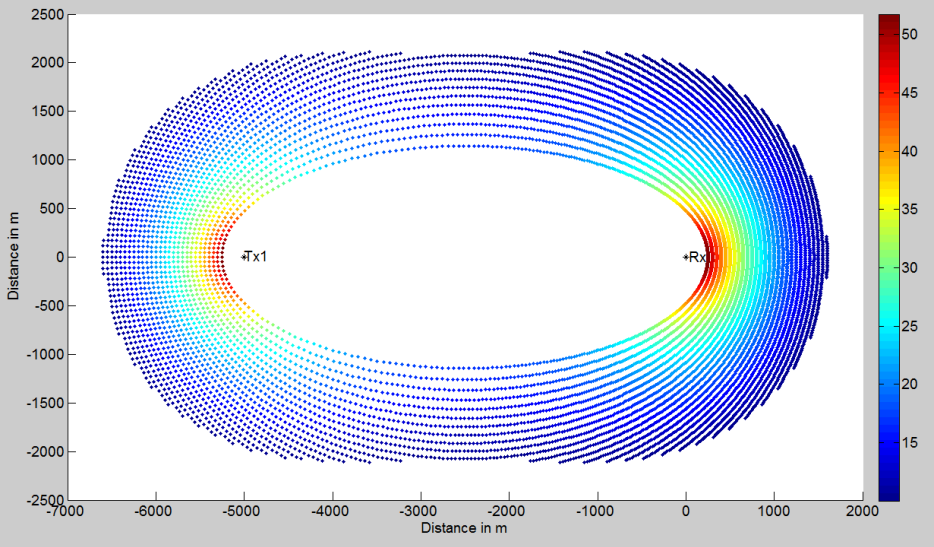


Figure 14. SNR detection plot (dB) using simulated median RCS at S-band CMR with Rx at the origin and single Tx at $(-5000,0)$.

With the minimum SNR set at 10 dB and the EW receiver bandwidth of 500 MHz over an integration time of 1 s, the radial detection coverage under such conditions extends to approximately 7500 m from the receiver with near 100% coverage. From Figure 14, the detection coverage with the use of simulated median RCS shows a drop in detection coverage range to that of 1500 m from the receiver. The observable gaps in the plot of Figure 14 are the result of plotting resolution and not actually detection gaps. The detection void between the transmitter and receiver is due to the limitation offered by the PBR geometry. As the target approaches the baseline formed by the transmitter and receiver for the TDOA calculation expressed in Eq. (8), the difference between the direct path $L$ and the reflected path $(R_T + R_R)$ converges to zero. All equations expressed in this thesis break down both in theory and in practice since the target is now directly between the transmitter and receiver line-of-sight. In such cases, the PBR functions as a forward scatter radar instead of a PBR.

## 2. Monostatic RCS with X-Band CMR

Using the Eq. (15), we can show the monostatic RCS of a typical frigate at X-band (9410 MHz) to be 28,875 $m^2$. A separate simulation using FEKO on the model based on RSN's Formidable-class frigate yields a more representative monostatic RCS plot (see Figure 15). The monostatic RCS fluctuates from $-10$ dBsm to 80 dBsm dependent on the incidence angle. Using the results shown in Figure 15, we find the estimated simulated median RCS to be 15 dBsm (32 $m^2$) for X-band.

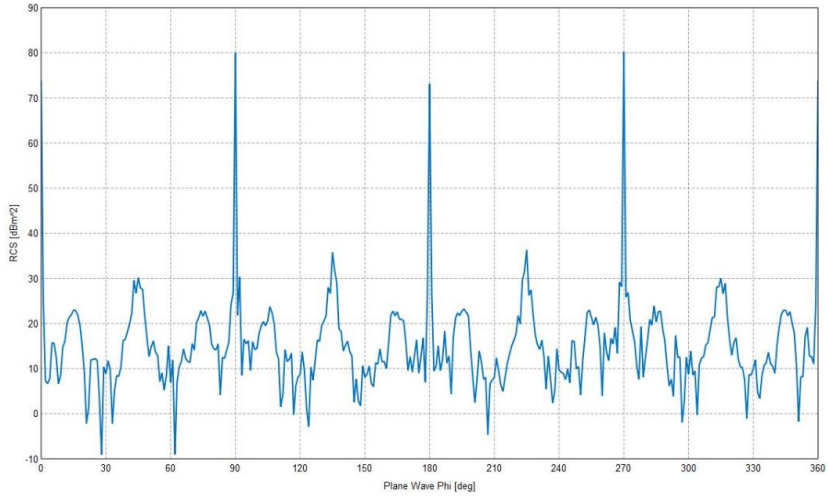


Figure 15. Monostatic RCS of RSN's Formidable-class frigate's model simulated at 9410 MHz using FEKO.

For the purpose of comparison, we put both median monostatic RCS values (median from formula and median from FEKO) into the simulation. The resulting detection coverage of a PBR with an X-band CMR at $(-5000,0)$ is shown in Figures 16 and 17. The magnitude of the SNR behaves in the same way for all PBR systems with high SNR around the vicinity of the transmitter and receiver and reduces in a linearly radial manner. This simulation is consistent with findings by [10].

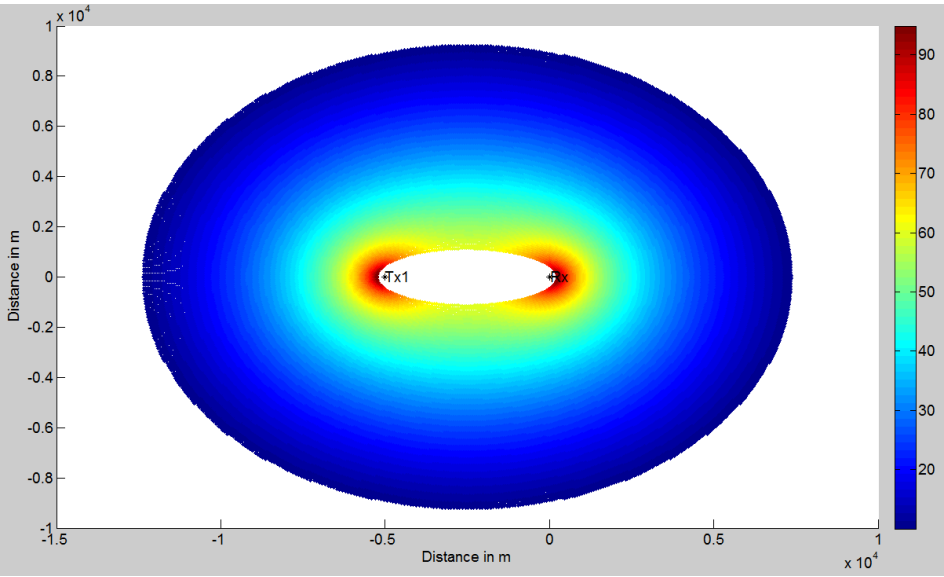


Figure 16. SNR detection plot (dB) using empirical median monstatic RCS from Eq. (15) at X-band CMR with Rx at the origin and single Tx at $(-5000,0)$.

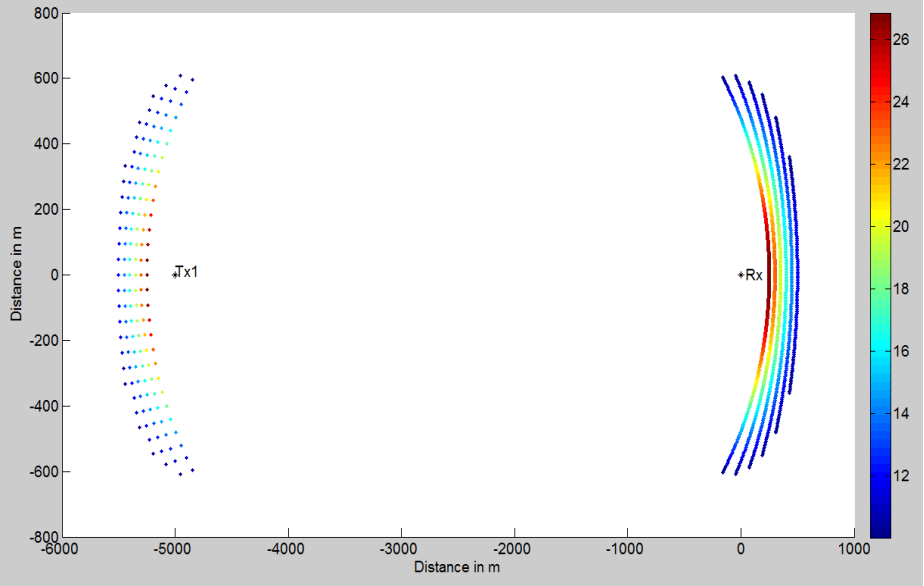


Figure 17. SNR detection plot (dB) using simulated median monostatic RCS from FEKO at X-band with Rx at the origin and single Tx at $(-5000,0)$.

The low FEKO simulated monostatic RCS has significantly reduced the detection coverage to be restricted to regions around the transmitter and receiver. This indicates that without using a PBR, the ability to detect a low-RCS target monostatically is severely limited.

### 3. Bistatic RCS with S-Band CMR

With the inclusion of bistatic RCS in the simulation, the detection coverage varies with the change in target aspect with respect to the transmitter and receiver. The effect of the bistatic RCS is most evident with changes made to bistatic angle $\beta$ by changing the course and heading of the target. Many possible combinations of $\beta$ with different bistatic geometry of Tx-Tgt-Rx exist. The most representative are those with the target's general direction headed towards the receiver and the other with the target's broadside directed towards the receiver on a crossing course. The former presents one of the smallest bistatic RCS returns, while the latter presents a larger bistatic RCS return. With the ship forward and aft line along the 0° and 180°, it can be seen from Figure 18 that the bistatic returns are mostly small with a narrow peak occurring at the negative of the incidence angle but always higher than the direct monostatic returns.

The RCS data was generated in 1° increments. When used in the PBR simulations, the incidence and observation angles were rounded to the nearest degree in order to obtain the RCS.

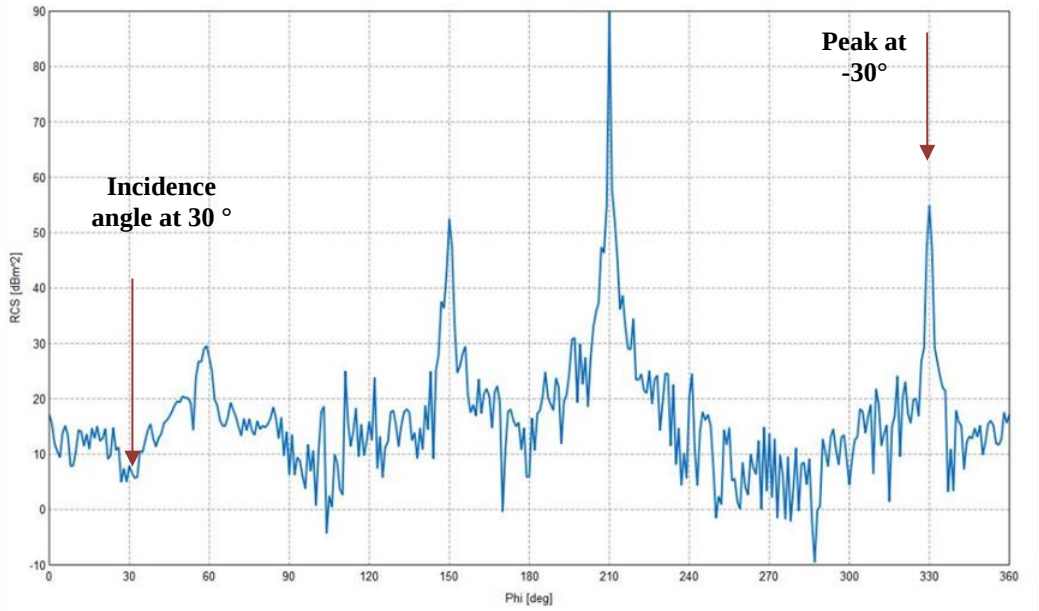


Figure 18. Bistatic RCS of RSN's Formidable-class frigate's model simulated at 3050 MHz using FEKO.

A comparison of Figures 17 and 19 shows clearly the difference in detection coverage when a different aspect of the low-RCS target is presented to the transmitter and receiver. The detection range increases from 3000 m to that of beyond 20,000 m with a change of target aspect. It is, therefore, important to understand a single PBR system is also limited in its ability to ensure consistent detection coverage and low detection gaps. The resultant detection coverage is dependent on the Tx-Tgt-Rx geometry and the aspect of the target.

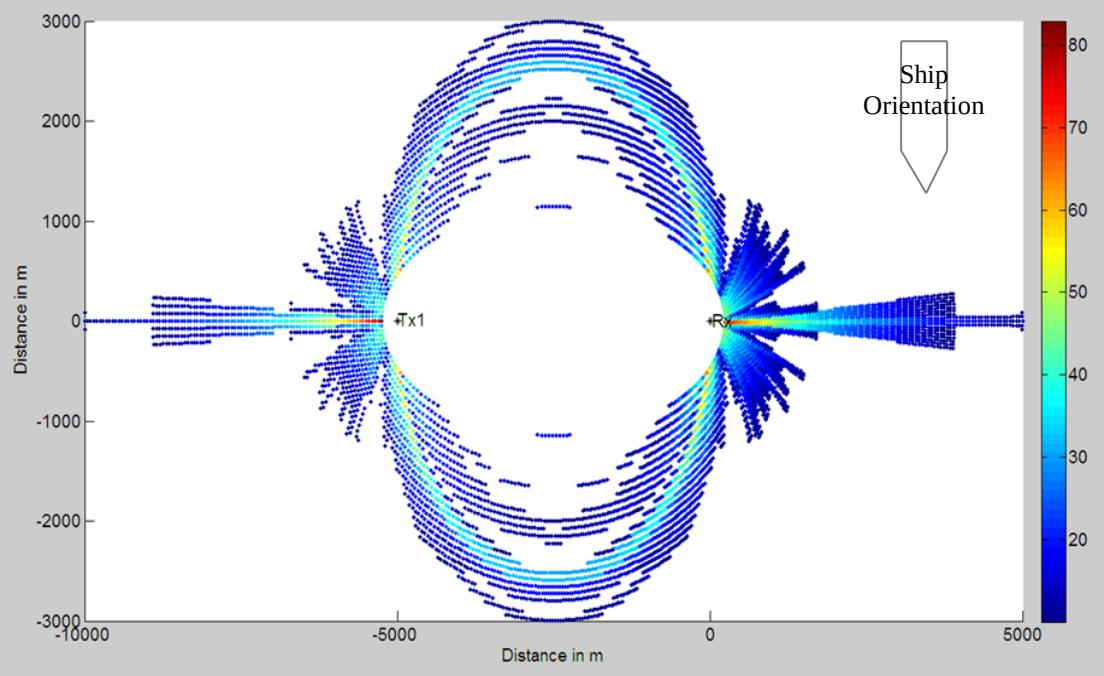


Figure 19. SNR detection plot (dB) using bistatic RCS at S-band having reflections off the forward aspect of the target ship by Tx1 ($-5000,0$).

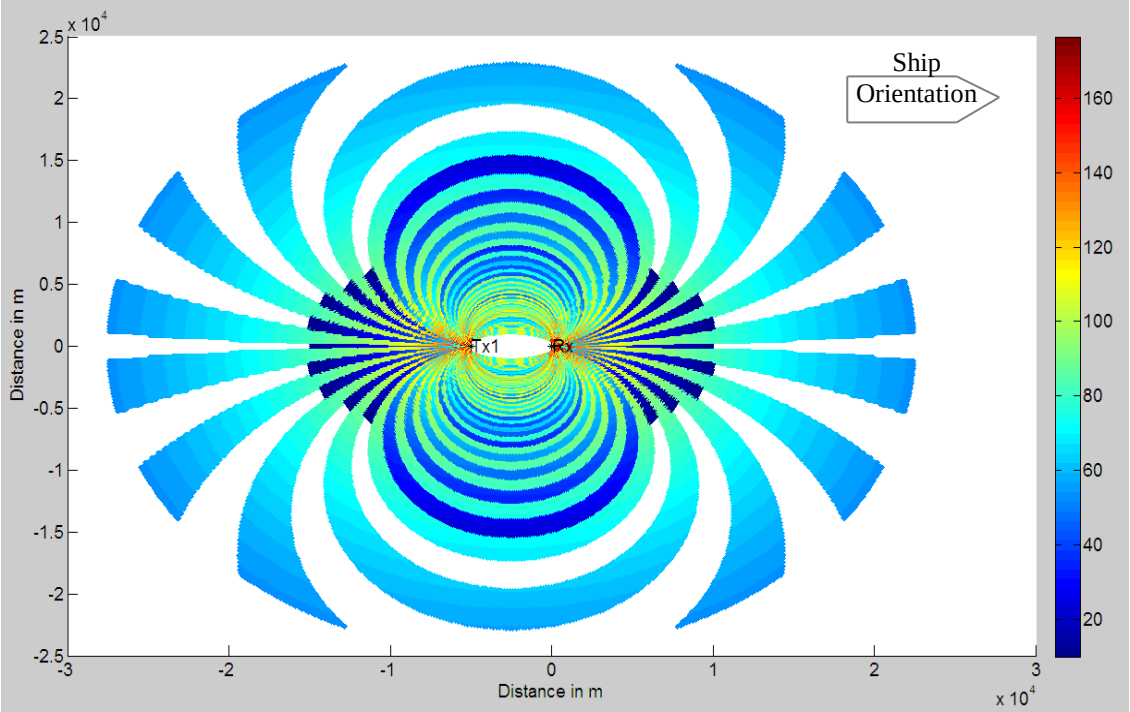


Figure 20. SNR detection plot (dB) using bistatic RCS at S-band having reflections off the broadside of the target ship by Tx1 $(-5000,0)$.

Due to the large comparative difference in the ship's dimensions with respect to the wavelength of the transmission, a higher resolution plot of the target RCS reveals more RCS fluctuations between the current sampling intervals of one degree.

### 4. Bistatic RCS with X-Band CMR

Similar conclusions can be drawn from the detection coverage plot, as shown in Figures 21 and 22, with an X-band CMR. In general, the X-band CMR as an opportunistic transmitter has a smaller detection coverage as compared to the S-band CMR. The detection gaps are also more pronounced. In a real-world scenario, the use of RAM becomes more practicable at small wavelengths. It follows that a low-RCS target is likely to have even lower RCS returns at higher frequencies, reducing the usefulness of X-band CMR as an opportunistic transmitter.

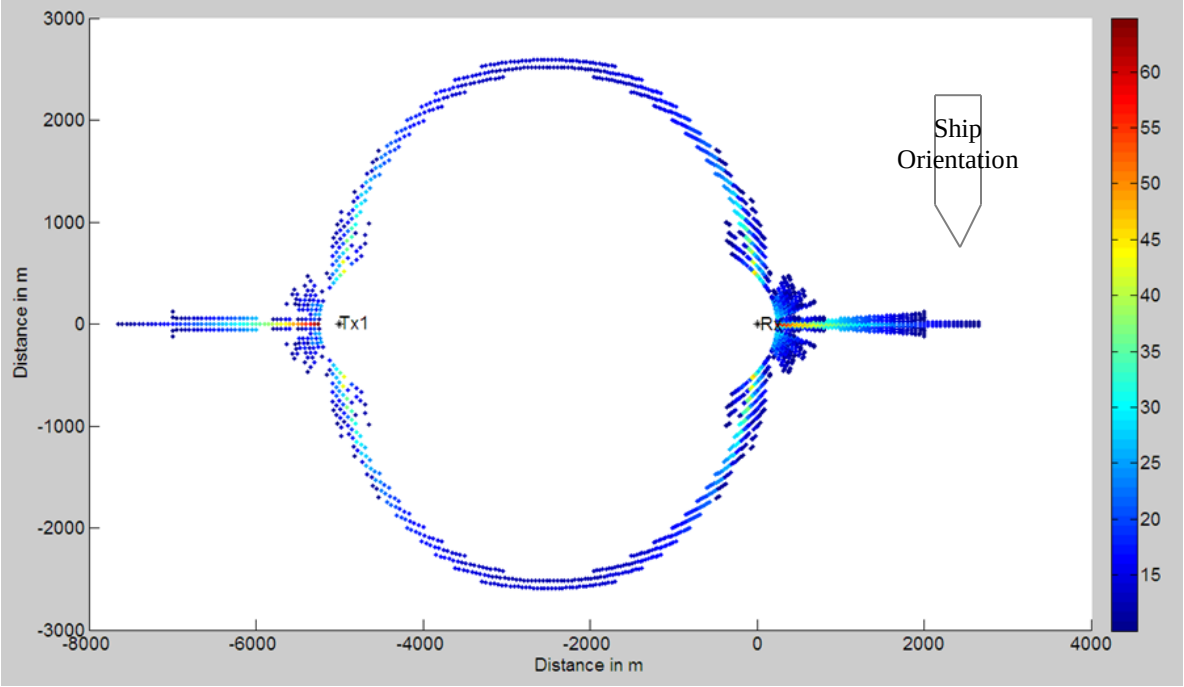


Figure 21. SNR detection plot (dB) using bistatic RCS at X-band having reflections off the forward aspect of the target ship by Tx1 (−5000,0).

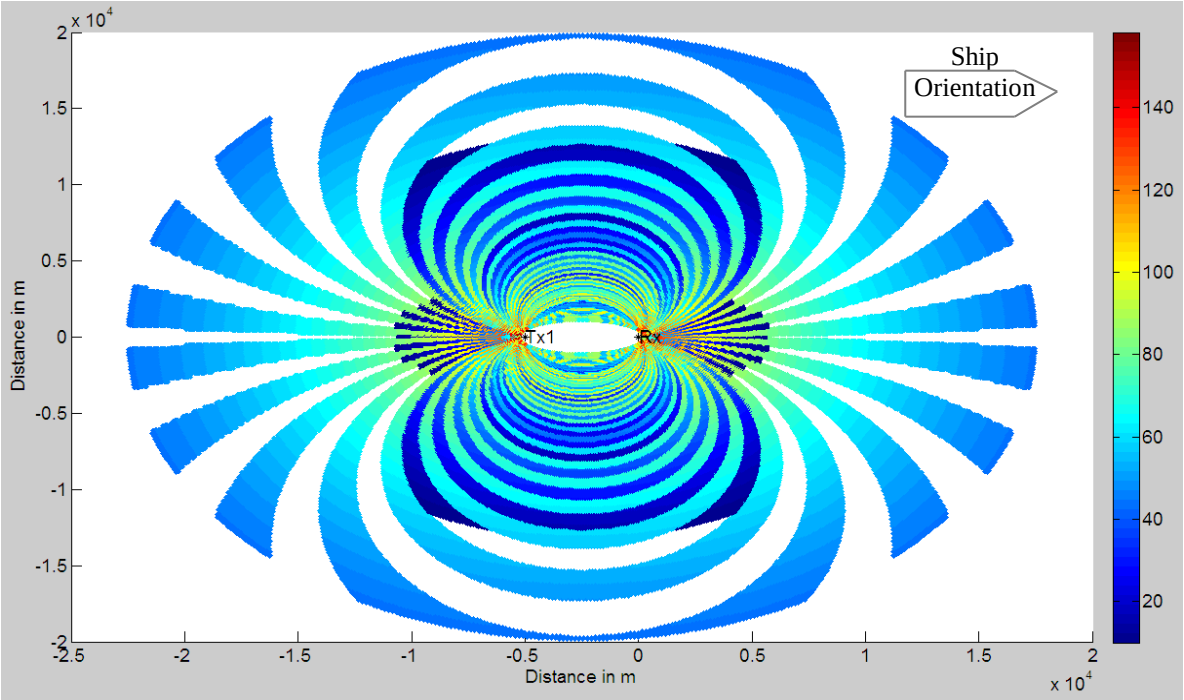


Figure 22. SNR detection plot (dB) using bistatic RCS at X-band having reflections off the broadside of the target ship by Tx1 (−5000,0).

## B. TWO TX-RX PAIR

Equipped with the knowledge of how a single PBR system is limited in its ability to provide consistent detection coverage, it is important to explore passive multistatic radar (PMR) and how a different transmitter constellation affects the detection coverage. The three parameters for transmitter constellation selection are the quantity of transmitters and their position relative to the receiver.

### 1. Bistatic RCS with Two S-Band CMRs

In this two-transmitter PMR system setup, the two transmitters (Tx1 and Tx2) are 90° degrees apart and share the same baseline distance of 5000 m. Although the subsequent detection plots bear semblance to the detection plots of a single Tx (Figure 23), it is important to note that detection gaps have been reduced in all cases (Figure 24), and the two-transmitter PMR system is now more tolerant of target RCS changes due to aspect. From Figures 25 and 26, the detection plots show the detection coverage of the Tx-Tgt-Rx geometry has at least one broadside reflection return from the low-RCS target.

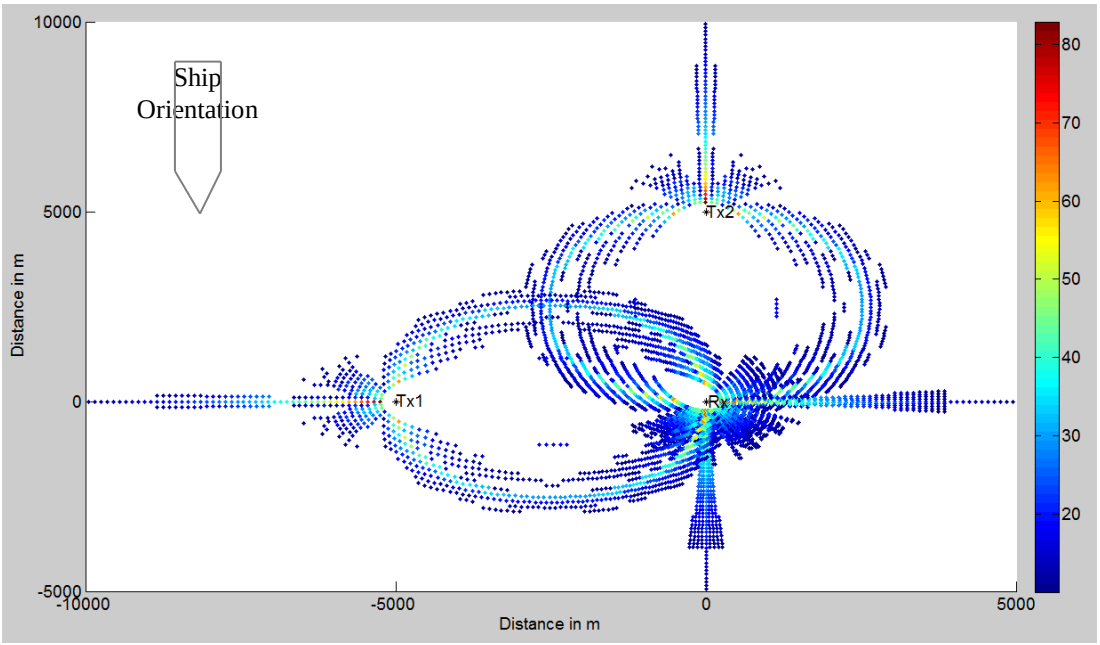


Figure 23. SNR detection plot (dB) with 2Tx at S-band (90° apart) having reflections off the forward aspect of the target ship.

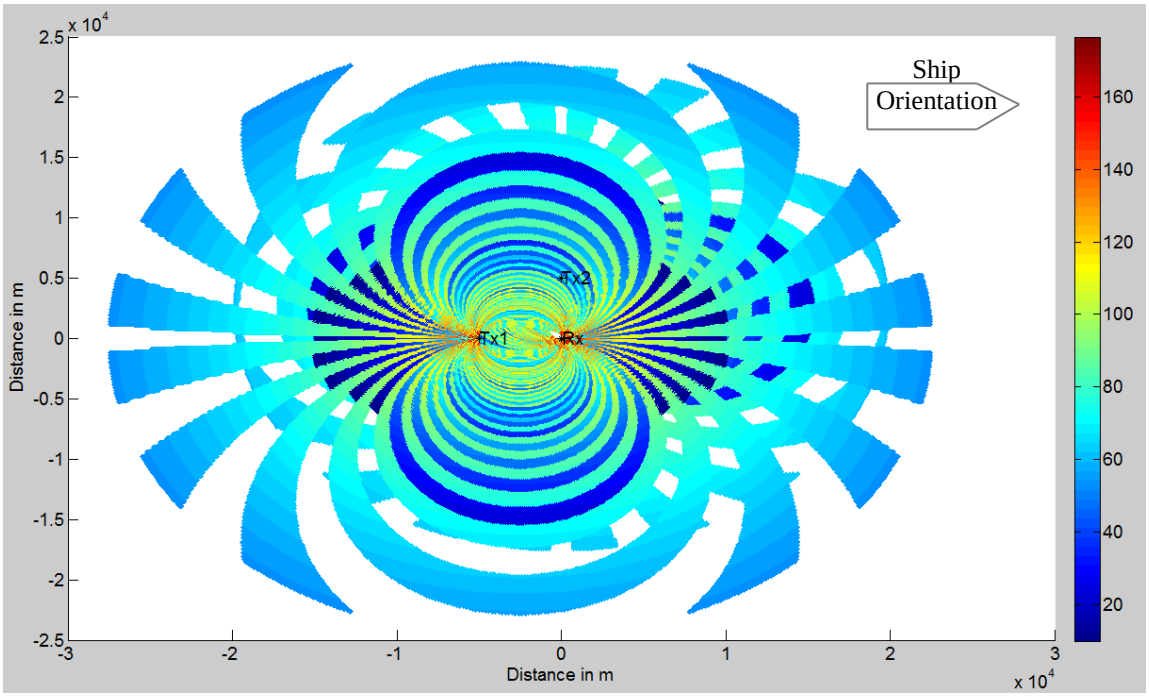


Figure 24. SNR detection plot (dB) with 2Tx at S-band having reflections off the broadside of the target ship.

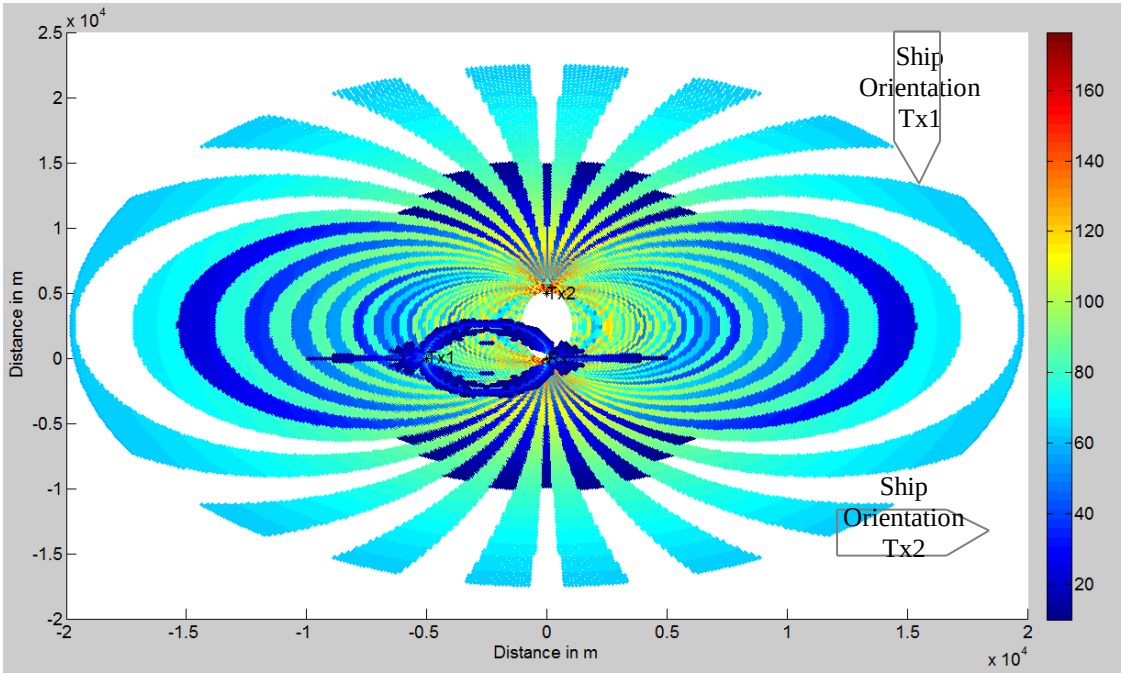


Figure 25. SNR detection plot (dB) at S-band with Tx1 with reflections off the forward aspect of the target ship and Tx2 off the broadside of the target ship.

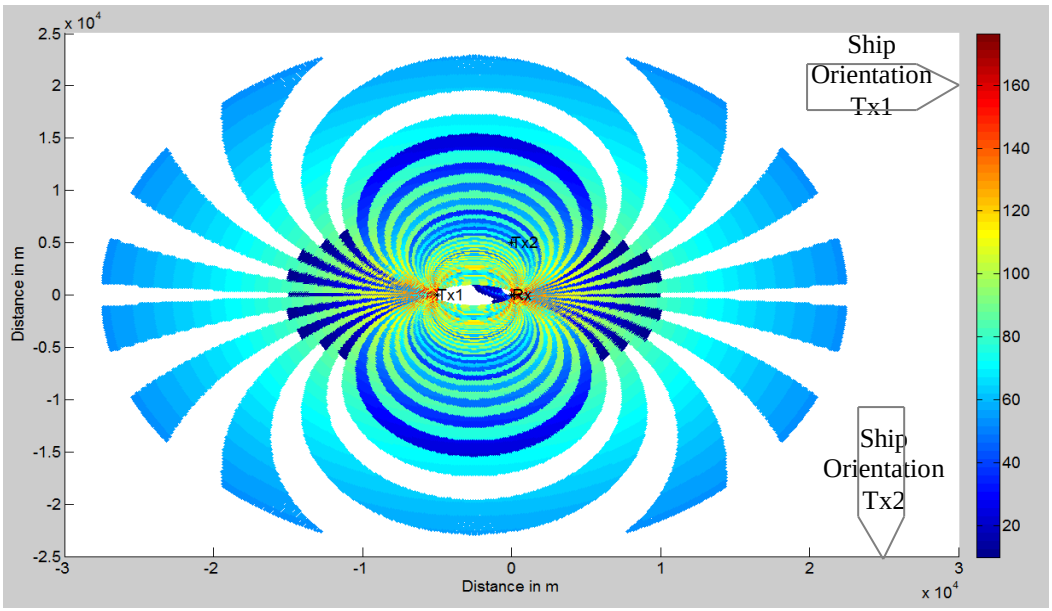


Figure 26. SNR detection plot (dB) at S-band with Tx1 with reflections off the broadside of the target ship and Tx2 off the forward aspect of the target ship.

## 2. Bistatic RCS with X-Band CMR

Extending the simulation using X-band CMR, we show the detection plots in Figures 27 through 30. They are consistent with that using S-band CMR as the opportunistic transmitter.

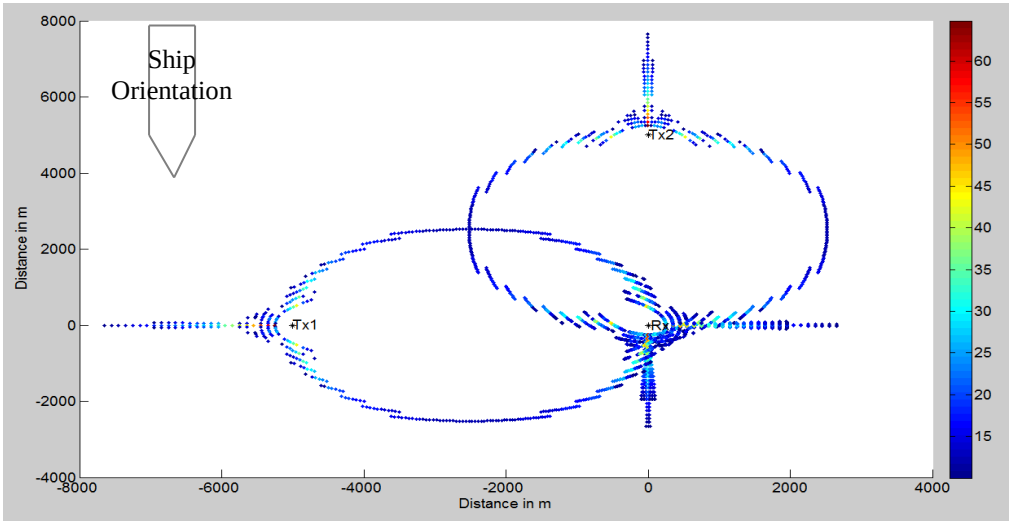


Figure 27. SNR detection plot (dB) with 2Tx at X-band (90° apart) with reflections off the forward aspect of the target ship.

From Figures 29 and 30, it can be observed that there two distinct shades of blue denoting the detection area about 5000 m further away from the receiver. The dark shades denote regions where the SNR is above the detection threshold of 10 dB but less than 40 dB. This dark shade of blue exists only between ranges above 5000 m and 12,000 m, while there are repeated patterns of coverage and non-coverage when the target range increases.

To explain this phenomenon, recall the variables in Eqs. (5) and (6) that affect the SNR. The obvious factor is the combined value of $R_T^2 R_R^2$ that is non-linear in nature acting as the denominator in Eq. (6). With $\beta$ constant, the change in $R_T^2 R_R^2$ affects the SNR. The more asymmetric the $R_T$ and $R_R$ are, the larger the SNR. This explains why the SNR increases at the ends of the constant $\beta$-contours; however, if the bistatic RCS returns corresponding to a $\beta$ are small, there are detection gaps for that value of $\beta$. In summary, there are two variables involved in determining the SNR, namely, the bistatic RCS returns which are sensitive to $\beta$ and $R_T^2 R_R^2$, where the latter loses its dominance as the target moves further away from the receiver.

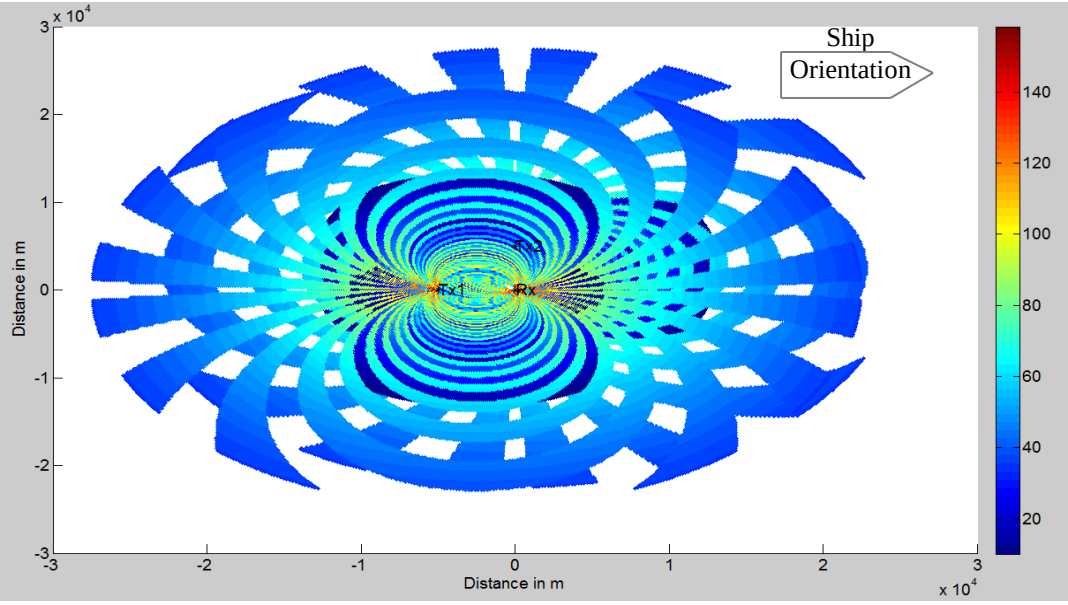


Figure 28. SNR detection plot (dB) with 2Tx at X-band with reflections off the broadside of the target ship.

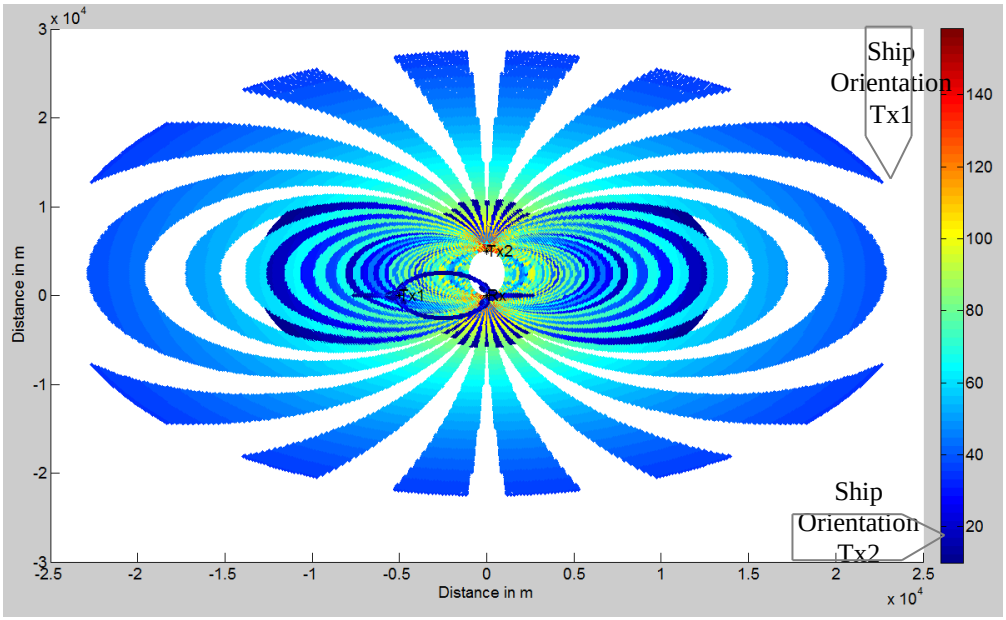


Figure 29. SNR detection plot (dB) at X-band with Tx1 with reflections off the forward aspect of the target ship and Tx2 off the broadside of the target ship.

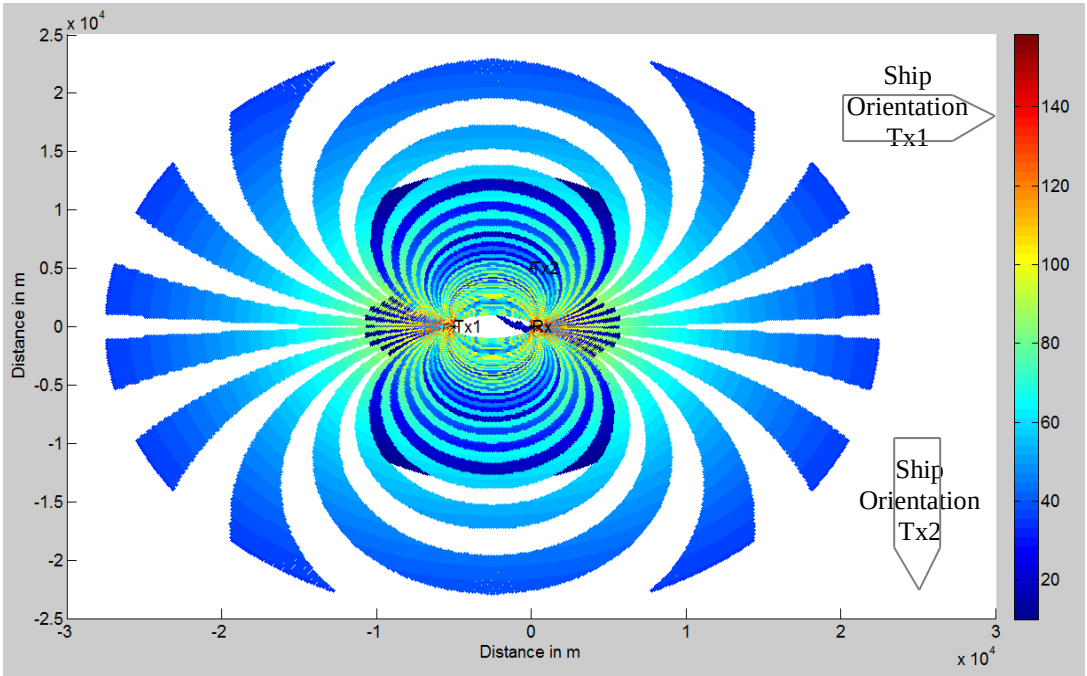


Figure 30. SNR detection plot (dB) at X-band with Tx1 with reflections off the broadside of the target ship and Tx2 off the forward aspect of the target ship.

## 3. Combination and Constellation

The approach taken to evaluate a transmitter constellation is to compare the detection coverage with a monostatic radar. That requirement is to achieve all-round coverage with a minimum number of detection gaps. A series of different constellations are explored to establish a decision matrix to choose the optimal number of opportunistic transmitters to maximize coverage and minimize gaps. To simplify the simulation without sacrificing validity, all subsequent detection plots are shown with strong RCS returns using S-band CMR. This is fair as the low-RCS target presents a different aspect to each transmitter, and at least one of these combinations invokes a strong RCS return back to the receiver.

As shown in Figures 31 through 36, both detection coverage and range can be improved by choosing an opportunistic transmitter that has a larger baseline distance from the receiver. The upper limit of the choice of baseline distance lies in the transmitter's power and the receiver's sensitivity. Complemented by another transmitter 90° or 180° apart, the detection gap is significantly reduced. It is also shown that detection gaps in a particular bearing can be reduced by a transmitter that lies orthogonally to it.

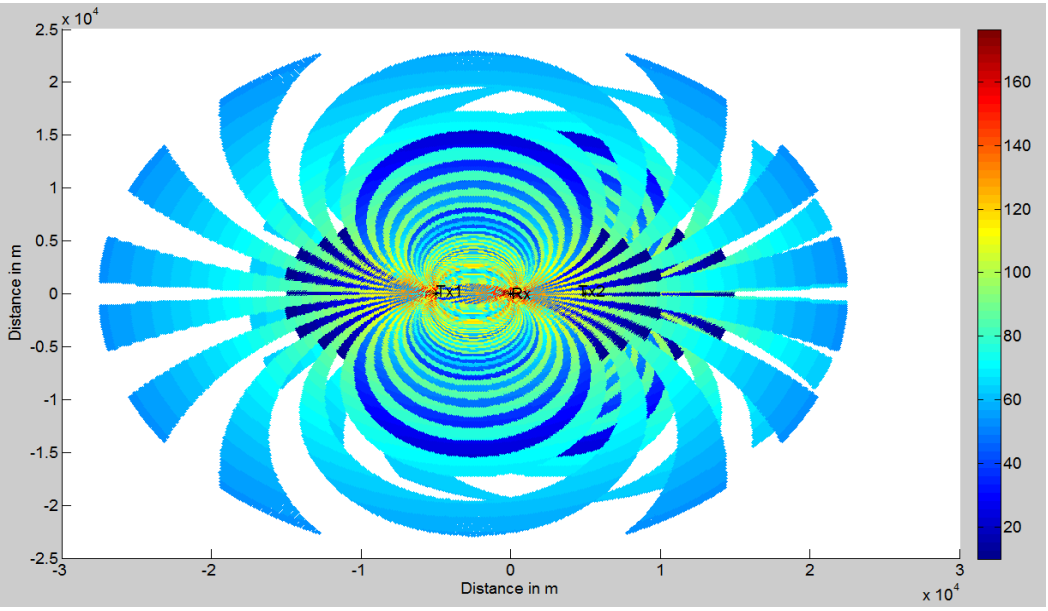


Figure 31. SNR detection plot with Tx1 at (−5000,0) and Tx2 at (5000,0).

Comparing Figures 31 and 32, we see that detection gaps to the right of the receiver are reduced with Tx2 at 90° as compared to 180°. The converse is also true for detection gaps that are reduced forward of the receiver if both Tx1 and Tx2 lie on the same baseline as the receiver.

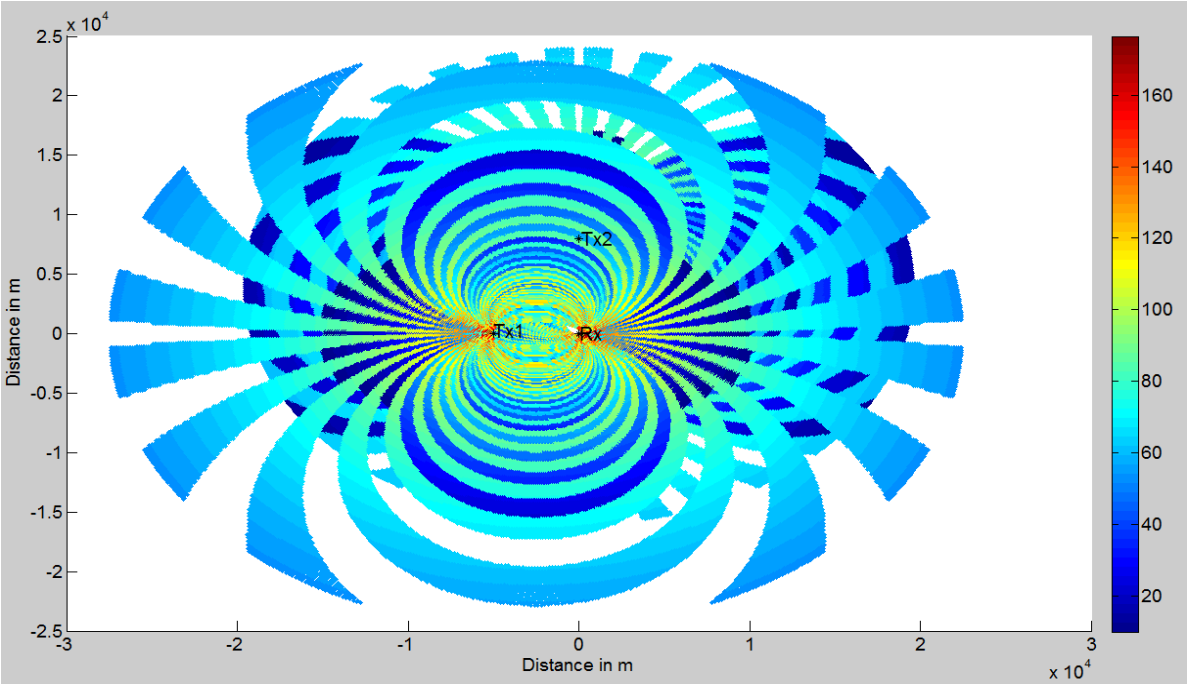


Figure 32. SNR detection plot with Tx1 at $(-5000,0)$ and Tx2 at $(0,8000)$.

It is noteworthy that the detection gaps can be classified into two types, interval gaps and through gaps. The interval gaps represent detection gaps that appear in a lateral manner and create loss in tracking as the target moves towards or away from the receiver. The through gaps are detection gaps that allow the target to evade detection and reach the receiver. Refer to Figure 32 for a depiction of how the interval gaps are detection gaps that form concentric ovals connecting the transmitter and receiver. The through gaps are detection gaps connecting with the transmitter (Tx1) on the left or the receiver on the right.

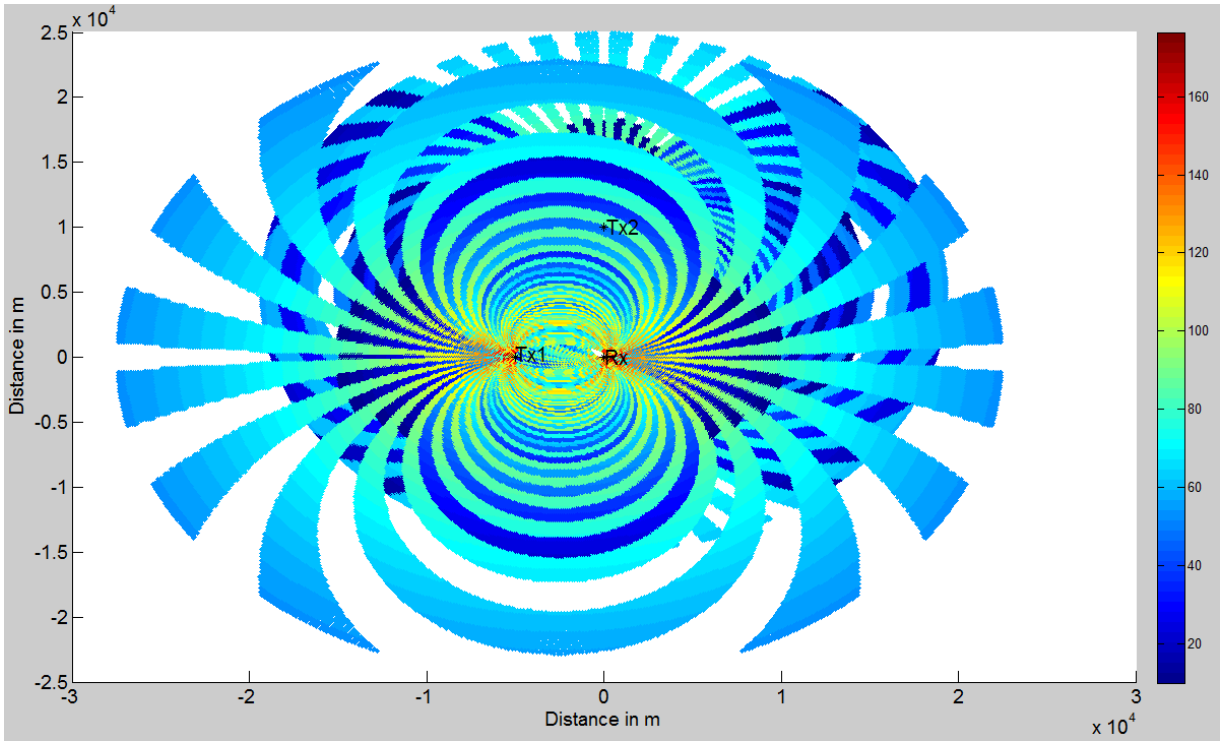


Figure 33. SNR detection plot with Tx1 at (−5000,0) and Tx2 at (0,10000).

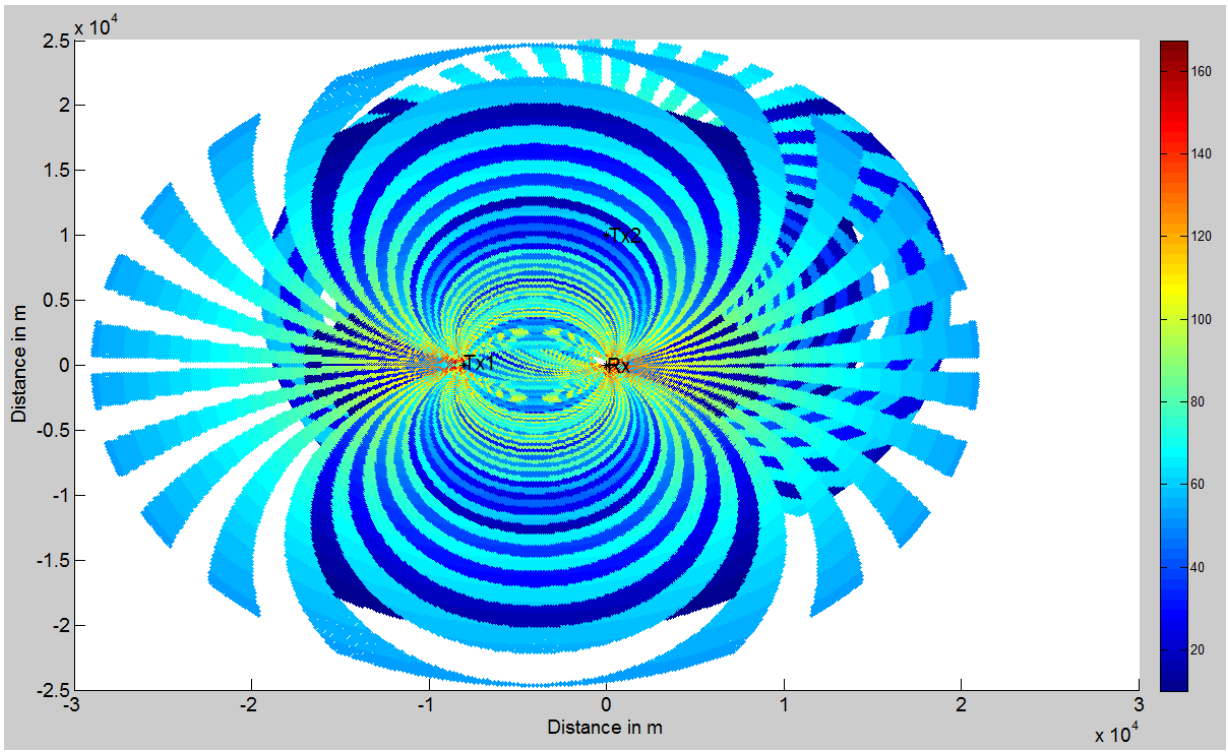


Figure 34. SNR detection plot with Tx1 at (−8000,0) and Tx2 at (0,10000).

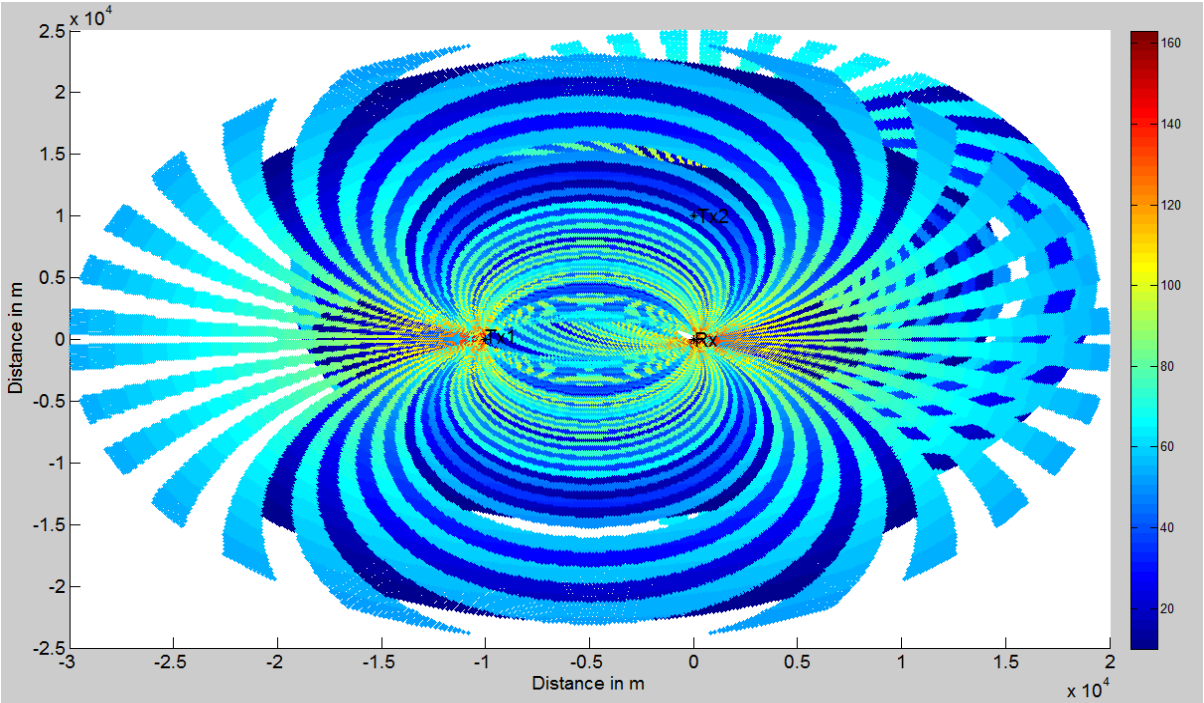


Figure 35. SNR detection plot with Tx1 at (−10000,0) and Tx2 at (0,10000).

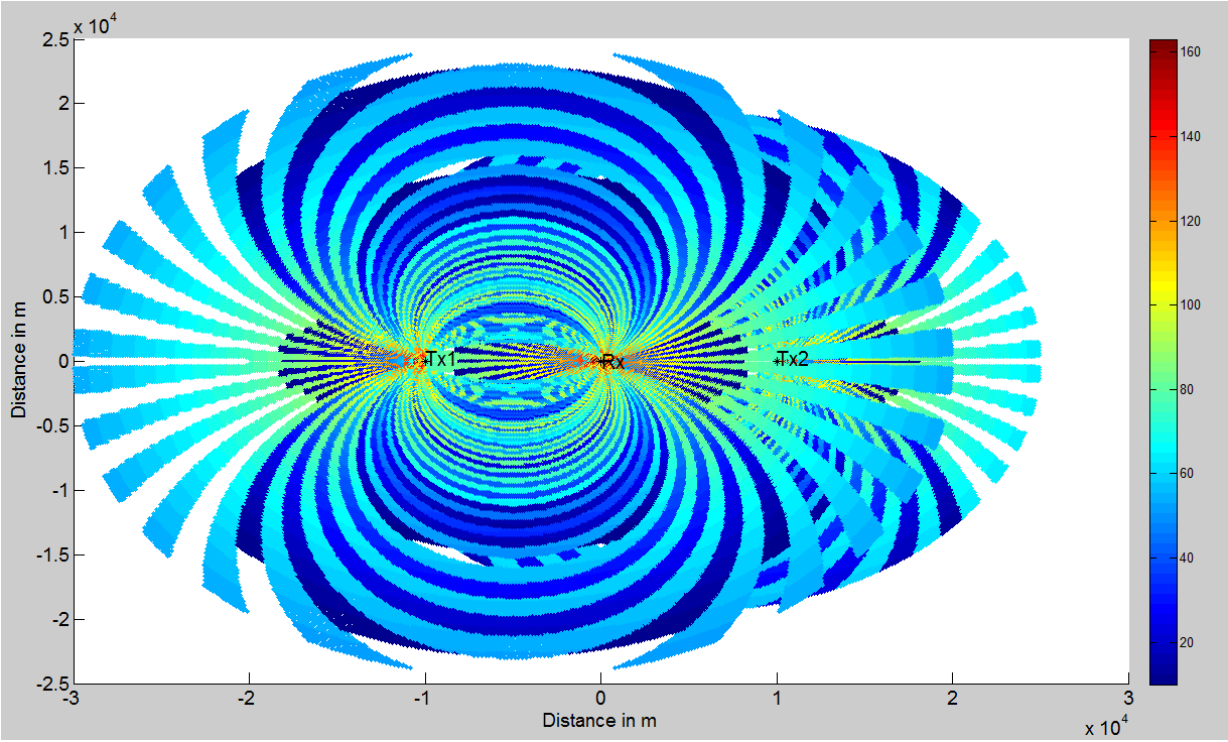


Figure 36. SNR detection plot with Tx1 at (−10000,0) and Tx2 at (10000,0).

To minimize detection gaps as a result of the bistatic angle formed between the Tx-Tgt-Rx, the optimal transmitter constellation should have transmitters at every quadrant and of varying baseline distance. This is consistent with the findings by [10].

## C. TRANSMITTER CONSTELLATIONS

How different constellations formed using 4Tx-Rx and 8Tx-Rx affects detection coverage is explored in this section.

### 1. Four Tx-Rx Pair

In this simulation, four transmitters are placed 10000 m away from the receiver, each occupying a quadrant at 90º apart (Figure 37). It is worth noting that 100% detection coverage is achieved within a 20 km radius of the receiver. The second detection tier between 20 km to 28 km has about 60% detection coverage. An increase in the baseline distance from 10 km to 15 km (Figure 38) also saw an improvement in detection range in the second detection tier with the reduction of through gaps. The improvement in detection coverage in the second tier increased from 60% to approximately 80%.

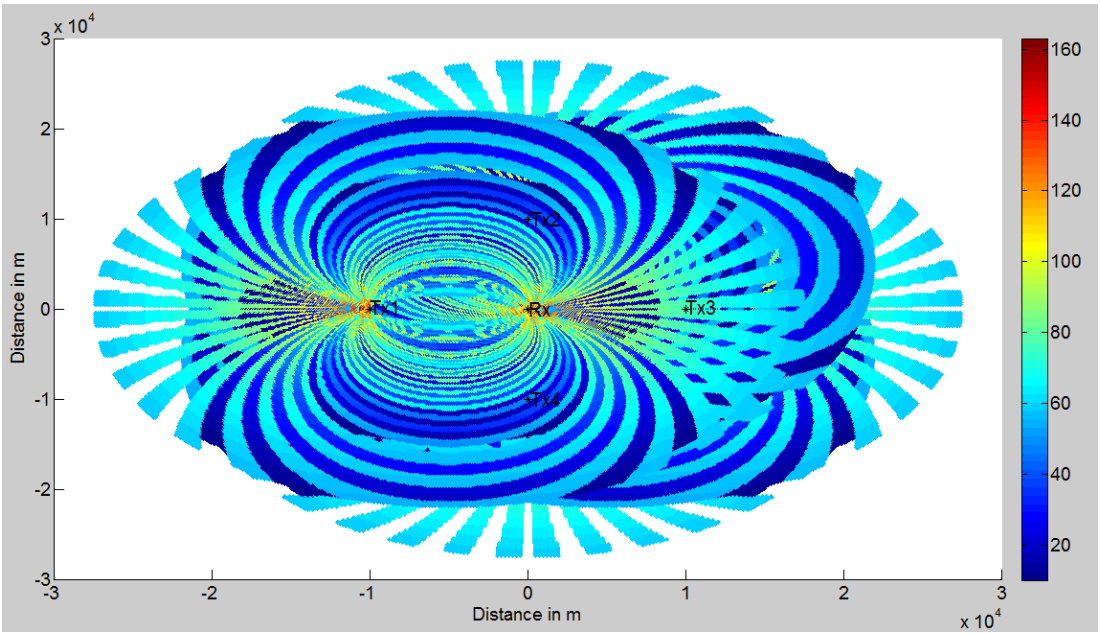


Figure 37. SNR detection coverage plot with 4Tx (0º, 90º, 180º and 270º) at 10000 m from the receiver.

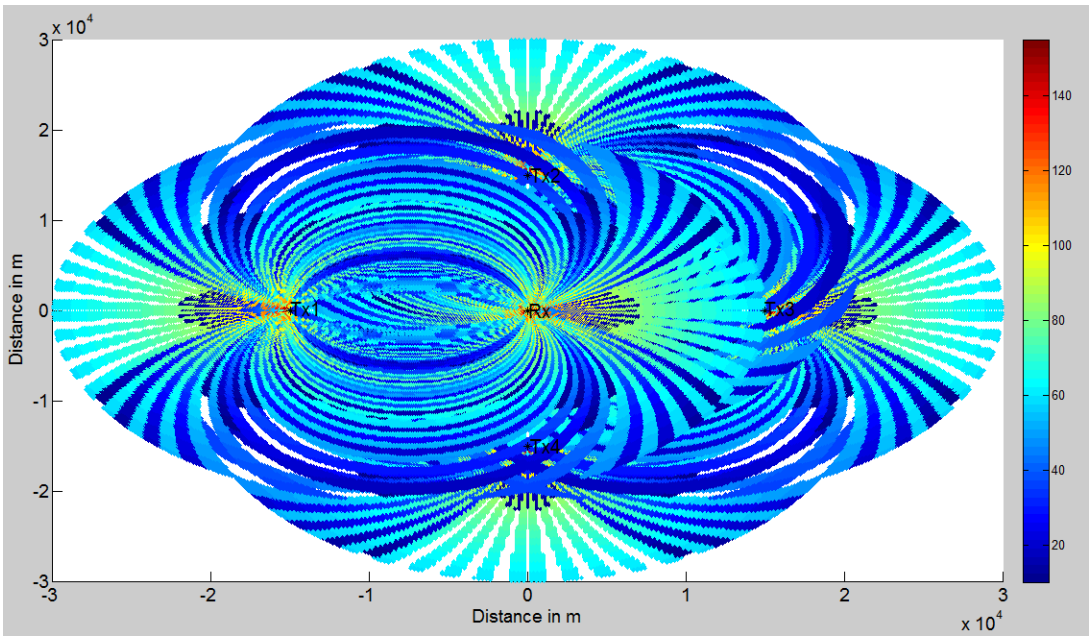


Figure 38. SNR detection coverage plot with 4Tx (0º, 90º, 180º and 270º) at 15000 m from the receiver.

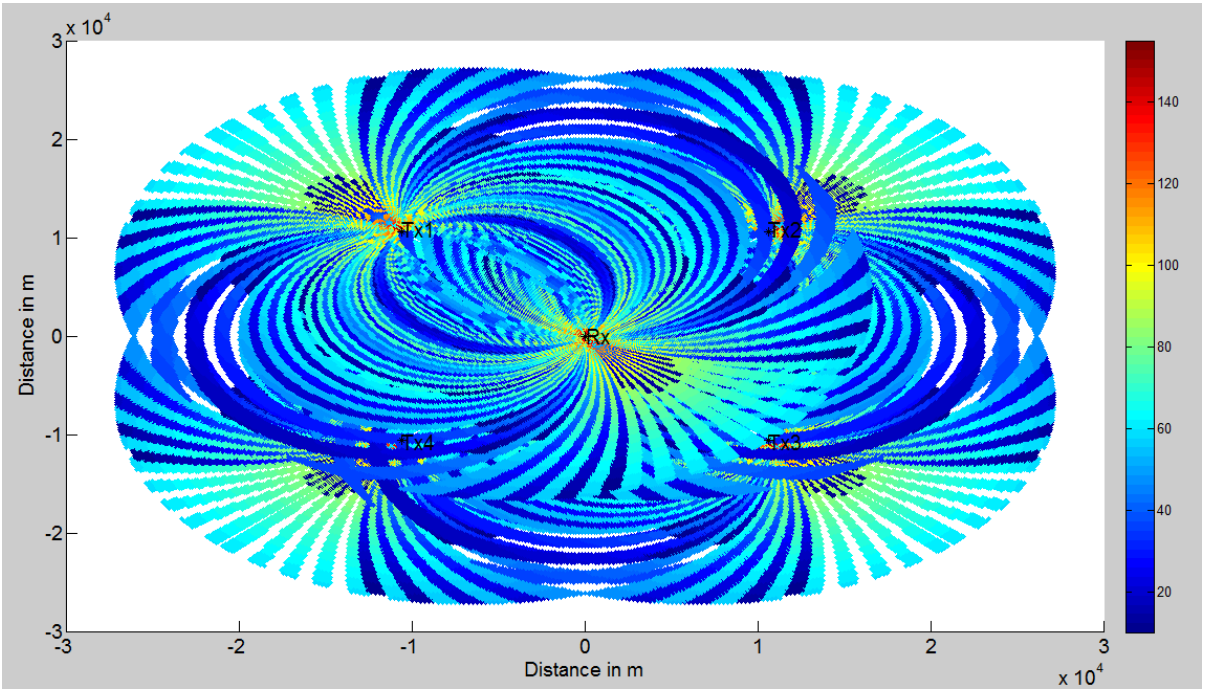


Figure 39. SNR detection coverage plot with 4Tx (45º, 135º, 225º and 315º) at 15000 m from the receiver.

As shown in Figure 39, the 4Tx constellation placement with transmitters at 45º, 135º, 225º and 315º, respectively, has modified the second tier detection coverage between 20 km and 28 km. By rotating the transmitter constellation by 45º, the location of through detection gaps in the second tier has also rotated. Essentially, the use of a different constellation of the four transmitters allows the receiver to direct optimal detection coverage in its quadrant of choice.

### 2. Eight Tx-Rx Pair

The use of eight transmitters offers the best all-round detection coverage with near 95% coverage up to a range of 30 km. From Figures 40 and 41, one can see the detection coverage by eight transmitters placed at 15000 m and 18000 m away from the receiver, respectively.

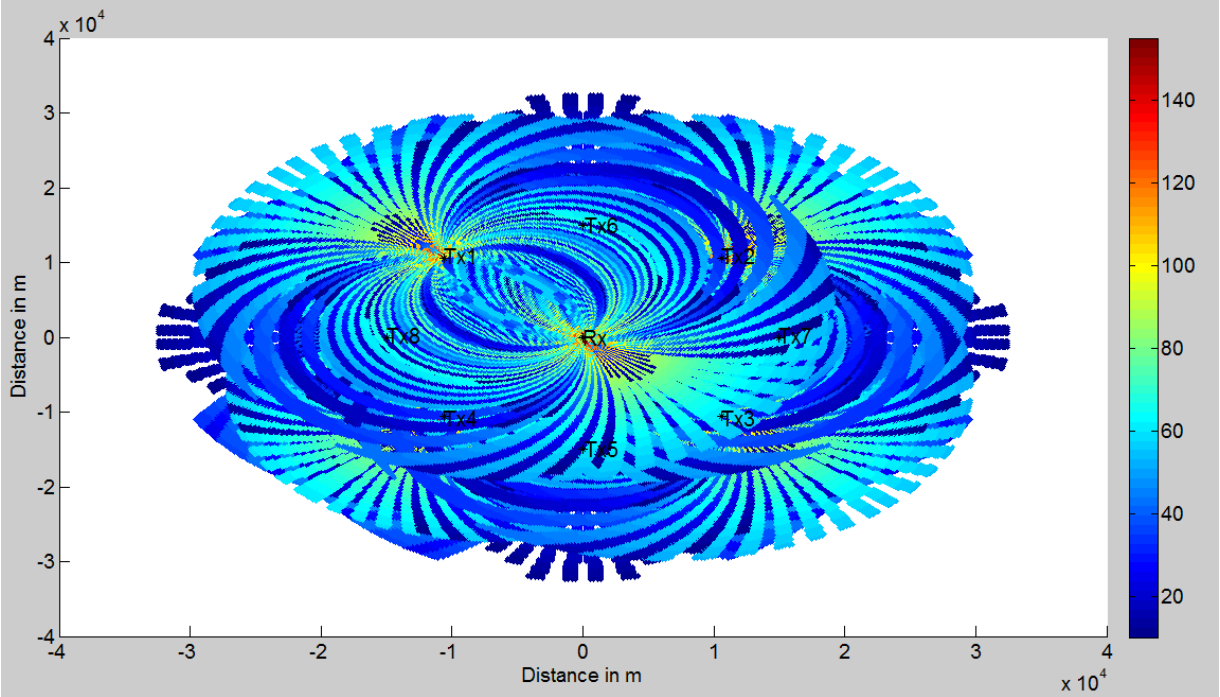


Figure 40. SNR detection coverage plot with 8Tx (0º, 45º, 90º, 135º, 180º, 225º, 270º and 315º) at 15000 m from the receiver.

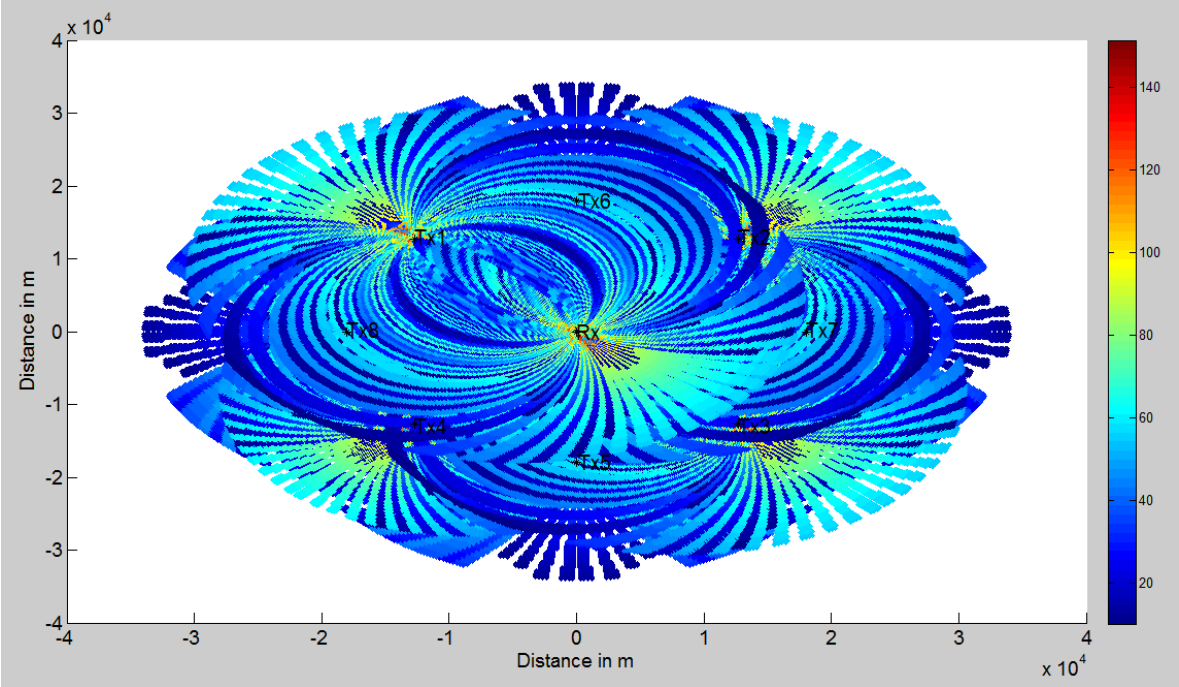


Figure 41. SNR detection coverage plot with 8Tx (0º, 45º, 90º, 135º, 180º, 225º, 270º and 315º) at 18000 m from the receiver.

In this chapter it was shown how the placement of the opportunistic transmitters affects detection range and detection coverage. In the next chapter the behavior of the measurement errors and how to minimize errors through the use of opportunistic transmitter placement is investigated.

# IV. SIMULATION RESULTS FOR MEASUREMENT ERRORS

Although an eight-transmitter constellation offers detection coverage nearly identical to that of a monostatic radar, there are measurement errors that have to factor into consideration. A target detection with an unacceptably large error is not useful. Depending on the geometry of the PBR, we found that the worst-case measurement error varies across range and bistatic angle. As shown in Eqs. (11) through (13), the RCS of the target does not have a role to play in measurement error; measurement error calculations come after target detection with a SNR of more than 10 dB. Despite the varying nature of the measurement errors, it is possible to use a careful choice of transmitter constellation to minimize the errors.

## A. UNCERTAINTY ELLIPSE

As explained earlier with the aid of Figure 9, every target position with a Tx-Rx geometry pair has its own measurement error. The measurement errors typically span three different axes and form an uncertainty ellipse around the target position. It should be interpreted as the target's actual location is anywhere within the ellipse. If the target is also tracked by another Tx-Rx pair, the resultant uncertainty ellipse is likely to have the dominant measurement error on a different axis. In such cases, the uncertainty of the target's position is further reduced to the overlapped area. This improvement extends to multiple pairs of Tx-Rx on the same target.

To be commensurate with the detection plots shown in Chapter III, the uncertainty ellipse of a different target location is plotted using the same transmitter constellations. The MATLAB source code for the following plots is included as Appendix G.

### 1. Two Tx-Rx Pairs

In this case, the target is 20.6 km away from the receiver with two transmitters 90$^{o}$ apart, as shown in Figure 42. The inputs to this simulation plot assume transmitter positioning update by the MAIS at 5 s and a net displacement of the target at 10 knots.

The uncertainty ellipse around the target ($-5000$, 20000) is the overlap area between the two uncertainty ellipses formed. At this extended distance, the target's measurement error area is approximately 120 m all round. Comparing with the target length of 114 m, we assess the error as reasonable.

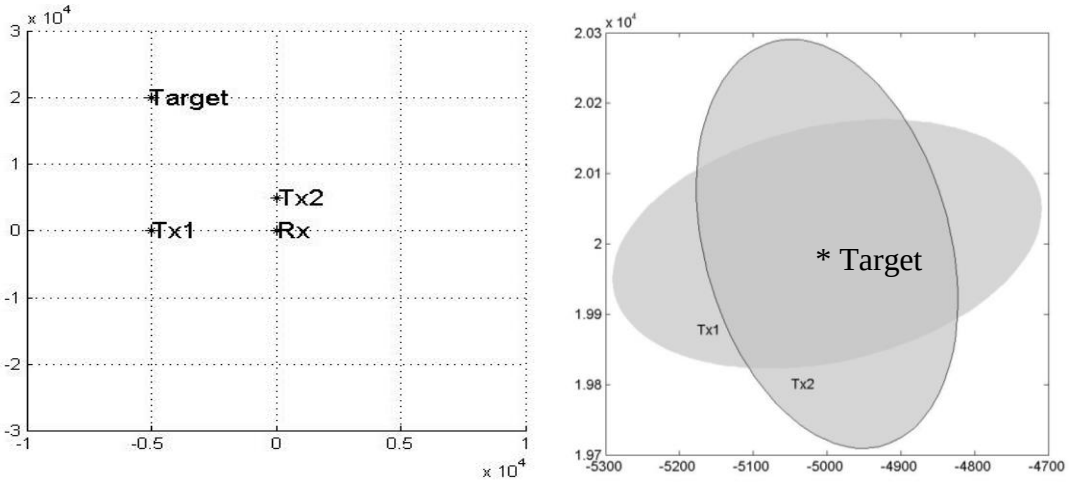


Figure 42. Uncertainty ellipse of Target ($-5000$,20000) with 2Tx at 90º apart.

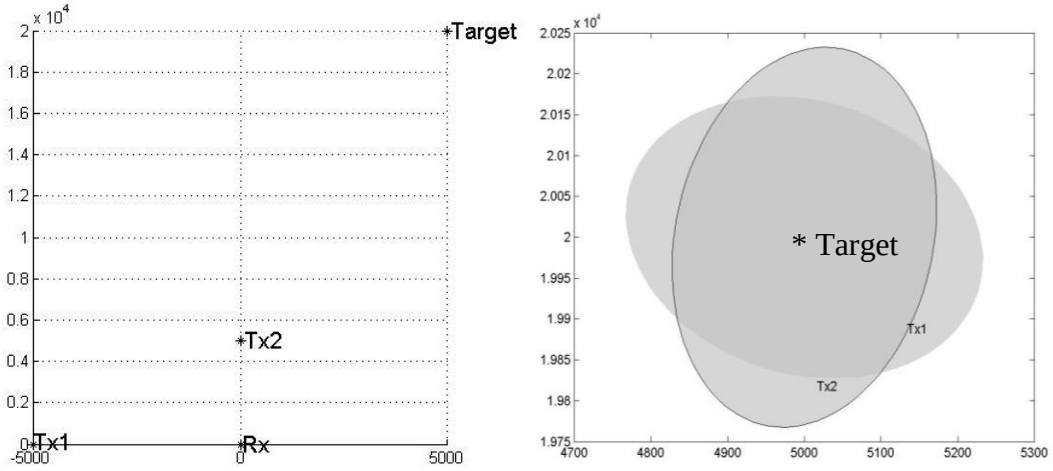


Figure 43. Uncertainty ellipse of Target (5000,20000) with 2Tx at 90º apart.

A change of target position to the right of the Tx-Tx constellation shows a slightly larger uncertainty ellipse due to geometry (Figure 43). As the target approaches the Tx-Rx geometry, one can see the uncertainty ellipse reduces with an all-round error of 40 m

as shown in Figure 42. In certain geometries (Figure 45), the uncertainty ellipse is the same from two different transmitter locations.

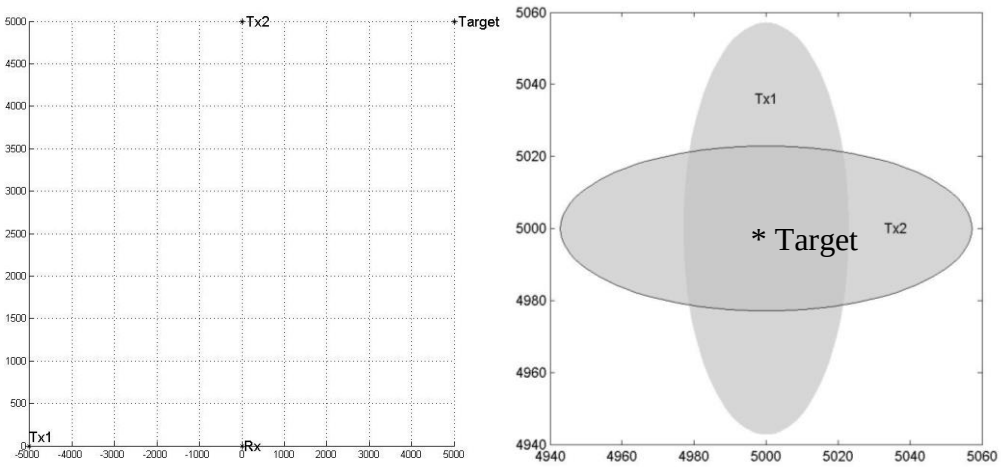


Figure 44. Uncertainty ellipse of Target (5000,5000) with 2Tx at 90º apart.

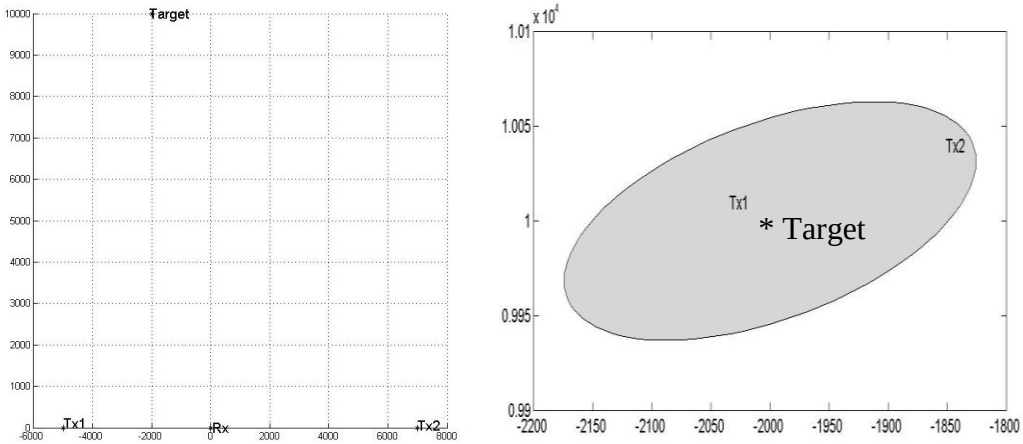


Figure 45. Uncertainty ellipse of Target ( – 2000,10000) with 2Tx at 180º apart.

### 2. Four Tx-Rx Pairs

In a four-transmitter constellation, the effect on the uncertainty ellipse is similar (Figure 46). The major factors affecting the size of the uncertainty ellipse are the beamwidth of the transmitter and DF accuracy of the receiver. As the target approaches the transmitter or the receiver, the dominant factor changes. The important observation here is that the movement of the transmitter, receiver and target has very little influence

in determining the uncertainty ellipse. With the target at (4500,4500) and using the S-band CMR with a beamwidth of 1.8°, one can see from Figure 47 that the shape of the uncertainty ellipse has changed. Extending this further, we see the uncertainty ellipse of the same constellation with the transmitter changed to X-band CMR with a beamwidth of 0.95° as illustrated in Figure 48. For Figure 49, the transmitter, receiver and target speeds have been reduced to zero from 10 knots. It can be seen that the data age and target speed have negligible effects on the measurement error in this setup.

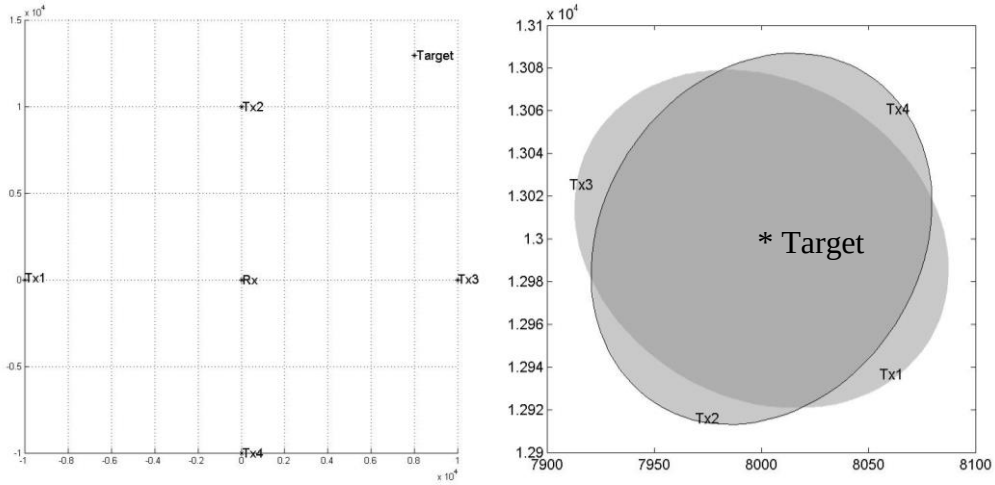


Figure 46. Uncertainty ellipse of Target (8000,13000) with 4Tx at 90º apart from each other.

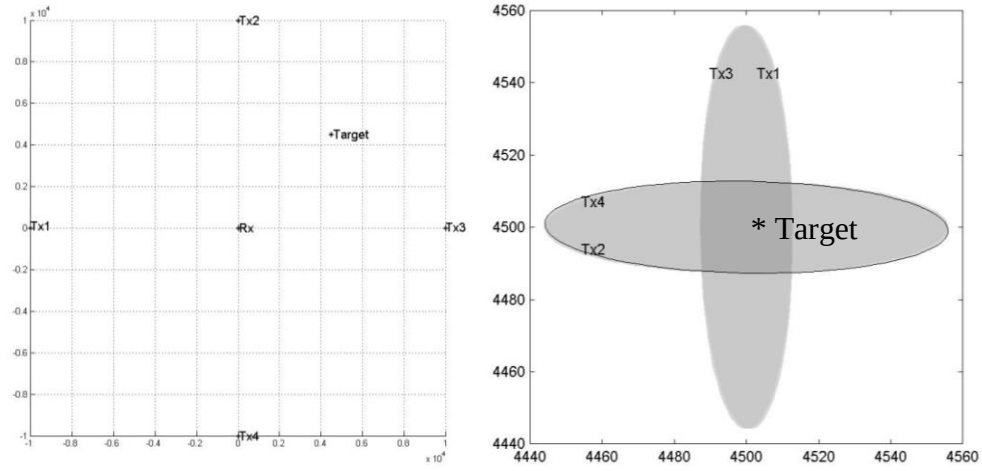


Figure 47. Uncertainty ellipse of Target (4500,4500) with 4Tx at 90º apart from each other using S-band CMR.

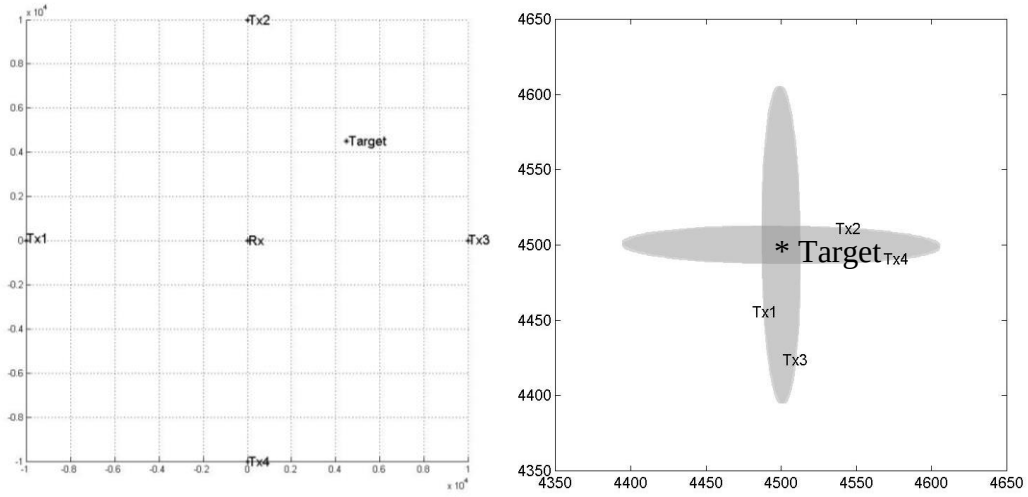


Figure 48. Uncertainty ellipse of Target (4500,4500) with 4Tx at 90º apart from each other using X-band CMR.

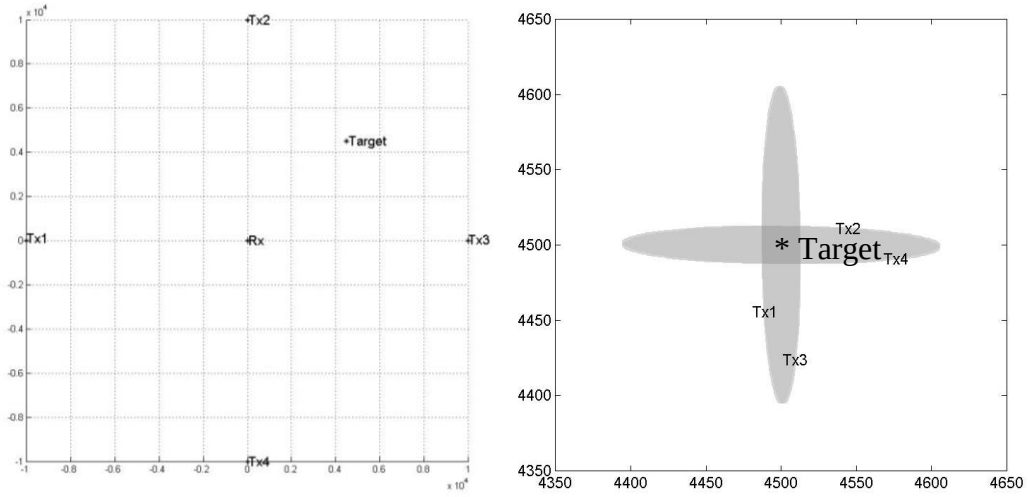


Figure 49. Uncertainty ellipse of Target (4500,4500) with 4Tx at 90º apart from each other using X-band CMR and zero net speed for transmitter, receiver and target.

### 3. Eight Tx-Rx Pairs

One can expect similar results from an eight-transmitter constellation when compared to the four-transmitter constellation; however, it is worthwhile to note that the higher the number of transmitters and the more they are spatially diversified, the higher the number of target positions that the PMR can achieve and the smaller the uncertainty ellipse that results. Therefore, a higher accuracy of detection can be obtained. In Figure

50, an eight-transmitter constellation is set up similar to that shown in Chapter III. Letting the target position be (4500,4500), it can be seen that a very small measurement error of approximately 20 m is achievable with only four transmitters out of the eight transmitters used. This should be interpreted as the PMR system now has eight data sets to compare and choose from, so the best sets can be used to represent the uncertainty ellipse. To achieve the same low measurement error, one needs to actively seek transmitter spatial diversity if one wishes to focus on obtaining high accuracy on one target.

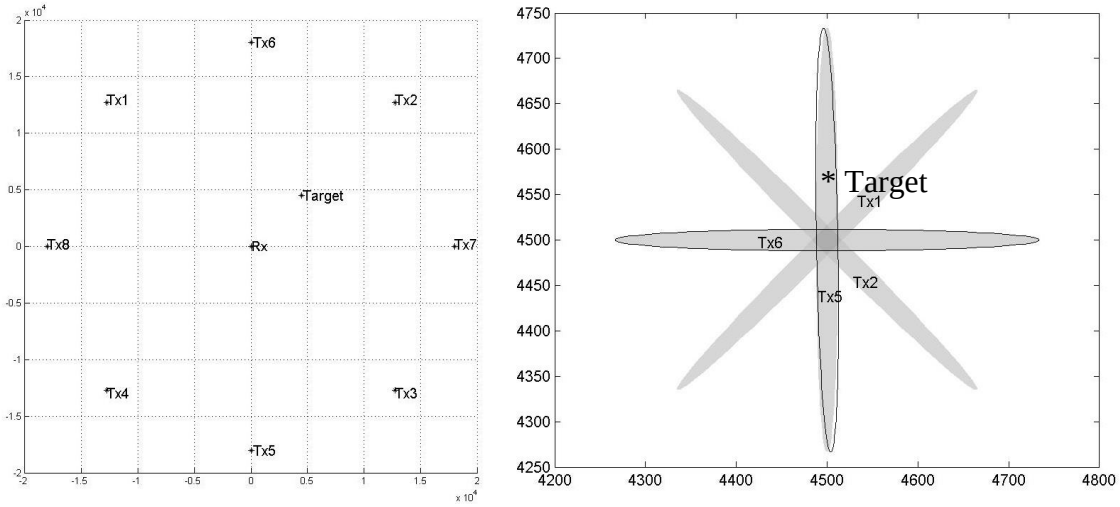


Figure 50. Uncertainty ellipse of Target (4500,4500) with 8Tx at 45º apart from each other using S-band CMR while the target is moving at the speed of 10 knots.

# V. CONCLUSION

## A. SUMMARY OF THESIS FINDINGS

Using opportunistic transmitters in the form of civil marine radar (S-band and X-band) to detect maritime targets passively is both viable and has comparable performance to monostatic radars. However, in the case of detecting low-RCS targets, the PMR outperforms the former. The highly regulated requirements instilled by the IMO have ensured that most of maritime vessels out-at-sea have the necessary information to support a PBR and PMR. With the world's trade routed via the sea, there is no shortage of suitable vessels possessing at least one CMR and one MAIS on the main shipping routes. Among all the suitable vessels, larger ships like oil tankers, container ships, etc., have their CMR installed at the highest point, which extends the radar horizon and detection range. The narrow beamwidth and high transmit power of the CMR conveniently lend themselves to exploitation by a PBR system in terms of both detection accuracy and detection range.

The unique geometry formed among the opportunistic transmitter, passive receiver and unsuspecting target provides exceptional military applications not achieved by current military technologies. It offers true passive detection (with zero transmission from the receiving warship) while at the same time supports detection coverage comparable to a monostatic radar. Passive detection means there is no minimum range detection that is unavoidable in a monostatic radar. In the same vein, there is no need for 'blanking' of the ESM receiver every time the onboard radar transmits. It allows for continuous monitoring of the EW spectrum for intelligence and threat. On the vulnerability front, this has removed the risk posed by ARM and, at the same time, has enhanced mission survivability, allowing the warship to continue with tracking information without a working radar or with a damaged radar.

This same unique geometry also improves the warship's probability of detecting a low-RCS ship treated both in shaping and RAM as compared to a monostatic radar. The use of low frequency S-band CMR poses serious limitations to the use of RAM treatment

on a low-RCS ship. It, therefore, restricts the effectiveness of low-RCS ships in the use of shaping. It was shown in the bistatic RCS measurement of the model based on the RSN Formidable-class stealthy frigate that shaping alone is capable of reducing the median RCS to values not higher than 200 $m^2$. With all else being equal with the effect of RCS on detection, the PBR system has an added advantage. The bistatic RCS simulation using FEKO shows that more incidence angles exist that demonstrate a spike in RCS returns. Simply put, there are more degrees-of-freedom created by the transmitter-target-receiver geometry that has a higher probability of directing spikes in the RCS returns toward the receiver. In the case of a monostatic radar, there are limited ways to maximize RCS returns because the shaping of a low-RCS is designed to reduce returns in the direction of the incidence angle.

The simplicity of PMR also lies in the fact that there are no expensive systems to build. Instead, all the information that the PMR system needs is already available on most warships. This information can be extracted and then used to carry out tracking.

### 1. Conclusion for Passive Detection Coverage

The passive detection range and coverage are related to many parameters on the transmitter, target and receiver. On the opportunistic transmitter end, the transmit power and antenna gain are the two parameters that determine the maximum detection range. However, it is the relative position of the transmitter in the PBR geometry that determines the detection coverage or detection gaps. On the receiver end, the deciding parameters are the sensitivity and bandwidth of the ESM receiver. These two parameters affect the SNR and, thereby, change maximum detection range. Similar to the opportunistic transmitter, it is the geometry of the PBR that affects the detection gaps. Collectively, the factor that is used here to quantify the geometry is the bistatic angle $\beta$, defined earlier in this thesis. Incidentally, the bistatic angle determines the bistatic RCS of what is presented to the receiver depending on the incidence angle of the transmitter's radar emission.

From the simulation plots presented in Chapter III, it was shown that when more transmitters are spaced further apart, they provide better overall coverage with small

detection gaps. The minimum number of transmitters is four, placed 90 degrees apart, with one in each quadrant. To achieve maximum coverage with this particular combination of system parameters and transmitter constellation, a baseline distance of 18000 m is recommended. By rotating the quadrant placement of transmitters, one can direct the detection gaps away from a specific bearing of choice to improve detection.

Using more than four transmitters in the suggested constellation does not significantly extend the detection range. As shown in the eight-transmitter simulation, it does improve detection coverage from approximately 80% to 95% through the reduction of detection gaps. This translates to the ability of the PMR to track a target continuously provided the target offers a strong bistatic return to all eight transmitters. In all likelihood, a low-RCS target would have presented at least two to four strong RCS returns to either the quadrant-based constellation using four transmitters or the two-layered quadrant-based constellation using eight transmitters. If the availability of such a constellation is not possible out at sea, one should position oneself to create such a constellation without jeopardizing a passive posture.

### 2. Conclusion for Detection Accuracy

There are two dominant factors that affect detection accuracy, namely the beamwidth of the transmitter and the DF accuracy of the receiver. It was shown in multiple figures that the worst-case measurement error comes up to approximately $\pm 120$ m for a low-RCS 114 m frigate at a range of 20 km. In most cases, a lower measurement can be achieved using multiple transmitters by overlapping their individual uncertainty ellipses. It was found that the four-transmitter and eight-transmitter constellations recommended for maximum detection coverage are also optimized to reduce the target's uncertainty ellipse. It was shown that with an eight-transmitter constellation, the area overlapped by all the uncertainty ellipses have given rise to a measurement error of 20 m for the same low-RCS target at a range of 6400 m.

## B. FUTURE WORK

Improvements are needed in the simulation model. Higher resolution RCS data should be provided. This is possible by calling FEKO directly from the Matlab simulation with the exact incidence and observation angles. Also, the effect of multipath from the sea surface should be included.

A natural extension of this research is to look into tracking algorithms for such a PMR given that there is only range and no Doppler information. There are a couple of proposed tracking methods that might be suitable for the PMR system. There are possibilities for extracting target Doppler information from opportunistic targets using the coherent-on-receive method [21]. Such receivers support a pseudo-coherent reception of radar signals to extract Doppler information. With both range and Doppler information in a pseudo-coherent form, the improved PMR system can generate ambiguity function for better detection accuracy and also adopt typical tracking methods used in monostatic radars.

With detection and tracking assured, it is possible to take a step further into classification and identification of targets. From [6], forward scatter and backscatter based ISAR are currently being investigated for their ability to detect target outline. It might be interesting to consider adding another dimension to this by using bistatic ISAR. In combination, the three ISAR plots might offer added information about the target to help in classification and identification.

# APPENDIX A. SPECIFICATION SHEET OF MANTADIGITAL RADAR BY KELVIN HUGHES

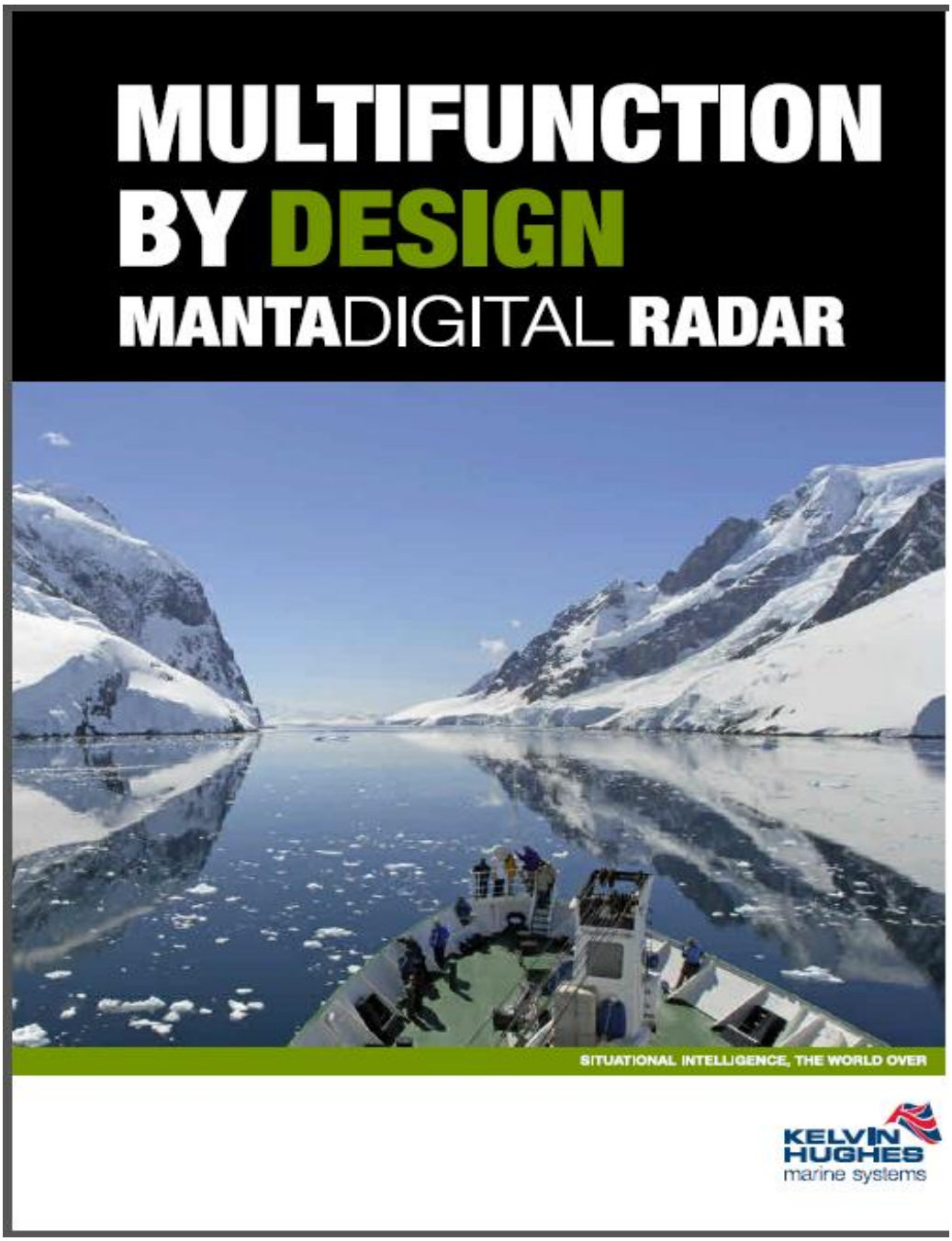

# Transceivers

## Transceiver Types

The Mantadigital™ range includes both magnetron and solid-state Radar transceivers. In both cases the latest low-profile aerials are used to reduce wind loading and increase in-service life. Upmast and downmast options are available in both X and S-Band for the magnetron transceivers. In all cases high reliability and performance have been the design criteria. In all systems a transmission

## Low-Profile Technology

Using the latest technology all Kelvin Hughes antennas use the polyrod lens principle. For both conventional and SharpEye™ systems this results in an antenna with reduced vertical dimension which is significantly lighter that a conventional unit. This has the effect of reducing motor and gearbox loading and results in an increase in service life.

**Transceiver Characteristics**

| | X-Band Systems | | | | S-Band Systems | | |
|---|---|---|---|---|---|---|---|
| **Transceiver** | **10kW Upmast** | **25kW Upmast** | **25kW Downmast** | **SharpEye™** | **30kW Upmast** | **30kW Downmast** | **SharpEye™** |
| **Peak Power** | 10kW | 25kW | 25kW | 170W | 30kW | 30kW | 170W |
| **Frequency** | 9410 +/-30MHz | 9410 +/-30MHz | 9410 +/-30MHz | 9220 –A3 9480MHz | 3050MHz +/- 10MHz | 3050MHz +/- 10MHz | 2900-3100MHz |
| **Pulse Length/PRF (Short)** | 55ns/3000Hz | 70ns/3000Hz | 70ns/3000Hz | N/A | 55ns/3000Hz | 70ns/3000Hz | N/A |
| **Pulse Length/PRF (Med)** | 230ns/1500Hz | 250ns/1500Hz | 260ns/1500Hz | N/A | 250ns/750Hz | 260ns/750Hz | N/A |
| **Pulse Length/PRF (Long)** | 600ns/750Hz | 900ns/750Hz | 900ns/750Hz | N/A | 950ns/750Hz | 900ns/750Hz | N/A |
| **Receiver Noise Figure** | <6dB | <6dB | <6dB | N/A | <6dB | <6dB | N/A |
| **Receiver IF Frequency** | 60MHz | 60MHz | 60MHz | N/A | 60MHz | 60MHz | N/A |
| **Receiver Bandwidth** | 6MHz / 22MHz | 6MHz / 22MHz | 6MHz / 22MHz | 20MHz | 6MHz/22MHz | 6MHz/22MHz | 20MHz |
| **Minimum Range** | <40m | <40m | <40m | <40m | <40m | <40m | <40m |
| **Range Resolution** | <2m | <2m | <2m | <15m | <2m | <2m | <15m |
| **Compass Safe Dist.** | 3.0m /1.8m | 3.0m / 1.8m | 3.0m/1.8m & 1.4m/0.8m | 3.0m / 1.8m | 3.0m/1.8m | 3.0m/1.8m & 1.4m/0.8m | 3.0m / 1.8m |

**Antenna Characteristics**

| | X-Band Systems | | | S-Band Systems |
|---|---|---|---|---|
| **Antenna Length** | 1.3m | 1.9m | 2.5m | 3.7m |
| **Beamwidth (H)** | 1.8° | 1.25° | 0.95° | 1.9° |
| **Beamwidth (V)** | 25° | | | 26° |
| **Antenna Gain** | 28dB | 30dB | 31dB | 28dB |
| **Polarisation** | Horizontal | Horizontal | Horizontal | Horizontal |
| **Sidelobes (+/- 10°)** | < -26dB | < -26dB | < -26dB | < -30dB |
| **Sidelobes (->10°)** | < -34dB | < -34dB | < -34dB | < -35dB |
| **Rotation Rate** | 24, 45 rpm option available | | | 24, 45 rpm option available |

10kW Upmast X-Band

25kW Upmast X-Band and 30kW Upmast S -Band Transceivers

KELVIN HUGHES
marine systems

# APPENDIX B. SPECIFICATION SHEET OF FAR28X7 SERIES BY FURUNO

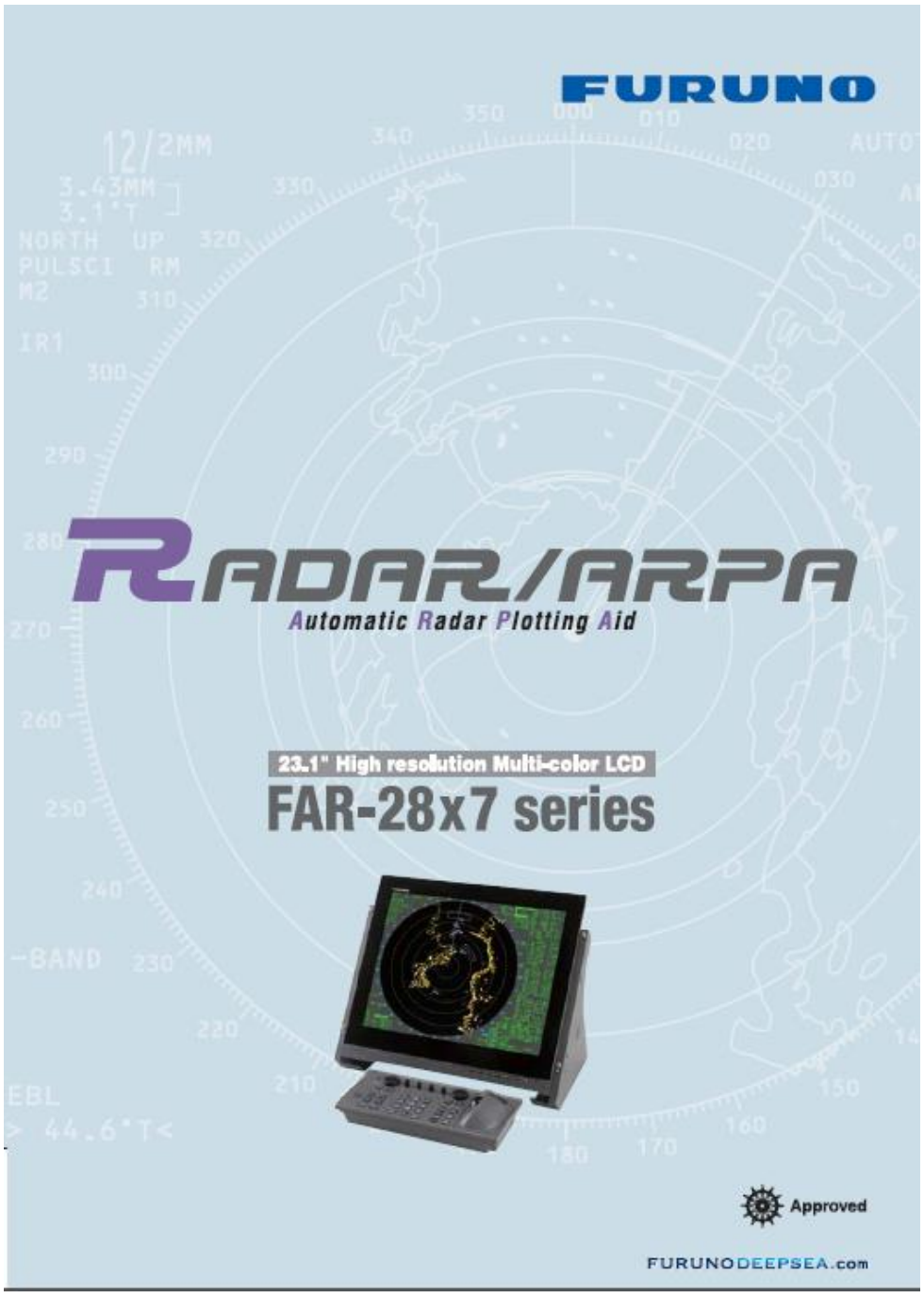

## Antenna Radiators

**1. Type** Slotted waveguide array

**2. Beamwidth and sidelobe attenuation**

| | X-Band | | | S-Band |
|---|---|---|---|---|
| Radiator Type | XN-12AF | XN-20AF | XN-24AF | SN-36AF |
| Length | 4 ft | 6.5 ft | 8 ft | 12 ft |
| Beamwidth(H) | 1.9 | 1.23 | 0.95 | 1.8 |
| Beamwidth(W) | 20 | 20 | 20 | 25 |
| Sidelobe (within 10) | -24 dB | -28 dB | -28 dB | -24 dB |
| Sidelobe (outside 10) | -30 dB | -32 dB | -32 dB | -30 dB |

**3. Rotation**

| | | |
|---|---|---|
| X-Band | | |
| Rotation | 24 rpm | 42 rpm |
| Gear Box | RSB-096/103 | RSB-097 |
| S-Band | | |
| Rotation | 21/26 rpm | 45 rpm |
| Gear Box | RSB-098/099/104/105 | RSB-100/101/102 |

## RF Transceiver

**1. Frequency**

X-band: 9410 MHz 30 MHz

S-band: 3050 MHz 30 MHz

**2. Output power**

| | FAR-2817 | FAR-2827 | FAR-2827W | FAR-2837S | FAR-2837SW |
|---|---|---|---|---|---|
| Output Power | 12 kW | 25 kW | 25 kW | 30 kW | 30 kW |
| Transceiver | RTR-078 | RTR-079 | RTR-081 | RTR-080 | RTR-082 |

**3. Pulselength/PRR**

| Range scale (nm) | Pulselength (s) | PRR (Hz) |
|---|---|---|
| 0.125, 0.25 | 0.07 | 3000 |
| 0.5 | 0.07, 0.15 | 3000 |
| 0.75, 1.5 | 0.07, 0.15, 0.3 | 3000, 1500 |
| 3 | 0.15, 0.3, 0.5, 0.7 | 3000, 1500, 1000 |
| 6 | 0.3, 0.5, 0.7, 1.2 | 1500, 1000, 600 |
| 12, 24 | 0.5, 0.7, 1.2 | 1000, 600 |
| 48, 96 | 1.2 | 600 |

**4. I.F.** 60 MHz, Logarithmic

**5. Bandwidth** Short pulse: 40 MHz
Middle pulse: 10 MHz
Long pulse: 3 MHz

## RADAR DISPLAY

**1. Display**

23.1" color LCD (UXGA 1600 x 1280 pixels),
470 (H) x 353 (V) mm,
Effective display diameter: 341 mm
Echo Color: Yellow, green or white in 32 levels

**2. Range scales and ring intervals (nm)**

| Range | .125, .25, .5, .75, 1.5, 3, 6, 12, 24, 48, 96 |
|---|---|
| Ring | .025, .05, .1, .25, .25, .5, 1, 2, 4, 8, 16 |

**3. Minimum range**
22 m

**4. Range discrimination**
26 m

**5. Range ring accuracy**
Within ±1 % of the current range scale or 10 m, whichever the greater

**6. Presentation modes**
Head-Up, Cursor-gyro, North-Up, Course-Up, True Motion (sea or ground stabilization)

**7. Heading information**
GPS compass SC-50/110 is a recommended heading sensor as a backup for a gyrocompass. Confirm if your Administrations permit its use.

**8. Parallel index lines**
1, 2, 3 or 6 lines (menu selectable)

**9. Radar map**
20,000 points to create coastlines, own ship safety contour, isolated underwater dangers, buoys, traffic routing systems, prohibited areas and fairways as required by IMO.

## Target Tracking

**1. Acquisition**
Auto or manual acquisition: 100 targets in 0.2-24 (32) nm

**2. Tracking**
Auto tracking on all acquired targets

**3. Guard zone (Target Acquisition Area)**
0.5 nm width sector, within 3-6 nm, desired bearing
1 nm width sector or polygon, desired range and bearing

**4. Past positions**
5 or 10 past positions on all targets

**5. Collision warning**
CPA Limit: 0.1-20 nm, TCPA Limit: 1-60 minutes

**6. Trial maneuver**
Dynamic or static, with selected delay time.

## AIS FUNCTIONS (Data input from AIS is required)

**1. Number of Targets**
1,000 targets max.

**2. Past Position Plot Intervals**
OFF, 30 s, 1-60 minutes

## POWER SUPPLY (specify when ordering)

**1. Processor Unit**
FAR-2817
100-115 VAC: 2.6 A (3.0 A for HSC), 220-230 VAC: 1.6 A (1.7 A for HSC), 1 ø, 50/60 Hz
FAR-2827
100-115 VAC: 3.0 A (3.4 A for HSC), 220-230 VAC: 1.8 A (1.9 A for HSC), 1 ø, 50/60 Hz
FAR-2827W
100-115 VAC: 3.2 A, 220-230 VAC: 1.6 A, 1 ø, 50/60 Hz
FAR-2837S/2837SW
100-115 VAC: 3.0 A, 220-230 VAC: 1.5 A, 1 ø, 50/60 Hz

**2. Display Unit**
100-230 VAC, 0.9 A, 1 ø, 50/60 Hz
440 VAC, 1 ø, 50/60 Hz with optional transformer RU-1803

**3. Antenna Unit**
FAR-2837S/2837SW:
200 VAC, 3.0 A, 3ø, 50 Hz; 220 VAC, 3.0 A (3.5 A for HSC*), 3ø, 60 Hz; 380 VAC, 1.5 A, 3ø, 50 Hz; 440 VAC, 1.5 A (1.7 A for HSC*), 3ø, 60 Hz
* for FAR-2837S only
110 VAC, 3ø, 60 Hz with RU-5693; 220 VAC, 3ø, 50 Hz with RU-6522; 440 VAC, 3ø, 50 Hz with RU-5466-1

## EQUIPMENT LIST

**Standard**

1. Display Unit MU-231
2. Processor Unit RPU-013
3. Full-keyboard Control Unit RCU-014
   Trackball Control Unit RCU-015
   (Specify when ordering)
4. Antenna Unit with cable (15/30/40/50 m)
5. Power Supply Unit PSU-007 for FAR-2837S
6. Standard Spare Parts and Installation Materials

**Option**

1. Performance Monitor PM-31 for X-band,
   PM-51 for S-band
2. Remote Control Unit RCU-016
3. Gyro Interface GC-10
4. DVI-Analog RGB Conversion Kit OP03-180 (SXGA output)
5. RGB Connector DSUB-BNC-1 (for VDR)
6. Memory Card Interface Unit CU-200
7. Transformer RU-1803/5466-1/5693/6522
8. Rectifier RU-3424/1746B
9. Junction Box RJB-001
10. Antenna Cable RW-9600
11. Hand Grip FP03-09840
12. Bracket FP03-09820
13. Switching Hub HUB-100

# APPENDIX C. SPECIFICATION SHEET OF QR026 EW RECEIVER BY TELEYDNE DEFENSE

TELEDYNE DEFENCE
A Teledyne Technologies Company

## 0.5 to 18GHz High Performance Receiver

**Technical Data QR026**

### Features

Full Band Coverage (options to >40GHz)
Fast Tune Speed
High Spurious Free Dynamic Range
Low Colouration
Simultaneous ELINT & ESM operation
Frequency Selective RF Protection
Compact, Expandable Architecture
Low power consumption
Optional 1GHz IF

### Applications

Electronic Intelligence (ELINT)
Electronic Support Measures (ESM)
Defensive Aids Suites (ECM Set-on)
Combined ELINT / ESM Sensors
Ground, Airborne & Naval Environments

### Product Description

The QR026 high performance receiver provides a new approach for ESM / ELINT applications incorporating patented features offering wide band synthesised capability from 500MHz to 18 GHz, with frequency extensions available up to 40 GHz. The QR026 builds on the concept developed for the QR010 receiver family and uses standard, interchangeable modules for maximum system flexibility.

The QR026 offers high pre-selection selectivity, but without the drawbacks of slow tune speeds and high DC power requirements associated with conventional YIG based receivers. Tune speeds of <125μsec are achievable over the full tuning range. Amplitude and group delay characteristics are excellent over the full 500MHz IF bandwidth, with even higher performance over the middle 80% (400MHz) bandwidth. Performance over the central 100MHz is exceptional (better than 1ns group delay), offering the lowest colouration for high quality ELINT signal collection. User control is via front panel Ethernet 10 / 100 Base T.

The temperature compensated unit exhibits low noise figure, high IP3 performance and consumes <80 Watts in single channel configuration.

The modular architecture of the receiver allows it to be configured as a single, dual, triple or quad channel unit with phase & amplitude matched performance across all channels. The receiver provides IF outputs at 960 and 160MHz, with user selectable IF bandwidths available. A 1GHz IF output is available as an option. The receiver can be supplied as an integrated rack or as cards for integration in a customer system.

TELEDYNE DEFENCE
A Teledyne Technologies Company

0.5 to 18GHz
High Performance Receiver
Technical Data QR026

## Electrical Specification

| Parameter | Specification |
|---|---|
| *RF Input Frequency Range:<br>Optional extensions to > 40GHz | 0.5-18GHz |
| *Maximum Input CW | +15dBm |
| *LO Re-radiation | -90dBm Max |
| *Gain 20dB nom. (960MHz IF)<br>28dB nom. (160MHz IF) | |
| *Gain Variation (500MHz IF BW) signal in the IF bandwidth | +/-3dB max for any tune frequency and any RF |
| *Gain Variation (any 100MHz of IF BW) | +/-1.25dB max |
| *Group Delay Variation (500MHz IF BW) | 6ns over the central 80% BW; 10ns over the full |
| bandwith; 3ns typ., <1ns in central 100MHz | |
| *Input Attenuator | 20dB (single step) |
| *IF Attenuator | 15dB Min, 1dB step size |
| *VSWR (RF in/IF out) | 2.5:1 |
| *Noise Figure | 18dB max (Typically 13.5dB) |
| *Input P1dB | -12dBm |
| *Input IP3 | -2dBm (Typically 0dBm) |
| *Single Tone SFDR | 60dB min (500MHz BW) |
| *In-band 2 Tone SFDR | 50dB min (500MHz BW) |
| *Internally Generated Spurious | -70dBm max equiv. input power |
| *Tune Speed | 125µs max – input tune command to Valid IF Output |
| *Tune Accuracy | 2kHz |
| *Tune Resolution | 1MHz (1kHz capable) |
| *Phase Noise | |
| 1kHz | -88dBc/Hz |
| 10kHz | -90dBc/Hz |
| 100kHz | -95dBc/Hz |
| 1MHz | -95dBc/Hz |
| 10MHz | -115dBc/Hz |
| *Size | 19 in rack x 2U high (single channel) |
| *Total Power Consumption: | <80W in full rack configuration |
| *Input Power Supply | 94 – 253 VAC, 47 – 63 Hz |
| *Weight: | < 12kg |
| *Operating Temperature Range | -10°C to +60°C |
| *Options | * Frequency Extension to beyond 40GHz<br>* Single, Dual or Quad Tracked Channels<br>* Digital IFM(s) with hi-PDI PDW outputs<br>* Alternative Speed / Accuracy Oscillators<br>* Alternative IF Outputs (3GHz, 1GHz, 70MHz)<br>* Alternative rack configurations or individual cards in transit frame for intergration in customer rack<br>* Alternative user control interfaces |

# APPENDIX D. SPECIFICATION SHEET FOR DF-A0062 DF RECEIVER BY POYNTING DEFENSE

Poynting Antennas

## Direction Finding and Monitoring Antenna

20 – 6000 MHz

Product Code: DF-A0062

**VERSION: 2.0**

**SPECIFICATIONS:**

**PRODUCT DESCRIPTION:**

This direction finding antenna covers a frequency range of 20 MHz to 6 GHz. A separate, but fully integrated active monitoring antenna gives high sensitivity omni-directional coverage on the same axis as the DF antenna, without interfering with the DF array.

The full-size elements on all bands give excellent DF sensitivity. Ultimate angular resolution for strong signals is well under 1° for most of the frequency range. Dipole elements provide good cross-polarisation rejection, and fair performance for signals arriving from up to 15° above or below the horizon.

The integrated monitoring antenna is in two bands, mounted above the Band C & D DF antenna module housed in the radome. Each band of the monitoring array is amplified at the top of the cable, and passively combined to give continuous coverage over the frequency range 20 MHz to 6 GHz, with a single output connector.

This DF antenna is designed to be usable with either a 5- or 2-channel phase-sensitive receiver and correlative algorithm. Characterisation of the antenna can be performed on request.

**Related products:** DF-A0064, DF-A0057-03, DF-A0038 and DF-A0098

| | | |
|---|---|---|
| **Product codes:** | | |
| DF-A0062 | | DF with monitoring up to 6 GHz |
| | | |
| **Electrical - DF:** | | |
| DF frequency range | | Band A: 20 – 300 MHz;<br>Band B: 300 – 1000 MHz;<br>Band C: 1000 – 3000 MHz;<br>Band D: 3000 – 6000 MHz |
| Nominal input impedance | | 50 Ω |
| Antenna type | | 5-element DF interferometer (From 5 to 2-channel receiver compatible) |
| Polarisation | | Vertical |
| Output cables | | RG 400 cables |
| DF connectors | | 20 x TNC male |
| Monitoring connector | | 1 x N male |
| | | |
| **Electrical - monitoring:** | | |
| Frequency range | | 20 – 6000 MHz |
| Nominal H-plane beamwidth | | 360° |
| Nominal E-plane beamwidth | | 60° |
| Typical VSWR* | | 2:1 |
| Polarisation | | Vertical |
| Connector type | | N-type male |
| Nominal impedance | | 50 Ω |
| Input voltage (via coax)* | | 13 – 24 V DC |
| Input current* | | < 150 mA |
| Power consumption (nom)* | | < 2.25 W |
| OP1dB (typ.)* | | > 11 dBm |
| OIP2 (typ.)* | | > 31 dBm |
| OIP3 (typ.)* | | > 21 dBm |
| Sensitivity (typ.) (S/N = 0 dB, BW = 1 Hz)* | 20 – 100 MHz | -20 dBµV/m |
| | 100 – 1000 MHz | -30 dBµV/m |
| | 1 – 3 GHz | -35 dBµV/m |
| | 3 – 6 GHz | -40 dBµV/m |
| | | |
| **Mechanical:** | | |
| Cross-sectional wind area | | 1.50 m² (including antenna switch) |
| Maximum wind speed | | 160 km/h (without ice load) |
| Assembled height | | 3.60 m |
| Assembled diameter (max) | | 2.70 m |
| Shipping dimensions | | 2.20 m x 0.90 m x 0.60 m |
| Weight of antenna<br>Including shipping container | | 60 kg<br>135 kg |

*in active mode

**ELECTRICAL FEATURES:**

- Full-size DF
- Wideband DF
- 5-element interferometer
- Optimised for 2-channel receivers
- High sensitivity omni antenna integrated
- Tactical rapid deploy/stow design with integrated dust caps

THIS PAGE INTENTIONALLY LEFT BLANK

# APPENDIX E. SAMPLE OF BISTATIC RCS RESULTS OF MODEL OF RSN'S FORMIDABLE-CLASS FRIGATE

The following table has a sample of the bistatic RCS values in dBsm for the frequency of 3050 MHz and the model shown in Figures 6 and 7 as generated by FEKO.

| Reflected Angle in ° | Incidence Angle in ° | | | | | | | | | |
|---|---|---|---|---|---|---|---|---|---|---|
| | 1 | 2 | 3 | 4 | 5 | 6 | 7 | 8 | 9 | 10 |
| 1 | 31.53 | 31.53 | 21.74 | 21.74 | 14.80 | 14.80 | 15.80 | 15.80 | 14.62 | 14.62 |
| 2 | 28.31 | 28.31 | 23.84 | 23.84 | 14.42 | 14.42 | 12.99 | 12.99 | 16.08 | 16.08 |
| 3 | 21.23 | 21.23 | 18.88 | 18.88 | 13.18 | 13.18 | 15.45 | 15.45 | 5.49 | 5.49 |
| 4 | 14.15 | 14.15 | 14.28 | 14.28 | 18.14 | 18.14 | 8.34 | 8.34 | 12.75 | 12.75 |
| 5 | 19.32 | 19.32 | 13.93 | 13.93 | 13.90 | 13.90 | 17.18 | 17.18 | 15.36 | 15.36 |
| 6 | 12.99 | 12.99 | 13.15 | 13.15 | 8.37 | 8.37 | 12.13 | 12.13 | 13.46 | 13.46 |
| 7 | 13.99 | 13.99 | 14.61 | 14.61 | 16.79 | 16.79 | 9.87 | 9.87 | 14.51 | 14.51 |
| 8 | 1.22 | 1.22 | 16.13 | 16.13 | 12.77 | 12.77 | 13.42 | 13.42 | 15.77 | 15.77 |
| 9 | 11.07 | 11.07 | 16.83 | 16.83 | 13.94 | 13.94 | 14.12 | 14.12 | 17.87 | 17.87 |
| 10 | 15.99 | 15.99 | 12.30 | 12.30 | 16.34 | 16.34 | 13.45 | 13.45 | 15.53 | 15.53 |
| 11 | 17.23 | 17.23 | 7.59 | 7.59 | 13.60 | 13.60 | 15.86 | 15.86 | 14.21 | 14.21 |
| 12 | 12.32 | 12.32 | 17.34 | 17.34 | 16.82 | 16.82 | 16.59 | 16.59 | 16.57 | 16.57 |
| 13 | 10.85 | 10.85 | 16.89 | 16.89 | 18.07 | 18.07 | 13.87 | 13.87 | 16.67 | 16.67 |
| 14 | 16.77 | 16.77 | 16.29 | 16.29 | 13.15 | 13.15 | 17.67 | 17.67 | 14.66 | 14.66 |
| 15 | 11.04 | 11.04 | 15.80 | 15.80 | 15.05 | 15.05 | 13.57 | 13.57 | 17.75 | 17.75 |
| 16 | 14.73 | 14.73 | 17.79 | 17.79 | 17.10 | 17.10 | 13.81 | 13.81 | 17.36 | 17.36 |
| 17 | 15.81 | 15.81 | 13.67 | 13.67 | 13.97 | 13.97 | 19.43 | 19.43 | 15.44 | 15.44 |
| 18 | 16.89 | 16.89 | 14.36 | 14.36 | 11.99 | 11.99 | 17.78 | 17.78 | 14.46 | 14.46 |
| 19 | 15.63 | 15.63 | 12.89 | 12.89 | 16.94 | 16.94 | 15.27 | 15.27 | 14.25 | 14.25 |
| 20 | 14.52 | 14.52 | 17.17 | 17.17 | 16.02 | 16.02 | 14.63 | 14.63 | 13.51 | 13.51 |
| 21 | 15.27 | 15.27 | 18.76 | 18.76 | 13.62 | 13.62 | 15.95 | 15.95 | 15.05 | 15.05 |
| 22 | 16.27 | 16.27 | 18.62 | 18.62 | 16.30 | 16.30 | 15.81 | 15.81 | 16.12 | 16.12 |
| 23 | 18.98 | 18.98 | 15.81 | 15.81 | 16.94 | 16.94 | 14.33 | 14.33 | 16.22 | 16.22 |
| 24 | 18.12 | 18.12 | 14.14 | 14.14 | 15.03 | 15.03 | 16.72 | 16.72 | 16.61 | 16.61 |
| 25 | 11.94 | 11.94 | 16.35 | 16.35 | 16.15 | 16.15 | 16.83 | 16.83 | 17.41 | 17.41 |
| 26 | 13.82 | 13.82 | 13.11 | 13.11 | 15.65 | 15.65 | 16.98 | 16.98 | 14.61 | 14.61 |
| 27 | 12.48 | 12.48 | 17.23 | 17.23 | 16.91 | 16.91 | 15.62 | 15.62 | 15.69 | 15.69 |
| 28 | 14.67 | 14.67 | 17.02 | 17.02 | 17.39 | 17.39 | 15.53 | 15.53 | 16.67 | 16.67 |
| 29 | 15.20 | 15.20 | 14.33 | 14.33 | 15.00 | 15.00 | 16.40 | 16.40 | 14.78 | 14.78 |
| 30 | 14.46 | 14.46 | 13.59 | 13.59 | 14.24 | 14.24 | 16.29 | 16.29 | 13.05 | 13.05 |
| 31 | 14.06 | 14.06 | 14.35 | 14.35 | 14.48 | 14.48 | 15.07 | 15.07 | 12.30 | 12.30 |
| 32 | 14.78 | 14.78 | 15.32 | 15.32 | 12.75 | 12.75 | 14.47 | 14.47 | 12.93 | 12.93 |
| 33 | 15.81 | 15.81 | 13.42 | 13.42 | 12.58 | 12.58 | 15.02 | 15.02 | 13.34 | 13.34 |
| 34 | 14.25 | 14.25 | 13.67 | 13.67 | 15.18 | 15.18 | 14.85 | 14.85 | 14.72 | 14.72 |
| 35 | 11.97 | 11.97 | 16.41 | 16.41 | 15.84 | 15.84 | 13.54 | 13.54 | 15.30 | 15.30 |
| 36 | 12.99 | 12.99 | 14.34 | 14.34 | 12.07 | 12.07 | 12.87 | 12.87 | 13.00 | 13.00 |
| 37 | 15.63 | 15.63 | 13.65 | 13.65 | 13.51 | 13.51 | 15.26 | 15.26 | 14.73 | 14.73 |
| 38 | 10.62 | 10.62 | 13.39 | 13.39 | 14.44 | 14.44 | 11.10 | 11.10 | 13.19 | 13.19 |
| 39 | 14.63 | 14.63 | 13.80 | 13.80 | 11.52 | 11.52 | 14.83 | 14.83 | 13.27 | 13.27 |
| 40 | 31.53 | 31.53 | 13.27 | 13.27 | 12.87 | 12.87 | 12.94 | 12.94 | 12.26 | 12.26 |

| Reflected Angle in ° | Incidence Angle in ° | | | | | | | | | |
|---|---|---|---|---|---|---|---|---|---|---|
| | 1 | 2 | 3 | 4 | 5 | 6 | 7 | 8 | 9 | 10 |
| 41 | 12.48 | 12.48 | 13.67 | 13.67 | 14.13 | 14.13 | 12.54 | 12.54 | 13.98 | 13.98 |
| 42 | 13.82 | 13.82 | 11.47 | 11.47 | 12.01 | 12.01 | 12.92 | 12.92 | 11.17 | 11.17 |
| 43 | 12.42 | 12.42 | 11.36 | 11.36 | 11.82 | 11.82 | 10.54 | 10.54 | 9.76 | 9.76 |
| 44 | 12.05 | 12.05 | 11.97 | 11.97 | 10.94 | 10.94 | 9.80 | 9.80 | 12.15 | 12.15 |
| 45 | 10.62 | 10.62 | 10.74 | 10.74 | 10.97 | 10.97 | 9.83 | 9.83 | 12.38 | 12.38 |
| 46 | 8.32 | 8.32 | 10.23 | 10.23 | 9.42 | 9.42 | 8.00 | 8.00 | 12.18 | 12.18 |
| 47 | 8.83 | 8.83 | 9.27 | 9.27 | 10.35 | 10.35 | 9.87 | 9.87 | 13.12 | 13.12 |
| 48 | 6.56 | 6.56 | 9.50 | 9.50 | 9.87 | 9.87 | 9.81 | 9.81 | 12.45 | 12.45 |
| 49 | 9.03 | 9.03 | 8.98 | 8.98 | 10.05 | 10.05 | 9.70 | 9.70 | 12.84 | 12.84 |
| 50 | 5.50 | 5.50 | 7.42 | 7.42 | 10.01 | 10.01 | 10.28 | 10.28 | 8.79 | 8.79 |
| 51 | 11.05 | 11.05 | 8.01 | 8.01 | 6.30 | 6.30 | 12.03 | 12.03 | 10.82 | 10.82 |
| 52 | 11.11 | 11.11 | 7.88 | 7.88 | 10.53 | 10.53 | 12.83 | 12.83 | 11.14 | 11.14 |
| 53 | 9.15 | 9.15 | 10.77 | 10.77 | 11.34 | 11.34 | 9.10 | 9.10 | 8.88 | 8.88 |
| 54 | 10.08 | 10.08 | 4.64 | 4.64 | 9.60 | 9.60 | 9.29 | 9.29 | 6.05 | 6.05 |
| 55 | 11.36 | 11.36 | 8.85 | 8.85 | 11.01 | 11.01 | 7.35 | 7.35 | 8.42 | 8.42 |
| 56 | 8.92 | 8.92 | 9.03 | 9.03 | 8.91 | 8.91 | 5.63 | 5.63 | 2.61 | 2.61 |
| 57 | 12.28 | 12.28 | 8.08 | 8.08 | 5.95 | 5.95 | 9.55 | 9.55 | -0.73 | -0.73 |
| 58 | 7.43 | 7.43 | 6.07 | 6.07 | 5.29 | 5.29 | 1.92 | 1.92 | 0.25 | 0.25 |
| 59 | 9.18 | 9.18 | 2.70 | 2.70 | 8.86 | 8.86 | 3.55 | 3.55 | 4.72 | 4.72 |
| 60 | 9.73 | 9.73 | 6.47 | 6.47 | 3.76 | 3.76 | 3.31 | 3.31 | 4.69 | 4.69 |
| 61 | 7.93 | 7.93 | 4.70 | 4.70 | 4.22 | 4.22 | 1.20 | 1.20 | 6.80 | 6.80 |
| 62 | 10.79 | 10.79 | -2.42 | -2.42 | 0.33 | 0.33 | 5.65 | 5.65 | 8.59 | 8.59 |
| 63 | -4.50 | -4.50 | 1.43 | 1.43 | 3.83 | 3.83 | 4.60 | 4.60 | 8.44 | 8.44 |
| 64 | 5.53 | 5.53 | -0.31 | -0.31 | 1.01 | 1.01 | 6.21 | 6.21 | 10.88 | 10.88 |
| 65 | 8.79 | 8.79 | -5.83 | -5.83 | -1.06 | -1.06 | 9.59 | 9.59 | 11.51 | 11.51 |
| 66 | -2.80 | -2.80 | -9.00 | -9.00 | 3.12 | 3.12 | 9.93 | 9.93 | 9.51 | 9.51 |
| 67 | -2.95 | -2.95 | 1.10 | 1.10 | 4.20 | 4.20 | 3.95 | 3.95 | 2.61 | 2.61 |
| 68 | 4.57 | 4.57 | 4.19 | 4.19 | 5.63 | 5.63 | -2.17 | -2.17 | 7.21 | 7.21 |
| 69 | 3.70 | 3.70 | -0.07 | -0.07 | 3.57 | 3.57 | -1.55 | -1.55 | 9.12 | 9.12 |
| 70 | 5.05 | 5.05 | 2.70 | 2.70 | 1.94 | 1.94 | 7.00 | 7.00 | 7.37 | 7.37 |
| 71 | 2.02 | 2.02 | 4.56 | 4.56 | 3.37 | 3.37 | 7.15 | 7.15 | 7.13 | 7.13 |
| 72 | 6.98 | 6.98 | 8.71 | 8.71 | 7.03 | 7.03 | 4.61 | 4.61 | 5.78 | 5.78 |
| 73 | 7.77 | 7.77 | 11.86 | 11.86 | 11.88 | 11.88 | -1.92 | -1.92 | 6.40 | 6.40 |
| 74 | 9.04 | 9.04 | 13.71 | 13.71 | 13.84 | 13.84 | 11.81 | 11.81 | 13.24 | 13.24 |
| 75 | 6.22 | 6.22 | 13.94 | 13.94 | 10.40 | 10.40 | 14.65 | 14.65 | 7.29 | 7.29 |
| 76 | 10.65 | 10.65 | 13.19 | 13.19 | 11.79 | 11.79 | 8.42 | 8.42 | 17.98 | 17.98 |
| 77 | 14.29 | 14.29 | 9.69 | 9.69 | 16.86 | 16.86 | 17.66 | 17.66 | 25.03 | 25.03 |
| 78 | 12.52 | 12.52 | 16.92 | 16.92 | 11.15 | 11.15 | 15.77 | 15.77 | 25.23 | 25.23 |
| 79 | 11.89 | 11.89 | 14.69 | 14.69 | 18.01 | 18.01 | 23.58 | 23.58 | 26.26 | 26.26 |
| 80 | 13.07 | 13.07 | 15.53 | 15.53 | 15.69 | 15.69 | 26.55 | 26.55 | 27.71 | 27.71 |
| 81 | 14.91 | 14.91 | 12.82 | 12.82 | 23.97 | 23.97 | 27.51 | 27.51 | 27.83 | 27.83 |
| 82 | 12.79 | 12.79 | 21.71 | 21.71 | 26.64 | 26.64 | 27.94 | 27.94 | 26.41 | 26.41 |
| 83 | 13.91 | 13.91 | 23.55 | 23.55 | 25.76 | 25.76 | 27.35 | 27.35 | 27.19 | 27.19 |
| 84 | 13.82 | 13.82 | 23.12 | 23.12 | 27.96 | 27.96 | 25.91 | 25.91 | 23.07 | 23.07 |
| 85 | 14.90 | 14.90 | 27.52 | 27.52 | 26.76 | 26.76 | 27.81 | 27.81 | 22.61 | 22.61 |
| 86 | 17.52 | 17.52 | 23.78 | 23.78 | 30.06 | 30.06 | 23.22 | 23.22 | 9.02 | 9.02 |
| 87 | 8.39 | 8.39 | 30.03 | 30.03 | 24.66 | 24.66 | 25.11 | 25.11 | 15.40 | 15.40 |
| 88 | 15.74 | 15.74 | 24.02 | 24.02 | 24.29 | 24.29 | 8.33 | 8.33 | 11.54 | 11.54 |
| 89 | 14.62 | 14.62 | 27.59 | 27.59 | 21.46 | 21.46 | 17.36 | 17.36 | 9.80 | 9.80 |
| 90 | 19.12 | 19.12 | 19.23 | 19.23 | 22.59 | 22.59 | 15.77 | 15.77 | 14.32 | 14.32 |

| Reflected Angle in ° | Incidence Angle in ° | | | | | | | | | |
|---|---|---|---|---|---|---|---|---|---|---|
| | 1 | 2 | 3 | 4 | 5 | 6 | 7 | 8 | 9 | 10 |
| 91 | 16.62 | 16.62 | 25.39 | 25.39 | 13.42 | 13.42 | 10.42 | 10.42 | 8.56 | 8.56 |
| 92 | 18.30 | 18.30 | 9.82 | 9.82 | 17.38 | 17.38 | 15.04 | 15.04 | 15.41 | 15.41 |
| 93 | 15.41 | 15.41 | 20.56 | 20.56 | 15.46 | 15.46 | 11.52 | 11.52 | 11.15 | 11.15 |
| 94 | 11.73 | 11.73 | 16.71 | 16.71 | 9.27 | 9.27 | 15.02 | 15.02 | 10.33 | 10.33 |
| 95 | 16.52 | 16.52 | 13.76 | 13.76 | 17.46 | 17.46 | 9.30 | 9.30 | 10.94 | 10.94 |
| 96 | 14.32 | 14.32 | 14.59 | 14.59 | 5.16 | 5.16 | 5.55 | 5.55 | 5.32 | 5.32 |
| 97 | 15.66 | 15.66 | 7.23 | 7.23 | 14.88 | 14.88 | 12.43 | 12.43 | 9.45 | 9.45 |
| 98 | 13.95 | 13.95 | 14.52 | 14.52 | 7.30 | 7.30 | 3.56 | 3.56 | 5.88 | 5.88 |
| 99 | 12.01 | 12.01 | 11.58 | 11.58 | 10.66 | 10.66 | 11.37 | 11.37 | 8.88 | 8.88 |
| 100 | 10.62 | 10.62 | 13.40 | 13.40 | 12.05 | 12.05 | 5.37 | 5.37 | 8.61 | 8.61 |
| 101 | 14.92 | 14.92 | 13.40 | 13.40 | 6.51 | 6.51 | 11.84 | 11.84 | 6.93 | 6.93 |
| 102 | 14.96 | 14.96 | 14.10 | 14.10 | 15.28 | 15.28 | 11.12 | 11.12 | 11.23 | 11.23 |
| 103 | 12.17 | 12.17 | 12.73 | 12.73 | 12.21 | 12.21 | 8.70 | 8.70 | 7.53 | 7.53 |
| 104 | 12.97 | 12.97 | 13.29 | 13.29 | 12.69 | 12.69 | 9.81 | 9.81 | 10.52 | 10.52 |
| 105 | 13.42 | 13.42 | 16.79 | 16.79 | 15.06 | 15.06 | 11.21 | 11.21 | 12.71 | 12.71 |
| 106 | 13.95 | 13.95 | 17.22 | 17.22 | 14.69 | 14.69 | 10.98 | 10.98 | 12.60 | 12.60 |
| 107 | 15.82 | 15.82 | 16.20 | 16.20 | 15.79 | 15.79 | 12.48 | 12.48 | 1.45 | 1.45 |
| 108 | 15.09 | 15.09 | 15.21 | 15.21 | 13.74 | 13.74 | 13.41 | 13.41 | 1.69 | 1.69 |
| 109 | 14.15 | 14.15 | 12.99 | 12.99 | 17.34 | 17.34 | 15.05 | 15.05 | 6.45 | 6.45 |
| 110 | 15.33 | 15.33 | 15.45 | 15.45 | 16.72 | 16.72 | 13.82 | 13.82 | 3.92 | 3.92 |
| 111 | 13.86 | 13.86 | 11.15 | 11.15 | 16.90 | 16.90 | 17.18 | 17.18 | 9.99 | 9.99 |
| 112 | 15.05 | 15.05 | 9.16 | 9.16 | 15.70 | 15.70 | 17.03 | 17.03 | 10.42 | 10.42 |
| 113 | 10.32 | 10.32 | 15.59 | 15.59 | 15.63 | 15.63 | 19.51 | 19.51 | 12.11 | 12.11 |
| 114 | 14.42 | 14.42 | 11.99 | 11.99 | 13.17 | 13.17 | 17.19 | 17.19 | 12.73 | 12.73 |
| 115 | 6.27 | 6.27 | 8.41 | 8.41 | 18.87 | 18.87 | 12.32 | 12.32 | 14.04 | 14.04 |
| 116 | 9.23 | 9.23 | 16.92 | 16.92 | 22.61 | 22.61 | 18.42 | 18.42 | 15.87 | 15.87 |
| 117 | 8.77 | 8.77 | 14.12 | 14.12 | 17.76 | 17.76 | 19.40 | 19.40 | 14.24 | 14.24 |
| 118 | 2.77 | 2.77 | 18.31 | 18.31 | 16.56 | 16.56 | 12.94 | 12.94 | 12.21 | 12.21 |
| 119 | 12.65 | 12.65 | 21.25 | 21.25 | 16.73 | 16.73 | 17.56 | 17.56 | 12.78 | 12.78 |
| 120 | 11.05 | 11.05 | 14.23 | 14.23 | 13.43 | 13.43 | 4.92 | 4.92 | 18.77 | 18.77 |
| 121 | 16.08 | 16.08 | 12.15 | 12.15 | 7.02 | 7.02 | 13.07 | 13.07 | 15.50 | 15.50 |
| 122 | 6.78 | 6.78 | 11.65 | 11.65 | 16.07 | 16.07 | 14.29 | 14.29 | 9.83 | 9.83 |
| 123 | 12.52 | 12.52 | 11.31 | 11.31 | 18.08 | 18.08 | 8.83 | 8.83 | 13.96 | 13.96 |
| 124 | 6.04 | 6.04 | 5.84 | 5.84 | 14.04 | 14.04 | 11.82 | 11.82 | 14.17 | 14.17 |
| 125 | 12.44 | 12.44 | 12.77 | 12.77 | -0.15 | -0.15 | 10.66 | 10.66 | 18.89 | 18.89 |
| 126 | 10.14 | 10.14 | 12.44 | 12.44 | 6.81 | 6.81 | 18.86 | 18.86 | 15.68 | 15.68 |
| 127 | 12.01 | 12.01 | 8.19 | 8.19 | 15.67 | 15.67 | 18.58 | 18.58 | 6.97 | 6.97 |
| 128 | 11.83 | 11.83 | 4.41 | 4.41 | 18.31 | 18.31 | 10.31 | 10.31 | 2.33 | 2.33 |
| 129 | 12.46 | 12.46 | 14.00 | 14.00 | 20.59 | 20.59 | 2.99 | 2.99 | 9.92 | 9.92 |
| 130 | 7.08 | 7.08 | 15.85 | 15.85 | 14.25 | 14.25 | 8.25 | 8.25 | 8.40 | 8.40 |
| 131 | 18.90 | 18.90 | 21.26 | 21.26 | 3.25 | 3.25 | 5.48 | 5.48 | 4.78 | 4.78 |
| 132 | 12.28 | 12.28 | 9.29 | 9.29 | -6.25 | -6.25 | 9.75 | 9.75 | 9.14 | 9.14 |
| 133 | 20.86 | 20.86 | 15.74 | 15.74 | 8.93 | 8.93 | 9.08 | 9.08 | 24.62 | 24.62 |
| 134 | 20.86 | 20.86 | 10.76 | 10.76 | 13.29 | 13.29 | 3.87 | 3.87 | 10.17 | 10.17 |
| 135 | 16.61 | 16.61 | 11.66 | 11.66 | 14.95 | 14.95 | 23.81 | 23.81 | 20.53 | 20.53 |
| 136 | 15.03 | 15.03 | 13.87 | 13.87 | 1.56 | 1.56 | 18.97 | 18.97 | 18.77 | 18.77 |
| 137 | 15.72 | 15.72 | 20.99 | 20.99 | 19.68 | 19.68 | 17.07 | 17.07 | 15.61 | 15.61 |
| 138 | 17.95 | 17.95 | 16.87 | 16.87 | 14.76 | 14.76 | 15.03 | 15.03 | 16.33 | 16.33 |
| 139 | 18.31 | 18.31 | 25.54 | 25.54 | 18.51 | 18.51 | 17.20 | 17.20 | 11.68 | 11.68 |
| 140 | 17.37 | 17.37 | 20.89 | 20.89 | 15.90 | 15.90 | 16.10 | 16.10 | 4.16 | 4.16 |

| Reflected Angle in ° | Incidence Angle in ° | | | | | | | | | |
|---|---|---|---|---|---|---|---|---|---|---|
| | 1 | 2 | 3 | 4 | 5 | 6 | 7 | 8 | 9 | 10 |
| 141 | 25.17 | 25.17 | 19.12 | 19.12 | 13.23 | 13.23 | 14.39 | 14.39 | 13.48 | 13.48 |
| 142 | 19.37 | 19.37 | 15.16 | 15.16 | 18.71 | 18.71 | 17.20 | 17.20 | 15.28 | 15.28 |
| 143 | 19.92 | 19.92 | 20.13 | 20.13 | 16.87 | 16.87 | 15.18 | 15.18 | 8.47 | 8.47 |
| 144 | 9.21 | 9.21 | 19.72 | 19.72 | 0.53 | 0.53 | 17.46 | 17.46 | 15.95 | 15.95 |
| 145 | 16.35 | 16.35 | 17.15 | 17.15 | 15.94 | 15.94 | 10.64 | 10.64 | 16.38 | 16.38 |
| 146 | 14.20 | 14.20 | 10.74 | 10.74 | 12.02 | 12.02 | 17.08 | 17.08 | 2.94 | 2.94 |
| 147 | 16.75 | 16.75 | 4.29 | 4.29 | 16.85 | 16.85 | 13.11 | 13.11 | 20.67 | 20.67 |
| 148 | 15.82 | 15.82 | 14.01 | 14.01 | 13.23 | 13.23 | 11.49 | 11.49 | 15.14 | 15.14 |
| 149 | 18.16 | 18.16 | 14.15 | 14.15 | 12.81 | 12.81 | 7.26 | 7.26 | 9.03 | 9.03 |
| 150 | 11.65 | 11.65 | 17.56 | 17.56 | 12.06 | 12.06 | 13.12 | 13.12 | 13.29 | 13.29 |
| 151 | 18.53 | 18.53 | 20.68 | 20.68 | 12.32 | 12.32 | 13.00 | 13.00 | 15.54 | 15.54 |
| 152 | 18.15 | 18.15 | 15.65 | 15.65 | 16.95 | 16.95 | 14.03 | 14.03 | 7.85 | 7.85 |
| 153 | 18.71 | 18.71 | 9.39 | 9.39 | 13.31 | 13.31 | 16.05 | 16.05 | 16.40 | 16.40 |
| 154 | 15.74 | 15.74 | 12.92 | 12.92 | 16.24 | 16.24 | 13.13 | 13.13 | 12.76 | 12.76 |
| 155 | 19.69 | 19.69 | 9.29 | 9.29 | 15.34 | 15.34 | 17.32 | 17.32 | 15.99 | 15.99 |
| 156 | 5.95 | 5.95 | 18.21 | 18.21 | 20.14 | 20.14 | 13.00 | 13.00 | 13.18 | 13.18 |
| 157 | 16.99 | 16.99 | 16.96 | 16.96 | 21.29 | 21.29 | 10.72 | 10.72 | 18.52 | 18.52 |
| 158 | 15.73 | 15.73 | 16.43 | 16.43 | 18.04 | 18.04 | 20.36 | 20.36 | 22.92 | 22.92 |
| 159 | 18.17 | 18.17 | 18.27 | 18.27 | 15.87 | 15.87 | 23.21 | 23.21 | 19.38 | 19.38 |
| 160 | 14.31 | 14.31 | 22.57 | 22.57 | 21.28 | 21.28 | 22.04 | 22.04 | 25.05 | 25.05 |
| 161 | 9.92 | 9.92 | 16.67 | 16.67 | 16.61 | 16.61 | 23.11 | 23.11 | 15.39 | 15.39 |
| 162 | 20.86 | 20.86 | 17.48 | 17.48 | 17.35 | 17.35 | 16.15 | 16.15 | 28.07 | 28.07 |
| 163 | 18.82 | 18.82 | 22.26 | 22.26 | 10.20 | 10.20 | 16.73 | 16.73 | 29.82 | 29.82 |
| 164 | 16.47 | 16.47 | 21.29 | 21.29 | 20.95 | 20.95 | 11.73 | 11.73 | 25.46 | 25.46 |
| 165 | 9.39 | 9.39 | 7.17 | 7.17 | 23.36 | 23.36 | 10.15 | 10.15 | 28.05 | 28.05 |
| 166 | 22.88 | 22.88 | 23.93 | 23.93 | 22.85 | 22.85 | 18.72 | 18.72 | 31.73 | 31.73 |
| 167 | 22.27 | 22.27 | 14.01 | 14.01 | 20.75 | 20.75 | 25.96 | 25.96 | 31.84 | 31.84 |
| 168 | 16.65 | 16.65 | 23.70 | 23.70 | 16.55 | 16.55 | 11.50 | 11.50 | 35.03 | 35.03 |
| 169 | 29.95 | 29.95 | 20.54 | 20.54 | 14.62 | 14.62 | 26.24 | 26.24 | 37.27 | 37.27 |
| 170 | 30.67 | 30.67 | 22.16 | 22.16 | 22.02 | 22.02 | 26.95 | 26.95 | 34.22 | 34.22 |
| 171 | 24.17 | 24.17 | 23.35 | 23.35 | 19.97 | 19.97 | 27.68 | 27.68 | 36.87 | 36.87 |
| 172 | 26.07 | 26.07 | 24.93 | 24.93 | 29.18 | 29.18 | 34.31 | 34.31 | 49.15 | 49.15 |
| 173 | 32.45 | 32.45 | 27.50 | 27.50 | 35.31 | 35.31 | 34.74 | 34.74 | 39.48 | 39.48 |
| 174 | 34.28 | 34.28 | 26.45 | 26.45 | 35.58 | 35.58 | 48.46 | 48.46 | 36.34 | 36.34 |
| 175 | 28.64 | 28.64 | 27.86 | 27.86 | 39.40 | 39.40 | 36.93 | 36.93 | 39.02 | 39.02 |
| 176 | 38.80 | 38.80 | 37.34 | 37.34 | 44.49 | 44.49 | 33.15 | 33.15 | 30.89 | 30.89 |
| 177 | 37.77 | 37.77 | 39.45 | 39.45 | 43.99 | 43.99 | 24.56 | 24.56 | 29.71 | 29.71 |
| 178 | 45.24 | 45.24 | 47.41 | 47.41 | 41.08 | 41.08 | 33.65 | 33.65 | 33.35 | 33.35 |
| 179 | 61.50 | 61.50 | 50.60 | 50.60 | 43.77 | 43.77 | 31.57 | 31.57 | 34.65 | 34.65 |
| 180 | 78.86 | 78.86 | 49.50 | 49.50 | 43.67 | 43.67 | 37.55 | 37.55 | 27.72 | 27.72 |
| 181 | 61.64 | 61.64 | 61.46 | 61.46 | 47.32 | 47.32 | 41.96 | 41.96 | 36.18 | 36.18 |
| 182 | 46.01 | 46.01 | 79.67 | 79.67 | 48.33 | 48.33 | 41.59 | 41.59 | 31.70 | 31.70 |
| 183 | 37.48 | 37.48 | 57.93 | 57.93 | 54.60 | 54.60 | 32.26 | 32.26 | 39.70 | 39.70 |
| 184 | 37.65 | 37.65 | 48.32 | 48.32 | 81.19 | 81.19 | 50.41 | 50.41 | 44.34 | 44.34 |
| 185 | 34.87 | 34.87 | 40.98 | 40.98 | 49.67 | 49.67 | 49.87 | 49.87 | 44.81 | 44.81 |
| 186 | 33.43 | 33.43 | 42.10 | 42.10 | 50.11 | 50.11 | 82.18 | 82.18 | 36.68 | 36.68 |
| 187 | 29.38 | 29.38 | 34.66 | 34.66 | 43.76 | 43.76 | 49.93 | 49.93 | 51.23 | 51.23 |
| 188 | 27.37 | 27.37 | 26.55 | 26.55 | 41.99 | 41.99 | 41.30 | 41.30 | 83.06 | 83.06 |
| 189 | 14.33 | 14.33 | 24.06 | 24.06 | 37.93 | 37.93 | 42.41 | 42.41 | 49.20 | 49.20 |
| 190 | 18.22 | 18.22 | 32.23 | 32.23 | 33.01 | 33.01 | 34.82 | 34.82 | 49.12 | 49.12 |

| Reflected Angle in ° | Incidence Angle in ° | | | | | | | | | |
|---|---|---|---|---|---|---|---|---|---|---|
| | 1 | 2 | 3 | 4 | 5 | 6 | 7 | 8 | 9 | 10 |
| 191 | 24.67 | 24.67 | 23.26 | 23.26 | 23.02 | 23.02 | 36.05 | 36.05 | 42.32 | 42.32 |
| 192 | 17.57 | 17.57 | 26.96 | 26.96 | 19.98 | 19.98 | 33.80 | 33.80 | 43.83 | 43.83 |
| 193 | 19.73 | 19.73 | 18.55 | 18.55 | 26.95 | 26.95 | 27.81 | 27.81 | 39.86 | 39.86 |
| 194 | 15.90 | 15.90 | 24.28 | 24.28 | 24.10 | 24.10 | 30.81 | 30.81 | 25.96 | 25.96 |
| 195 | 22.61 | 22.61 | 22.61 | 22.61 | 16.25 | 16.25 | 29.32 | 29.32 | 26.83 | 26.83 |
| 196 | 11.71 | 11.71 | 20.60 | 20.60 | 21.07 | 21.07 | 30.66 | 30.66 | 34.41 | 34.41 |
| 197 | 16.66 | 16.66 | 2.21 | 2.21 | 22.57 | 22.57 | 31.86 | 31.86 | 31.80 | 31.80 |
| 198 | 19.92 | 19.92 | 17.74 | 17.74 | 18.11 | 18.11 | 29.69 | 29.69 | 22.77 | 22.77 |
| 199 | 7.48 | 7.48 | 14.07 | 14.07 | 16.59 | 16.59 | 23.17 | 23.17 | 29.77 | 29.77 |
| 200 | 8.04 | 8.04 | 20.62 | 20.62 | 12.40 | 12.40 | 11.70 | 11.70 | 26.32 | 26.32 |
| 201 | 16.45 | 16.45 | 9.21 | 9.21 | 8.05 | 8.05 | 16.75 | 16.75 | 16.01 | 16.01 |
| 202 | 17.43 | 17.43 | 10.46 | 10.46 | 17.62 | 17.62 | 22.39 | 22.39 | 21.75 | 21.75 |
| 203 | 14.45 | 14.45 | 16.91 | 16.91 | 16.50 | 16.50 | 20.13 | 20.13 | 22.61 | 22.61 |
| 204 | 3.37 | 3.37 | 18.38 | 18.38 | 22.88 | 22.88 | 19.21 | 19.21 | 14.36 | 14.36 |
| 205 | 17.14 | 17.14 | 22.68 | 22.68 | 24.40 | 24.40 | 15.20 | 15.20 | 8.64 | 8.64 |
| 206 | 18.44 | 18.44 | 21.96 | 21.96 | 18.99 | 18.99 | 19.07 | 19.07 | 17.71 | 17.71 |
| 207 | 17.47 | 17.47 | 11.83 | 11.83 | 10.29 | 10.29 | 22.84 | 22.84 | 18.80 | 18.80 |
| 208 | 19.00 | 19.00 | 21.17 | 21.17 | 17.39 | 17.39 | 14.10 | 14.10 | 23.08 | 23.08 |
| 209 | 15.51 | 15.51 | 8.20 | 8.20 | 10.79 | 10.79 | 18.46 | 18.46 | 18.48 | 18.48 |
| 210 | 13.66 | 13.66 | 20.60 | 20.60 | 22.07 | 22.07 | 23.80 | 23.80 | 27.02 | 27.02 |
| 211 | 19.13 | 19.13 | 8.35 | 8.35 | 16.75 | 16.75 | 20.60 | 20.60 | 18.58 | 18.58 |
| 212 | 16.43 | 16.43 | 12.76 | 12.76 | 15.63 | 15.63 | 27.42 | 27.42 | 24.24 | 24.24 |
| 213 | 16.80 | 16.80 | 16.04 | 16.04 | 15.93 | 15.93 | 22.22 | 22.22 | 17.35 | 17.35 |
| 214 | 13.54 | 13.54 | 18.88 | 18.88 | 18.29 | 18.29 | 14.52 | 14.52 | 14.30 | 14.30 |
| 215 | 15.00 | 15.00 | 17.92 | 17.92 | 24.64 | 24.64 | 2.38 | 2.38 | 13.60 | 13.60 |
| 216 | 12.31 | 12.31 | 22.16 | 22.16 | 15.44 | 15.44 | 8.73 | 8.73 | 13.77 | 13.77 |
| 217 | 17.63 | 17.63 | 19.36 | 19.36 | 13.22 | 13.22 | 4.40 | 4.40 | 13.54 | 13.54 |
| 218 | 17.13 | 17.13 | 16.26 | 16.26 | 2.58 | 2.58 | 7.52 | 7.52 | 10.42 | 10.42 |
| 219 | 25.13 | 25.13 | 12.47 | 12.47 | -2.71 | -2.71 | 14.27 | 14.27 | 18.56 | 18.56 |
| 220 | 11.46 | 11.46 | 12.77 | 12.77 | -0.74 | -0.74 | 17.41 | 17.41 | 18.56 | 18.56 |
| 221 | 13.62 | 13.62 | 4.67 | 4.67 | 11.39 | 11.39 | 18.06 | 18.06 | 18.52 | 18.52 |
| 222 | 14.73 | 14.73 | 5.61 | 5.61 | 14.56 | 14.56 | 19.44 | 19.44 | 13.22 | 13.22 |
| 223 | 14.01 | 14.01 | 13.29 | 13.29 | 19.75 | 19.75 | 19.19 | 19.19 | 13.59 | 13.59 |
| 224 | 12.99 | 12.99 | 19.66 | 19.66 | 20.67 | 20.67 | 17.67 | 17.67 | 14.49 | 14.49 |
| 225 | 12.31 | 12.31 | 20.20 | 20.20 | 17.90 | 17.90 | 10.82 | 10.82 | 6.52 | 6.52 |
| 226 | 18.75 | 18.75 | 19.30 | 19.30 | 14.68 | 14.68 | 5.17 | 5.17 | 14.82 | 14.82 |
| 227 | 20.83 | 20.83 | 3.06 | 3.06 | 15.17 | 15.17 | 2.18 | 2.18 | 12.77 | 12.77 |
| 228 | 15.47 | 15.47 | 11.32 | 11.32 | 17.92 | 17.92 | 1.76 | 1.76 | 14.52 | 14.52 |
| 229 | 17.75 | 17.75 | 14.50 | 14.50 | 16.50 | 16.50 | 11.15 | 11.15 | 11.96 | 11.96 |
| 230 | 2.76 | 2.76 | 12.22 | 12.22 | 10.17 | 10.17 | 11.95 | 11.95 | 12.22 | 12.22 |
| 231 | 12.11 | 12.11 | 8.65 | 8.65 | -1.00 | -1.00 | 7.61 | 7.61 | 15.03 | 15.03 |
| 232 | 10.97 | 10.97 | 13.05 | 13.05 | 7.87 | 7.87 | 1.35 | 1.35 | 15.80 | 15.80 |
| 233 | 14.41 | 14.41 | 1.19 | 1.19 | 8.89 | 8.89 | 11.83 | 11.83 | 13.59 | 13.59 |
| 234 | 2.83 | 2.83 | 4.93 | 4.93 | 1.01 | 1.01 | 12.37 | 12.37 | 10.72 | 10.72 |
| 235 | 8.00 | 8.00 | 4.25 | 4.25 | 4.50 | 4.50 | 5.05 | 5.05 | 14.45 | 14.45 |
| 236 | 3.85 | 3.85 | 8.27 | 8.27 | 6.18 | 6.18 | 7.26 | 7.26 | 10.84 | 10.84 |
| 237 | 3.61 | 3.61 | -3.69 | -3.69 | -2.64 | -2.64 | -2.80 | -2.80 | 8.14 | 8.14 |
| 238 | 1.33 | 1.33 | 4.27 | 4.27 | 8.60 | 8.60 | 3.87 | 3.87 | 8.86 | 8.86 |
| 239 | -9.57 | -9.57 | -0.57 | -0.57 | -0.70 | -0.70 | 8.61 | 8.61 | 5.38 | 5.38 |
| 240 | 0.19 | 0.19 | 9.39 | 9.39 | 6.38 | 6.38 | 7.85 | 7.85 | 4.06 | 4.06 |

| Reflected Angle in ° | Incidence Angle in ° | | | | | | | | | |
|---|---|---|---|---|---|---|---|---|---|---|
| | 1 | 2 | 3 | 4 | 5 | 6 | 7 | 8 | 9 | 10 |
| 241 | 2.96 | 2.96 | 4.61 | 4.61 | -5.00 | -5.00 | 6.40 | 6.40 | -4.28 | -4.28 |
| 242 | -8.96 | -8.96 | 8.27 | 8.27 | 5.12 | 5.12 | 11.02 | 11.02 | -1.57 | -1.57 |
| 243 | 3.56 | 3.56 | 6.51 | 6.51 | 6.81 | 6.81 | 8.94 | 8.94 | 6.10 | 6.10 |
| 244 | 7.16 | 7.16 | 4.97 | 4.97 | 7.35 | 7.35 | 10.16 | 10.16 | 2.75 | 2.75 |
| 245 | 3.54 | 3.54 | 9.32 | 9.32 | 8.24 | 8.24 | 11.69 | 11.69 | 8.49 | 8.49 |
| 246 | 8.96 | 8.96 | 8.77 | 8.77 | 9.89 | 9.89 | 9.92 | 9.92 | 7.71 | 7.71 |
| 247 | 12.29 | 12.29 | 3.82 | 3.82 | 12.23 | 12.23 | 8.38 | 8.38 | 13.11 | 13.11 |
| 248 | 12.29 | 12.29 | 6.66 | 6.66 | 13.03 | 13.03 | 3.44 | 3.44 | 3.69 | 3.69 |
| 249 | 11.86 | 11.86 | 9.73 | 9.73 | 11.40 | 11.40 | 11.95 | 11.95 | 13.05 | 13.05 |
| 250 | 11.44 | 11.44 | 10.68 | 10.68 | 13.84 | 13.84 | 10.24 | 10.24 | 13.55 | 13.55 |
| 251 | 9.53 | 9.53 | 13.26 | 13.26 | 11.94 | 11.94 | 0.63 | 0.63 | 13.23 | 13.23 |
| 252 | 10.77 | 10.77 | 9.76 | 9.76 | 5.61 | 5.61 | 4.81 | 4.81 | 13.52 | 13.52 |
| 253 | 12.57 | 12.57 | 3.04 | 3.04 | 0.01 | 0.01 | 12.44 | 12.44 | 11.17 | 11.17 |
| 254 | 12.24 | 12.24 | 7.27 | 7.27 | 0.01 | 0.01 | 14.19 | 14.19 | 8.13 | 8.13 |
| 255 | 11.28 | 11.28 | 11.12 | 11.12 | 6.35 | 6.35 | 10.74 | 10.74 | 11.85 | 11.85 |
| 256 | 9.95 | 9.95 | 10.86 | 10.86 | 11.12 | 11.12 | 11.17 | 11.17 | 9.41 | 9.41 |
| 257 | 8.75 | 8.75 | 9.12 | 9.12 | 13.11 | 13.11 | -1.54 | -1.54 | 13.79 | 13.79 |
| 258 | 11.58 | 11.58 | 12.08 | 12.08 | 11.88 | 11.88 | 9.50 | 9.50 | 11.91 | 11.91 |
| 259 | 11.37 | 11.37 | 8.47 | 8.47 | 10.04 | 10.04 | 9.99 | 9.99 | 19.07 | 19.07 |
| 260 | 5.68 | 5.68 | 11.20 | 11.20 | 6.83 | 6.83 | 10.66 | 10.66 | 18.75 | 18.75 |
| 261 | 10.29 | 10.29 | 12.08 | 12.08 | 5.38 | 5.38 | 12.67 | 12.67 | 13.82 | 13.82 |
| 262 | 14.52 | 14.52 | 10.31 | 10.31 | 7.33 | 7.33 | 14.87 | 14.87 | 8.35 | 8.35 |
| 263 | 9.93 | 9.93 | 12.57 | 12.57 | 8.39 | 8.39 | 15.47 | 15.47 | 20.23 | 20.23 |
| 264 | 13.86 | 13.86 | 8.91 | 8.91 | 14.77 | 14.77 | 15.69 | 15.69 | 17.03 | 17.03 |
| 265 | 15.81 | 15.81 | 15.20 | 15.20 | 16.57 | 16.57 | 19.34 | 19.34 | 16.31 | 16.31 |
| 266 | 9.23 | 9.23 | 16.34 | 16.34 | 14.99 | 14.99 | 15.98 | 15.98 | 15.59 | 15.59 |
| 267 | 16.71 | 16.71 | 10.81 | 10.81 | 16.32 | 16.32 | 12.48 | 12.48 | 13.48 | 13.48 |
| 268 | 18.03 | 18.03 | 6.84 | 6.84 | 14.29 | 14.29 | 9.46 | 9.46 | 12.34 | 12.34 |
| 269 | 21.80 | 21.80 | 9.97 | 9.97 | 13.20 | 13.20 | 7.81 | 7.81 | 12.78 | 12.78 |
| 270 | 19.58 | 19.58 | 13.79 | 13.79 | 11.30 | 11.30 | 11.61 | 11.61 | 14.50 | 14.50 |
| 271 | 16.63 | 16.63 | 12.93 | 12.93 | 7.47 | 7.47 | 7.77 | 7.77 | 15.45 | 15.45 |
| 272 | 16.64 | 16.64 | 9.37 | 9.37 | 9.23 | 9.23 | 14.63 | 14.63 | 12.82 | 12.82 |
| 273 | 9.34 | 9.34 | 10.89 | 10.89 | 7.38 | 7.38 | 13.91 | 13.91 | 11.58 | 11.58 |
| 274 | 19.72 | 19.72 | 2.42 | 2.42 | 15.11 | 15.11 | 11.94 | 11.94 | 10.95 | 10.95 |
| 275 | 14.22 | 14.22 | 8.66 | 8.66 | 13.63 | 13.63 | 10.44 | 10.44 | 10.95 | 10.95 |
| 276 | 14.68 | 14.68 | 13.08 | 13.08 | 10.97 | 10.97 | 12.84 | 12.84 | 12.36 | 12.36 |
| 277 | 12.37 | 12.37 | 14.22 | 14.22 | 9.57 | 9.57 | 12.26 | 12.26 | 10.68 | 10.68 |
| 278 | 13.01 | 13.01 | 10.64 | 10.64 | 7.30 | 7.30 | 13.37 | 13.37 | 8.52 | 8.52 |
| 279 | 13.78 | 13.78 | 10.23 | 10.23 | 11.62 | 11.62 | 6.83 | 6.83 | 12.23 | 12.23 |
| 280 | 14.87 | 14.87 | 6.94 | 6.94 | 11.51 | 11.51 | 5.48 | 5.48 | 9.36 | 9.36 |
| 281 | 12.52 | 12.52 | 13.53 | 13.53 | 13.09 | 13.09 | 7.14 | 7.14 | 10.95 | 10.95 |
| 282 | 15.11 | 15.11 | 11.54 | 11.54 | 8.54 | 8.54 | 9.93 | 9.93 | 5.50 | 5.50 |
| 283 | 15.01 | 15.01 | 12.27 | 12.27 | 7.25 | 7.25 | 4.99 | 4.99 | 11.24 | 11.24 |
| 284 | 12.69 | 12.69 | 11.46 | 11.46 | 9.88 | 9.88 | 7.29 | 7.29 | 10.45 | 10.45 |
| 285 | 12.04 | 12.04 | 9.92 | 9.92 | 6.50 | 6.50 | 9.64 | 9.64 | 10.68 | 10.68 |
| 286 | 12.95 | 12.95 | 8.86 | 8.86 | 8.28 | 8.28 | 7.82 | 7.82 | 12.98 | 12.98 |
| 287 | 11.67 | 11.67 | 8.52 | 8.52 | 8.52 | 8.52 | 11.03 | 11.03 | 10.50 | 10.50 |
| 288 | 10.55 | 10.55 | 8.28 | 8.28 | 8.40 | 8.40 | 10.74 | 10.74 | 12.14 | 12.14 |
| 289 | 8.64 | 8.64 | 9.51 | 9.51 | 7.42 | 7.42 | 11.05 | 11.05 | 6.96 | 6.96 |
| 290 | 9.96 | 9.96 | 8.87 | 8.87 | 9.22 | 9.22 | 9.10 | 9.10 | 6.27 | 6.27 |

| Reflected Angle in ° | Incidence Angle in ° | | | | | | | | | |
|---|---|---|---|---|---|---|---|---|---|---|
| | 1 | 2 | 3 | 4 | 5 | 6 | 7 | 8 | 9 | 10 |
| 291 | 8.08 | 8.08 | 10.18 | 10.18 | 11.69 | 11.69 | 8.81 | 8.81 | 6.23 | 6.23 |
| 292 | 9.47 | 9.47 | 10.47 | 10.47 | 10.41 | 10.41 | 11.00 | 11.00 | 8.35 | 8.35 |
| 293 | 8.51 | 8.51 | 11.43 | 11.43 | 9.25 | 9.25 | 8.42 | 8.42 | 8.85 | 8.85 |
| 294 | 9.18 | 9.18 | 8.90 | 8.90 | 10.61 | 10.61 | 4.49 | 4.49 | 5.06 | 5.06 |
| 295 | 12.32 | 12.32 | 8.85 | 8.85 | 8.55 | 8.55 | 6.65 | 6.65 | 0.56 | 0.56 |
| 296 | 8.52 | 8.52 | 11.78 | 11.78 | 5.17 | 5.17 | 5.64 | 5.64 | 1.62 | 1.62 |
| 297 | 5.55 | 5.55 | 10.23 | 10.23 | 8.19 | 8.19 | 3.00 | 3.00 | 5.50 | 5.50 |
| 298 | 11.90 | 11.90 | 7.46 | 7.46 | 4.35 | 4.35 | 4.08 | 4.08 | -8.89 | -8.89 |
| 299 | 7.79 | 7.79 | 10.47 | 10.47 | 6.92 | 6.92 | 6.78 | 6.78 | 8.63 | 8.63 |
| 300 | 8.57 | 8.57 | 4.41 | 4.41 | 3.42 | 3.42 | 4.05 | 4.05 | -0.04 | -0.04 |
| 301 | 7.91 | 7.91 | 8.78 | 8.78 | 7.63 | 7.63 | 7.66 | 7.66 | 10.54 | 10.54 |
| 302 | 2.38 | 2.38 | 5.85 | 5.85 | 7.28 | 7.28 | 9.81 | 9.81 | 7.09 | 7.09 |
| 303 | 7.77 | 7.77 | 2.38 | 2.38 | 6.90 | 6.90 | 11.37 | 11.37 | 9.10 | 9.10 |
| 304 | 2.71 | 2.71 | 5.41 | 5.41 | 7.97 | 7.97 | 6.92 | 6.92 | 7.06 | 7.06 |
| 305 | 4.58 | 4.58 | 6.62 | 6.62 | 9.33 | 9.33 | 11.00 | 11.00 | 11.62 | 11.62 |
| 306 | 3.84 | 3.84 | 7.78 | 7.78 | 11.16 | 11.16 | 6.97 | 6.97 | 11.13 | 11.13 |
| 307 | 3.41 | 3.41 | 7.08 | 7.08 | 8.27 | 8.27 | 12.84 | 12.84 | 12.98 | 12.98 |
| 308 | 6.57 | 6.57 | 10.16 | 10.16 | 11.24 | 11.24 | 12.66 | 12.66 | 11.77 | 11.77 |
| 309 | 8.73 | 8.73 | 8.99 | 8.99 | 11.13 | 11.13 | 14.50 | 14.50 | 13.75 | 13.75 |
| 310 | 1.50 | 1.50 | 11.96 | 11.96 | 14.41 | 14.41 | 12.70 | 12.70 | 15.07 | 15.07 |
| 311 | 9.35 | 9.35 | 10.15 | 10.15 | 11.87 | 11.87 | 14.82 | 14.82 | 14.94 | 14.94 |
| 312 | 4.39 | 4.39 | 11.87 | 11.87 | 14.20 | 14.20 | 15.19 | 15.19 | 18.15 | 18.15 |
| 313 | 9.07 | 9.07 | 13.44 | 13.44 | 12.91 | 12.91 | 15.97 | 15.97 | 12.02 | 12.02 |
| 314 | 6.52 | 6.52 | 15.09 | 15.09 | 15.07 | 15.07 | 11.27 | 11.27 | 16.30 | 16.30 |
| 315 | 10.51 | 10.51 | 13.50 | 13.50 | 8.85 | 8.85 | 17.31 | 17.31 | 12.86 | 12.86 |
| 316 | 12.71 | 12.71 | 12.99 | 12.99 | 16.83 | 16.83 | 14.16 | 14.16 | 14.09 | 14.09 |
| 317 | 13.43 | 13.43 | 15.21 | 15.21 | 17.61 | 17.61 | 12.15 | 12.15 | 14.97 | 14.97 |
| 318 | 13.79 | 13.79 | 14.59 | 14.59 | 14.50 | 14.50 | 15.23 | 15.23 | 16.49 | 16.49 |
| 319 | 13.06 | 13.06 | 14.55 | 14.55 | 15.40 | 15.40 | 14.73 | 14.73 | 16.36 | 16.36 |
| 320 | 11.07 | 11.07 | 10.16 | 10.16 | 12.97 | 12.97 | 13.65 | 13.65 | 14.61 | 14.61 |
| 321 | 11.06 | 11.06 | 13.40 | 13.40 | 14.52 | 14.52 | 16.75 | 16.75 | 15.26 | 15.26 |
| 322 | 9.14 | 9.14 | 14.25 | 14.25 | 15.83 | 15.83 | 15.09 | 15.09 | 14.85 | 14.85 |
| 323 | 15.06 | 15.06 | 13.41 | 13.41 | 14.76 | 14.76 | 12.63 | 12.63 | 15.99 | 15.99 |
| 324 | 11.54 | 11.54 | 12.98 | 12.98 | 14.67 | 14.67 | 14.95 | 14.95 | 15.41 | 15.41 |
| 325 | 12.49 | 12.49 | 13.09 | 13.09 | 12.37 | 12.37 | 14.62 | 14.62 | 14.81 | 14.81 |
| 326 | 13.56 | 13.56 | 16.38 | 16.38 | 15.29 | 15.29 | 11.18 | 11.18 | 17.04 | 17.04 |
| 327 | 14.74 | 14.74 | 15.45 | 15.45 | 15.58 | 15.58 | 16.13 | 16.13 | 15.64 | 15.64 |
| 328 | 14.17 | 14.17 | 11.87 | 11.87 | 14.51 | 14.51 | 14.00 | 14.00 | 17.37 | 17.37 |
| 329 | 11.48 | 11.48 | 13.29 | 13.29 | 13.16 | 13.16 | 18.12 | 18.12 | 16.84 | 16.84 |
| 330 | 11.77 | 11.77 | 14.88 | 14.88 | 16.60 | 16.60 | 13.19 | 13.19 | 15.59 | 15.59 |
| 331 | 13.22 | 13.22 | 16.18 | 16.18 | 16.45 | 16.45 | 15.34 | 15.34 | 17.36 | 17.36 |
| 332 | 15.03 | 15.03 | 11.67 | 11.67 | 14.88 | 14.88 | 14.30 | 14.30 | 19.35 | 19.35 |
| 333 | 10.79 | 10.79 | 12.57 | 12.57 | 9.40 | 9.40 | 18.89 | 18.89 | 11.99 | 11.99 |
| 334 | 10.66 | 10.66 | 18.71 | 18.71 | 17.38 | 17.38 | 17.11 | 17.11 | 14.10 | 14.10 |
| 335 | 17.69 | 17.69 | 21.58 | 21.58 | 16.66 | 16.66 | 17.24 | 17.24 | 13.33 | 13.33 |
| 336 | 20.71 | 20.71 | 17.27 | 17.27 | 19.21 | 19.21 | 10.41 | 10.41 | 9.35 | 9.35 |
| 337 | 24.64 | 24.64 | 17.59 | 17.59 | 11.52 | 11.52 | 8.86 | 8.86 | 17.63 | 17.63 |
| 338 | 20.11 | 20.11 | 19.68 | 19.68 | 14.41 | 14.41 | 14.94 | 14.94 | 20.71 | 20.71 |
| 339 | 18.73 | 18.73 | 14.60 | 14.60 | 15.13 | 15.13 | 15.33 | 15.33 | 18.52 | 18.52 |
| 340 | 13.35 | 13.35 | 12.40 | 12.40 | 17.67 | 17.67 | 13.11 | 13.11 | 19.48 | 19.48 |

| Reflected Angle in ° | Incidence Angle in ° | | | | | | | | | |
|---|---|---|---|---|---|---|---|---|---|---|
| | 1 | 2 | 3 | 4 | 5 | 6 | 7 | 8 | 9 | 10 |
| 341 | 13.75 | 13.75 | 14.04 | 14.04 | 16.69 | 16.69 | 10.31 | 10.31 | 13.62 | 13.62 |
| 342 | 16.64 | 16.64 | 14.48 | 14.48 | 13.24 | 13.24 | 13.56 | 13.56 | 14.19 | 14.19 |
| 343 | 16.88 | 16.88 | 18.26 | 18.26 | 18.09 | 18.09 | 17.68 | 17.68 | 24.58 | 24.58 |
| 344 | 16.87 | 16.87 | 11.88 | 11.88 | 20.61 | 20.61 | 13.88 | 13.88 | 19.38 | 19.38 |
| 345 | 8.19 | 8.19 | 14.83 | 14.83 | 19.87 | 19.87 | 25.56 | 25.56 | 16.03 | 16.03 |
| 346 | 17.94 | 17.94 | 24.24 | 24.24 | 13.24 | 13.24 | 21.75 | 21.75 | 16.67 | 16.67 |
| 347 | 17.19 | 17.19 | 7.26 | 7.26 | 24.64 | 24.64 | 5.61 | 5.61 | 19.10 | 19.10 |
| 348 | 24.78 | 24.78 | 20.85 | 20.85 | 17.46 | 17.46 | 14.20 | 14.20 | 22.48 | 22.48 |
| 349 | 18.67 | 18.67 | 25.25 | 25.25 | 17.22 | 17.22 | 17.89 | 17.89 | 24.02 | 24.02 |
| 350 | 20.67 | 20.67 | 9.57 | 9.57 | 16.23 | 16.23 | 15.73 | 15.73 | 29.56 | 29.56 |
| 351 | 24.58 | 24.58 | 10.26 | 10.26 | 17.52 | 17.52 | 24.12 | 24.12 | 37.39 | 37.39 |
| 352 | 11.74 | 11.74 | 9.75 | 9.75 | 16.80 | 16.80 | 33.99 | 33.99 | 64.51 | 64.51 |
| 353 | 15.73 | 15.73 | 21.41 | 21.41 | 25.53 | 25.53 | 36.90 | 36.90 | 38.93 | 38.93 |
| 354 | 15.63 | 15.63 | 18.43 | 18.43 | 36.39 | 36.39 | 64.58 | 64.58 | 31.57 | 31.57 |
| 355 | 18.67 | 18.67 | 26.36 | 26.36 | 38.28 | 38.28 | 31.76 | 31.76 | 22.49 | 22.49 |
| 356 | 14.94 | 14.94 | 33.68 | 33.68 | 64.43 | 64.43 | 28.69 | 28.69 | 11.89 | 11.89 |
| 357 | 26.43 | 26.43 | 37.85 | 37.85 | 35.23 | 35.23 | 22.89 | 22.89 | 19.38 | 19.38 |
| 358 | 28.28 | 28.28 | 64.52 | 64.52 | 31.68 | 31.68 | 15.21 | 15.21 | 6.34 | 6.34 |
| 359 | 37.85 | 37.85 | 35.69 | 35.69 | 23.48 | 23.48 | 14.92 | 14.92 | 11.42 | 11.42 |
| 360 | 64.43 | 64.43 | 28.41 | 28.41 | 13.76 | 13.76 | 12.60 | 12.60 | 4.39 | 4.39 |

| Reflected Angle in ° | Incidence Angle in ° | | | | | | | | | |
|---|---|---|---|---|---|---|---|---|---|---|
| | 11 | 12 | 13 | 14 | 15 | 16 | 17 | 18 | 19 | 20 |
| 1 | 17.59 | 17.59 | 8.33 | 8.33 | 16.04 | 16.04 | 14.31 | 14.31 | 15.99 | 15.99 |
| 2 | 11.82 | 11.82 | 17.41 | 17.41 | 16.51 | 16.51 | 17.35 | 17.35 | 15.04 | 15.04 |
| 3 | 15.12 | 15.12 | 15.12 | 15.12 | 18.11 | 18.11 | 14.44 | 14.44 | 17.95 | 17.95 |
| 4 | 16.28 | 16.28 | 17.05 | 17.05 | 13.37 | 13.37 | 16.77 | 16.77 | 12.33 | 12.33 |
| 5 | 14.11 | 14.11 | 14.97 | 14.97 | 14.80 | 14.80 | 13.27 | 13.27 | 18.12 | 18.12 |
| 6 | 13.52 | 13.52 | 16.50 | 16.50 | 17.74 | 17.74 | 13.87 | 13.87 | 18.00 | 18.00 |
| 7 | 14.74 | 14.74 | 17.82 | 17.82 | 16.02 | 16.02 | 19.83 | 19.83 | 14.92 | 14.92 |
| 8 | 15.55 | 15.55 | 16.59 | 16.59 | 14.73 | 14.73 | 17.64 | 17.64 | 14.95 | 14.95 |
| 9 | 13.56 | 13.56 | 15.96 | 15.96 | 18.93 | 18.93 | 16.79 | 16.79 | 14.96 | 14.96 |
| 10 | 11.98 | 11.98 | 16.00 | 16.00 | 15.42 | 15.42 | 16.47 | 16.47 | 15.38 | 15.38 |
| 11 | 15.01 | 15.01 | 19.29 | 19.29 | 16.55 | 16.55 | 15.72 | 15.72 | 16.61 | 16.61 |
| 12 | 15.96 | 15.96 | 14.08 | 14.08 | 13.21 | 13.21 | 15.19 | 15.19 | 15.61 | 15.61 |
| 13 | 17.36 | 17.36 | 16.82 | 16.82 | 15.48 | 15.48 | 16.83 | 16.83 | 13.94 | 13.94 |
| 14 | 15.36 | 15.36 | 13.22 | 13.22 | 16.37 | 16.37 | 13.99 | 13.99 | 16.42 | 16.42 |
| 15 | 15.97 | 15.97 | 17.20 | 17.20 | 17.13 | 17.13 | 17.01 | 17.01 | 16.08 | 16.08 |
| 16 | 15.82 | 15.82 | 14.84 | 14.84 | 14.15 | 14.15 | 15.54 | 15.54 | 13.94 | 13.94 |
| 17 | 16.97 | 16.97 | 15.64 | 15.64 | 16.46 | 16.46 | 15.10 | 15.10 | 16.35 | 16.35 |
| 18 | 15.01 | 15.01 | 15.83 | 15.83 | 16.87 | 16.87 | 13.95 | 13.95 | 15.80 | 15.80 |
| 19 | 15.61 | 15.61 | 16.93 | 16.93 | 16.48 | 16.48 | 14.85 | 14.85 | 15.30 | 15.30 |
| 20 | 16.24 | 16.24 | 17.10 | 17.10 | 16.41 | 16.41 | 14.97 | 14.97 | 15.73 | 15.73 |
| 21 | 17.37 | 17.37 | 16.26 | 16.26 | 15.61 | 15.61 | 14.10 | 14.10 | 16.24 | 16.24 |
| 22 | 18.11 | 18.11 | 15.86 | 15.86 | 13.99 | 13.99 | 15.28 | 15.28 | 15.51 | 15.51 |
| 23 | 16.54 | 16.54 | 16.87 | 16.87 | 13.83 | 13.83 | 16.41 | 16.41 | 13.33 | 13.33 |
| 24 | 15.18 | 15.18 | 14.79 | 14.79 | 14.77 | 14.77 | 13.76 | 13.76 | 13.92 | 13.92 |
| 25 | 15.65 | 15.65 | 14.14 | 14.14 | 15.09 | 15.09 | 14.93 | 14.93 | 14.14 | 14.14 |
| 26 | 15.22 | 15.22 | 15.31 | 15.31 | 14.45 | 14.45 | 12.94 | 12.94 | 15.46 | 15.46 |
| 27 | 13.97 | 13.97 | 15.60 | 15.60 | 15.00 | 15.00 | 15.45 | 15.45 | 14.57 | 14.57 |
| 28 | 15.89 | 15.89 | 13.44 | 13.44 | 12.30 | 12.30 | 14.88 | 14.88 | 12.06 | 12.06 |
| 29 | 15.77 | 15.77 | 13.48 | 13.48 | 14.58 | 14.58 | 13.86 | 13.86 | 14.32 | 14.32 |
| 30 | 14.37 | 14.37 | 14.82 | 14.82 | 15.82 | 15.82 | 13.85 | 13.85 | 15.93 | 15.93 |
| 31 | 14.74 | 14.74 | 15.39 | 15.39 | 14.84 | 14.84 | 14.31 | 14.31 | 15.58 | 15.58 |
| 32 | 15.02 | 15.02 | 14.54 | 14.54 | 15.21 | 15.21 | 14.67 | 14.67 | 15.29 | 15.29 |
| 33 | 15.40 | 15.40 | 14.29 | 14.29 | 14.64 | 14.64 | 14.12 | 14.12 | 15.19 | 15.19 |
| 34 | 14.76 | 14.76 | 14.08 | 14.08 | 12.64 | 12.64 | 13.99 | 13.99 | 12.59 | 12.59 |
| 35 | 13.10 | 13.10 | 13.65 | 13.65 | 13.26 | 13.26 | 13.81 | 13.81 | 10.40 | 10.40 |
| 36 | 14.14 | 14.14 | 14.93 | 14.93 | 13.89 | 13.89 | 14.16 | 14.16 | 12.97 | 12.97 |
| 37 | 14.15 | 14.15 | 11.84 | 11.84 | 11.93 | 11.93 | 10.17 | 10.17 | 9.57 | 9.57 |
| 38 | 13.00 | 13.00 | 13.84 | 13.84 | 12.51 | 12.51 | 13.58 | 13.58 | 9.09 | 9.09 |
| 39 | 13.10 | 13.10 | 11.50 | 11.50 | 13.57 | 13.57 | 8.38 | 8.38 | 9.99 | 9.99 |
| 40 | 10.40 | 10.40 | 11.79 | 11.79 | 12.22 | 12.22 | 9.67 | 9.67 | 8.79 | 8.79 |
| 41 | 12.89 | 12.89 | 10.54 | 10.54 | 10.86 | 10.86 | 9.60 | 9.60 | 6.82 | 6.82 |
| 42 | 11.09 | 11.09 | 12.60 | 12.60 | 12.70 | 12.70 | 8.19 | 8.19 | 9.10 | 9.10 |
| 43 | 10.44 | 10.44 | 13.29 | 13.29 | 12.55 | 12.55 | 9.77 | 9.77 | 7.81 | 7.81 |
| 44 | 10.17 | 10.17 | 12.23 | 12.23 | 12.05 | 12.05 | 9.13 | 9.13 | 6.05 | 6.05 |
| 45 | 11.39 | 11.39 | 12.88 | 12.88 | 11.55 | 11.55 | 9.63 | 9.63 | 9.80 | 9.80 |
| 46 | 13.87 | 13.87 | 12.32 | 12.32 | 9.57 | 9.57 | 11.15 | 11.15 | 8.22 | 8.22 |
| 47 | 11.96 | 11.96 | 10.67 | 10.67 | 5.61 | 5.61 | 4.05 | 4.05 | 2.83 | 2.83 |
| 48 | 12.61 | 12.61 | 12.07 | 12.07 | 6.90 | 6.90 | 11.01 | 11.01 | 6.76 | 6.76 |
| 49 | 9.37 | 9.37 | 8.64 | 8.64 | 2.11 | 2.11 | 3.61 | 3.61 | 7.38 | 7.38 |
| 50 | 10.28 | 10.28 | 9.12 | 9.12 | 7.28 | 7.28 | 4.42 | 4.42 | 5.30 | 5.30 |

| Reflected Angle in ° | Incidence Angle in ° | | | | | | | | | |
|---|---|---|---|---|---|---|---|---|---|---|
| | 11 | 12 | 13 | 14 | 15 | 16 | 17 | 18 | 19 | 20 |
| 51 | 8.81 | 8.81 | -0.67 | -0.67 | 2.82 | 2.82 | 4.40 | 4.40 | 4.83 | 4.83 |
| 52 | 5.03 | 5.03 | 2.79 | 2.79 | 2.24 | 2.24 | 8.24 | 8.24 | 5.27 | 5.27 |
| 53 | 5.82 | 5.82 | -3.64 | -3.64 | 4.26 | 4.26 | 2.06 | 2.06 | 8.64 | 8.64 |
| 54 | 0.31 | 0.31 | 0.77 | 0.77 | 4.68 | 4.68 | 4.35 | 4.35 | 7.13 | 7.13 |
| 55 | -0.42 | -0.42 | 1.28 | 1.28 | 5.07 | 5.07 | 8.13 | 8.13 | 11.17 | 11.17 |
| 56 | 0.78 | 0.78 | 1.59 | 1.59 | 10.21 | 10.21 | 7.65 | 7.65 | 13.48 | 13.48 |
| 57 | 5.18 | 5.18 | 4.87 | 4.87 | 9.62 | 9.62 | 12.55 | 12.55 | 12.75 | 12.75 |
| 58 | 3.92 | 3.92 | 11.13 | 11.13 | 12.28 | 12.28 | 14.32 | 14.32 | 14.44 | 14.44 |
| 59 | 7.24 | 7.24 | 9.87 | 9.87 | 12.88 | 12.88 | 14.69 | 14.69 | 15.56 | 15.56 |
| 60 | 7.43 | 7.43 | 12.89 | 12.89 | 15.62 | 15.62 | 15.48 | 15.48 | 17.71 | 17.71 |
| 61 | 9.83 | 9.83 | 13.96 | 13.96 | 13.84 | 13.84 | 16.77 | 16.77 | 16.75 | 16.75 |
| 62 | 11.79 | 11.79 | 12.50 | 12.50 | 14.31 | 14.31 | 17.36 | 17.36 | 17.83 | 17.83 |
| 63 | 11.00 | 11.00 | 14.68 | 14.68 | 16.53 | 16.53 | 15.29 | 15.29 | 18.11 | 18.11 |
| 64 | 11.25 | 11.25 | 15.24 | 15.24 | 15.64 | 15.64 | 18.12 | 18.12 | 16.54 | 16.54 |
| 65 | 9.80 | 9.80 | 15.86 | 15.86 | 15.96 | 15.96 | 17.84 | 17.84 | 14.34 | 14.34 |
| 66 | 12.59 | 12.59 | 11.63 | 11.63 | 18.09 | 18.09 | 16.31 | 16.31 | 15.39 | 15.39 |
| 67 | 9.35 | 9.35 | 12.30 | 12.30 | 17.85 | 17.85 | 14.72 | 14.72 | 19.30 | 19.30 |
| 68 | 8.74 | 8.74 | 12.33 | 12.33 | 14.26 | 14.26 | 17.71 | 17.71 | 23.06 | 23.06 |
| 69 | 12.56 | 12.56 | 11.20 | 11.20 | 7.09 | 7.09 | 19.49 | 19.49 | 25.86 | 25.86 |
| 70 | 13.83 | 13.83 | 12.59 | 12.59 | 16.21 | 16.21 | 22.44 | 22.44 | 26.23 | 26.23 |
| 71 | 10.27 | 10.27 | 16.50 | 16.50 | 23.71 | 23.71 | 26.23 | 26.23 | 29.53 | 29.53 |
| 72 | 7.76 | 7.76 | 16.88 | 16.88 | 27.90 | 27.90 | 30.05 | 30.05 | 30.17 | 30.17 |
| 73 | 15.41 | 15.41 | 18.38 | 18.38 | 28.33 | 28.33 | 31.16 | 31.16 | 29.14 | 29.14 |
| 74 | 15.39 | 15.39 | 26.00 | 26.00 | 25.83 | 25.83 | 28.80 | 28.80 | 19.09 | 19.09 |
| 75 | 18.98 | 18.98 | 29.17 | 29.17 | 28.08 | 28.08 | 22.18 | 22.18 | 16.63 | 16.63 |
| 76 | 26.82 | 26.82 | 26.84 | 26.84 | 29.72 | 29.72 | 25.42 | 25.42 | 20.33 | 20.33 |
| 77 | 27.36 | 27.36 | 26.50 | 26.50 | 25.49 | 25.49 | 24.10 | 24.10 | 14.15 | 14.15 |
| 78 | 26.57 | 26.57 | 29.60 | 29.60 | 20.42 | 20.42 | 8.67 | 8.67 | 16.44 | 16.44 |
| 79 | 29.61 | 29.61 | 25.07 | 25.07 | 24.00 | 24.00 | 16.74 | 16.74 | 12.74 | 12.74 |
| 80 | 28.11 | 28.11 | 22.41 | 22.41 | 18.01 | 18.01 | 10.34 | 10.34 | 11.95 | 11.95 |
| 81 | 26.16 | 26.16 | 23.21 | 23.21 | 13.21 | 13.21 | 15.57 | 15.57 | 9.81 | 9.81 |
| 82 | 24.69 | 24.69 | 12.97 | 12.97 | 8.77 | 8.77 | 11.95 | 11.95 | 6.43 | 6.43 |
| 83 | 19.12 | 19.12 | 13.01 | 13.01 | 15.79 | 15.79 | 8.88 | 8.88 | 8.37 | 8.37 |
| 84 | 16.34 | 16.34 | 2.29 | 2.29 | 11.86 | 11.86 | 10.66 | 10.66 | 4.80 | 4.80 |
| 85 | 10.77 | 10.77 | 14.62 | 14.62 | 11.53 | 11.53 | 13.58 | 13.58 | 10.74 | 10.74 |
| 86 | 10.64 | 10.64 | 8.20 | 8.20 | 8.35 | 8.35 | 8.85 | 8.85 | 2.29 | 2.29 |
| 87 | 5.73 | 5.73 | 15.99 | 15.99 | 12.98 | 12.98 | 13.58 | 13.58 | 10.30 | 10.30 |
| 88 | 15.33 | 15.33 | 11.34 | 11.34 | 12.06 | 12.06 | 10.48 | 10.48 | 11.93 | 11.93 |
| 89 | 8.87 | 8.87 | 12.20 | 12.20 | 14.74 | 14.74 | 10.46 | 10.46 | 9.67 | 9.67 |
| 90 | 15.98 | 15.98 | 12.75 | 12.75 | 10.10 | 10.10 | 11.48 | 11.48 | 6.59 | 6.59 |
| 91 | 13.26 | 13.26 | 10.41 | 10.41 | 7.80 | 7.80 | 8.73 | 8.73 | 0.91 | 0.91 |
| 92 | 9.80 | 9.80 | 14.98 | 14.98 | 10.63 | 10.63 | 6.41 | 6.41 | 4.38 | 4.38 |
| 93 | 11.87 | 11.87 | 8.53 | 8.53 | 10.93 | 10.93 | 10.57 | 10.57 | 10.18 | 10.18 |
| 94 | 11.37 | 11.37 | 2.33 | 2.33 | 8.64 | 8.64 | 8.81 | 8.81 | 4.86 | 4.86 |
| 95 | 8.96 | 8.96 | 5.60 | 5.60 | 6.25 | 6.25 | 7.27 | 7.27 | 12.71 | 12.71 |
| 96 | 5.03 | 5.03 | 4.74 | 4.74 | 6.89 | 6.89 | 10.01 | 10.01 | 7.65 | 7.65 |
| 97 | 8.06 | 8.06 | 9.02 | 9.02 | 7.69 | 7.69 | 15.85 | 15.85 | 8.54 | 8.54 |
| 98 | 2.30 | 2.30 | 7.93 | 7.93 | 11.04 | 11.04 | 14.10 | 14.10 | 11.99 | 11.99 |
| 99 | 9.46 | 9.46 | 8.97 | 8.97 | 4.29 | 4.29 | 15.07 | 15.07 | 10.01 | 10.01 |
| 100 | 8.12 | 8.12 | 11.81 | 11.81 | 14.60 | 14.60 | 13.22 | 13.22 | 10.06 | 10.06 |

| Reflected Angle in ° | Incidence Angle in ° | | | | | | | | | |
|---|---|---|---|---|---|---|---|---|---|---|
| | 11 | 12 | 13 | 14 | 15 | 16 | 17 | 18 | 19 | 20 |
| 101 | 10.68 | 10.68 | 4.44 | 4.44 | 9.91 | 9.91 | 14.41 | 14.41 | 10.51 | 10.51 |
| 102 | 7.26 | 7.26 | 13.24 | 13.24 | 13.05 | 13.05 | 12.18 | 12.18 | 12.41 | 12.41 |
| 103 | 13.60 | 13.60 | 10.05 | 10.05 | 11.40 | 11.40 | 11.65 | 11.65 | 11.46 | 11.46 |
| 104 | 14.30 | 14.30 | 11.65 | 11.65 | 12.71 | 12.71 | 14.10 | 14.10 | 9.89 | 9.89 |
| 105 | 8.95 | 8.95 | 11.43 | 11.43 | 12.47 | 12.47 | 10.70 | 10.70 | 8.26 | 8.26 |
| 106 | 4.47 | 4.47 | 10.15 | 10.15 | 13.28 | 13.28 | 9.30 | 9.30 | 10.99 | 10.99 |
| 107 | 6.38 | 6.38 | 12.15 | 12.15 | 11.81 | 11.81 | 12.14 | 12.14 | 9.87 | 9.87 |
| 108 | 7.64 | 7.64 | 10.50 | 10.50 | 12.22 | 12.22 | 12.93 | 12.93 | 15.91 | 15.91 |
| 109 | -2.55 | -2.55 | 10.25 | 10.25 | 12.97 | 12.97 | 10.96 | 10.96 | 14.80 | 14.80 |
| 110 | -1.28 | -1.28 | 8.55 | 8.55 | 12.03 | 12.03 | 14.63 | 14.63 | 3.91 | 3.91 |
| 111 | 4.63 | 4.63 | 5.51 | 5.51 | 10.56 | 10.56 | 15.03 | 15.03 | 8.76 | 8.76 |
| 112 | 1.06 | 1.06 | 5.99 | 5.99 | 11.24 | 11.24 | 7.39 | 7.39 | 9.28 | 9.28 |
| 113 | 2.90 | 2.90 | 3.35 | 3.35 | 13.32 | 13.32 | 8.88 | 8.88 | 10.99 | 10.99 |
| 114 | 7.26 | 7.26 | 11.48 | 11.48 | 13.18 | 13.18 | 12.55 | 12.55 | 21.19 | 21.19 |
| 115 | 10.30 | 10.30 | 12.28 | 12.28 | 7.29 | 7.29 | -1.36 | -1.36 | 21.23 | 21.23 |
| 116 | 6.53 | 6.53 | 9.76 | 9.76 | 8.97 | 8.97 | 15.38 | 15.38 | 13.13 | 13.13 |
| 117 | 16.10 | 16.10 | -1.59 | -1.59 | -6.16 | -6.16 | 16.31 | 16.31 | 4.87 | 4.87 |
| 118 | 13.78 | 13.78 | 8.08 | 8.08 | 17.84 | 17.84 | 11.11 | 11.11 | 8.48 | 8.48 |
| 119 | 10.90 | 10.90 | 2.39 | 2.39 | 18.99 | 18.99 | 12.25 | 12.25 | 8.68 | 8.68 |
| 120 | 15.62 | 15.62 | 19.00 | 19.00 | 3.99 | 3.99 | 9.62 | 9.62 | 8.51 | 8.51 |
| 121 | 14.13 | 14.13 | 18.04 | 18.04 | -3.29 | -3.29 | 7.63 | 7.63 | 9.46 | 9.46 |
| 122 | 17.68 | 17.68 | 10.38 | 10.38 | 5.94 | 5.94 | 10.90 | 10.90 | 11.62 | 11.62 |
| 123 | 21.62 | 21.62 | 12.74 | 12.74 | 2.75 | 2.75 | 10.60 | 10.60 | 24.58 | 24.58 |
| 124 | 10.10 | 10.10 | 3.16 | 3.16 | 11.19 | 11.19 | 10.52 | 10.52 | 12.99 | 12.99 |
| 125 | 14.20 | 14.20 | 11.31 | 11.31 | 6.89 | 6.89 | 24.70 | 24.70 | 11.18 | 11.18 |
| 126 | 10.80 | 10.80 | 11.91 | 11.91 | 8.59 | 8.59 | 6.02 | 6.02 | 16.74 | 16.74 |
| 127 | 7.36 | 7.36 | 9.80 | 9.80 | 25.48 | 25.48 | 13.89 | 13.89 | 9.60 | 9.60 |
| 128 | 7.68 | 7.68 | 8.76 | 8.76 | 11.18 | 11.18 | 17.92 | 17.92 | 18.73 | 18.73 |
| 129 | 6.78 | 6.78 | 22.86 | 22.86 | 13.99 | 13.99 | 18.28 | 18.28 | 8.53 | 8.53 |
| 130 | 9.00 | 9.00 | 6.44 | 6.44 | 8.74 | 8.74 | 15.49 | 15.49 | 11.10 | 11.10 |
| 131 | 23.50 | 23.50 | 10.69 | 10.69 | 10.95 | 10.95 | 10.00 | 10.00 | 16.72 | 16.72 |
| 132 | 15.13 | 15.13 | 12.46 | 12.46 | 12.76 | 12.76 | 12.76 | 12.76 | 16.54 | 16.54 |
| 133 | 17.40 | 17.40 | 13.77 | 13.77 | 9.26 | 9.26 | 14.86 | 14.86 | 19.61 | 19.61 |
| 134 | 18.21 | 18.21 | 16.74 | 16.74 | 5.08 | 5.08 | 13.61 | 13.61 | 15.50 | 15.50 |
| 135 | 1.45 | 1.45 | 14.24 | 14.24 | 11.09 | 11.09 | 9.14 | 9.14 | 13.37 | 13.37 |
| 136 | 18.06 | 18.06 | 11.50 | 11.50 | 7.42 | 7.42 | 18.17 | 18.17 | 9.98 | 9.98 |
| 137 | 8.48 | 8.48 | 1.70 | 1.70 | 9.42 | 9.42 | 9.47 | 9.47 | 14.11 | 14.11 |
| 138 | 3.52 | 3.52 | 13.33 | 13.33 | 16.23 | 16.23 | 11.10 | 11.10 | 16.03 | 16.03 |
| 139 | 7.95 | 7.95 | 8.36 | 8.36 | 12.11 | 12.11 | 10.50 | 10.50 | 16.52 | 16.52 |
| 140 | 15.69 | 15.69 | 22.12 | 22.12 | 9.07 | 9.07 | 11.21 | 11.21 | 9.73 | 9.73 |
| 141 | 15.90 | 15.90 | 16.04 | 16.04 | 4.56 | 4.56 | 8.77 | 8.77 | 14.84 | 14.84 |
| 142 | 20.79 | 20.79 | 16.65 | 16.65 | 12.86 | 12.86 | 12.12 | 12.12 | 14.92 | 14.92 |
| 143 | 7.87 | 7.87 | 6.29 | 6.29 | 12.45 | 12.45 | 11.67 | 11.67 | 11.66 | 11.66 |
| 144 | 9.72 | 9.72 | 13.41 | 13.41 | 9.43 | 9.43 | 18.09 | 18.09 | 16.16 | 16.16 |
| 145 | 15.70 | 15.70 | 11.12 | 11.12 | 17.31 | 17.31 | 12.11 | 12.11 | 12.86 | 12.86 |
| 146 | 10.03 | 10.03 | 16.41 | 16.41 | 7.30 | 7.30 | 12.32 | 12.32 | 15.34 | 15.34 |
| 147 | 9.46 | 9.46 | 11.70 | 11.70 | 18.18 | 18.18 | 16.90 | 16.90 | 21.60 | 21.60 |
| 148 | 8.73 | 8.73 | 12.57 | 12.57 | 18.92 | 18.92 | 18.78 | 18.78 | 20.02 | 20.02 |
| 149 | 11.96 | 11.96 | 14.32 | 14.32 | 18.05 | 18.05 | 15.39 | 15.39 | 15.90 | 15.90 |
| 150 | 7.73 | 7.73 | 15.66 | 15.66 | 20.87 | 20.87 | 16.15 | 16.15 | 21.16 | 21.16 |

| Reflected Angle in ° | Incidence Angle in ° | | | | | | | | | |
|---|---|---|---|---|---|---|---|---|---|---|
| | 11 | 12 | 13 | 14 | 15 | 16 | 17 | 18 | 19 | 20 |
| 151 | 9.66 | 9.66 | 14.74 | 14.74 | 16.43 | 16.43 | 17.13 | 17.13 | 15.55 | 15.55 |
| 152 | 10.69 | 10.69 | 11.68 | 11.68 | 16.60 | 16.60 | 15.64 | 15.64 | 13.44 | 13.44 |
| 153 | 18.65 | 18.65 | 18.04 | 18.04 | 18.21 | 18.21 | 17.20 | 17.20 | 21.33 | 21.33 |
| 154 | 18.47 | 18.47 | 11.43 | 11.43 | 17.83 | 17.83 | 11.98 | 11.98 | 23.36 | 23.36 |
| 155 | 20.81 | 20.81 | 8.87 | 8.87 | 8.40 | 8.40 | 14.01 | 14.01 | 27.01 | 27.01 |
| 156 | 16.17 | 16.17 | 14.74 | 14.74 | 19.41 | 19.41 | 29.56 | 29.56 | 26.58 | 26.58 |
| 157 | 14.37 | 14.37 | 11.35 | 11.35 | 24.99 | 24.99 | 32.88 | 32.88 | 32.84 | 32.84 |
| 158 | 21.56 | 21.56 | 19.58 | 19.58 | 26.64 | 26.64 | 32.65 | 32.65 | 36.11 | 36.11 |
| 159 | 24.22 | 24.22 | 22.44 | 22.44 | 30.23 | 30.23 | 29.60 | 29.60 | 39.23 | 39.23 |
| 160 | 18.62 | 18.62 | 26.54 | 26.54 | 31.02 | 31.02 | 29.36 | 29.36 | 38.50 | 38.50 |
| 161 | 19.23 | 19.23 | 24.40 | 24.40 | 33.88 | 33.88 | 34.25 | 34.25 | 41.75 | 41.75 |
| 162 | 27.19 | 27.19 | 21.68 | 21.68 | 31.56 | 31.56 | 35.21 | 35.21 | 54.47 | 54.47 |
| 163 | 30.19 | 30.19 | 28.26 | 28.26 | 34.43 | 34.43 | 40.25 | 40.25 | 43.28 | 43.28 |
| 164 | 28.93 | 28.93 | 33.02 | 33.02 | 30.40 | 30.40 | 52.28 | 52.28 | 36.20 | 36.20 |
| 165 | 33.03 | 33.03 | 34.80 | 34.80 | 36.93 | 36.93 | 40.23 | 40.23 | 28.58 | 28.58 |
| 166 | 28.18 | 28.18 | 37.36 | 37.36 | 46.81 | 46.81 | 36.30 | 36.30 | 30.53 | 30.53 |
| 167 | 34.73 | 34.73 | 37.38 | 37.38 | 39.51 | 39.51 | 32.44 | 32.44 | 34.91 | 34.91 |
| 168 | 40.28 | 40.28 | 47.95 | 47.95 | 41.66 | 41.66 | 21.85 | 21.85 | 35.35 | 35.35 |
| 169 | 39.35 | 39.35 | 40.01 | 40.01 | 36.37 | 36.37 | 32.66 | 32.66 | 25.63 | 25.63 |
| 170 | 50.69 | 50.69 | 40.69 | 40.69 | 28.49 | 28.49 | 31.44 | 31.44 | 31.03 | 31.03 |
| 171 | 37.33 | 37.33 | 37.37 | 37.37 | 35.07 | 35.07 | 32.70 | 32.70 | 26.56 | 26.56 |
| 172 | 37.94 | 37.94 | 35.89 | 35.89 | 32.91 | 32.91 | 27.00 | 27.00 | 32.41 | 32.41 |
| 173 | 37.27 | 37.27 | 36.60 | 36.60 | 34.32 | 34.32 | 31.23 | 31.23 | 31.82 | 31.82 |
| 174 | 34.86 | 34.86 | 28.22 | 28.22 | 30.51 | 30.51 | 32.62 | 32.62 | 17.80 | 17.80 |
| 175 | 32.68 | 32.68 | 32.99 | 32.99 | 33.10 | 33.10 | 34.89 | 34.89 | 32.87 | 32.87 |
| 176 | 31.38 | 31.38 | 29.22 | 29.22 | 23.01 | 23.01 | 31.49 | 31.49 | 22.49 | 22.49 |
| 177 | 33.01 | 33.01 | 26.73 | 26.73 | 35.09 | 35.09 | 32.50 | 32.50 | 32.50 | 32.50 |
| 178 | 22.70 | 22.70 | 33.06 | 33.06 | 35.15 | 35.15 | 11.79 | 11.79 | 32.61 | 32.61 |
| 179 | 31.53 | 31.53 | 37.49 | 37.49 | 32.11 | 32.11 | 30.74 | 30.74 | 23.67 | 23.67 |
| 180 | 29.61 | 29.61 | 35.13 | 35.13 | 30.06 | 30.06 | 34.77 | 34.77 | 27.86 | 27.86 |
| 181 | 32.42 | 32.42 | 31.90 | 31.90 | 27.43 | 27.43 | 37.66 | 37.66 | 26.77 | 26.77 |
| 182 | 33.26 | 33.26 | 31.96 | 31.96 | 32.34 | 32.34 | 39.75 | 39.75 | 28.89 | 28.89 |
| 183 | 28.02 | 28.02 | 38.76 | 38.76 | 38.59 | 38.59 | 38.83 | 38.83 | 29.97 | 29.97 |
| 184 | 42.72 | 42.72 | 41.91 | 41.91 | 41.66 | 41.66 | 26.19 | 26.19 | 35.39 | 35.39 |
| 185 | 45.36 | 45.36 | 35.09 | 35.09 | 37.95 | 37.95 | 38.96 | 38.96 | 37.70 | 37.70 |
| 186 | 39.30 | 39.30 | 40.98 | 40.98 | 38.72 | 38.72 | 41.36 | 41.36 | 30.89 | 30.89 |
| 187 | 40.59 | 40.59 | 39.56 | 39.56 | 41.12 | 41.12 | 38.74 | 38.74 | 38.75 | 38.75 |
| 188 | 50.11 | 50.11 | 46.48 | 46.48 | 38.01 | 38.01 | 41.69 | 41.69 | 27.07 | 27.07 |
| 189 | 50.90 | 50.90 | 37.73 | 37.73 | 42.80 | 42.80 | 43.06 | 43.06 | 42.86 | 42.86 |
| 190 | 83.95 | 83.95 | 37.84 | 37.84 | 36.81 | 36.81 | 41.47 | 41.47 | 41.85 | 41.85 |
| 191 | 55.81 | 55.81 | 58.30 | 58.30 | 45.54 | 45.54 | 39.89 | 39.89 | 41.62 | 41.62 |
| 192 | 40.31 | 40.31 | 84.69 | 84.69 | 52.59 | 52.59 | 45.87 | 45.87 | 43.66 | 43.66 |
| 193 | 44.33 | 44.33 | 60.30 | 60.30 | 60.51 | 60.51 | 43.02 | 43.02 | 44.69 | 44.69 |
| 194 | 32.20 | 32.20 | 51.64 | 51.64 | 85.36 | 85.36 | 44.65 | 44.65 | 42.19 | 42.19 |
| 195 | 33.14 | 33.14 | 41.08 | 41.08 | 55.51 | 55.51 | 50.19 | 50.19 | 39.39 | 39.39 |
| 196 | 39.00 | 39.00 | 44.49 | 44.49 | 46.14 | 46.14 | 85.92 | 85.92 | 51.24 | 51.24 |
| 197 | 35.15 | 35.15 | 43.09 | 43.09 | 35.30 | 35.30 | 57.27 | 57.27 | 60.06 | 60.06 |
| 198 | 33.91 | 33.91 | 41.61 | 41.61 | 37.11 | 37.11 | 49.93 | 49.93 | 86.58 | 86.58 |
| 199 | 28.76 | 28.76 | 37.96 | 37.96 | 41.21 | 41.21 | 43.63 | 43.63 | 60.17 | 60.17 |
| 200 | 24.61 | 24.61 | 18.10 | 18.10 | 28.91 | 28.91 | 46.88 | 46.88 | 40.60 | 40.60 |

| Reflected Angle in ° | Incidence Angle in ° | | | | | | | | | |
|---|---|---|---|---|---|---|---|---|---|---|
| | 11 | 12 | 13 | 14 | 15 | 16 | 17 | 18 | 19 | 20 |
| 201 | 26.93 | 26.93 | 28.86 | 28.86 | 33.44 | 33.44 | 37.48 | 37.48 | 46.33 | 46.33 |
| 202 | 19.69 | 19.69 | 23.90 | 23.90 | 28.74 | 28.74 | 34.07 | 34.07 | 37.44 | 37.44 |
| 203 | 21.25 | 21.25 | 19.67 | 19.67 | 32.42 | 32.42 | 27.21 | 27.21 | 29.36 | 29.36 |
| 204 | 18.66 | 18.66 | 19.73 | 19.73 | 22.56 | 22.56 | 30.18 | 30.18 | 33.55 | 33.55 |
| 205 | 10.44 | 10.44 | 22.40 | 22.40 | 24.29 | 24.29 | 23.99 | 23.99 | 33.37 | 33.37 |
| 206 | 24.83 | 24.83 | 30.02 | 30.02 | 23.95 | 23.95 | 10.09 | 10.09 | 30.32 | 30.32 |
| 207 | 22.80 | 22.80 | 25.21 | 25.21 | 16.82 | 16.82 | 18.88 | 18.88 | 31.67 | 31.67 |
| 208 | 25.08 | 25.08 | 25.10 | 25.10 | 20.90 | 20.90 | 22.73 | 22.73 | 17.32 | 17.32 |
| 209 | 25.88 | 25.88 | 18.85 | 18.85 | 16.69 | 16.69 | 17.23 | 17.23 | 27.69 | 27.69 |
| 210 | 4.64 | 4.64 | 5.57 | 5.57 | 5.99 | 5.99 | 27.32 | 27.32 | 19.74 | 19.74 |
| 211 | 23.53 | 23.53 | 16.59 | 16.59 | 15.15 | 15.15 | 14.88 | 14.88 | 19.19 | 19.19 |
| 212 | 19.98 | 19.98 | 18.79 | 18.79 | 12.65 | 12.65 | 14.87 | 14.87 | 23.79 | 23.79 |
| 213 | 20.63 | 20.63 | 21.88 | 21.88 | 22.70 | 22.70 | 21.13 | 21.13 | 14.20 | 14.20 |
| 214 | 19.24 | 19.24 | 23.21 | 23.21 | 18.60 | 18.60 | 22.92 | 22.92 | 12.72 | 12.72 |
| 215 | 22.14 | 22.14 | 25.15 | 25.15 | 22.06 | 22.06 | 21.86 | 21.86 | 9.77 | 9.77 |
| 216 | 22.93 | 22.93 | 20.15 | 20.15 | 24.08 | 24.08 | 13.52 | 13.52 | 18.52 | 18.52 |
| 217 | 23.33 | 23.33 | 22.29 | 22.29 | 24.36 | 24.36 | 20.28 | 20.28 | 23.44 | 23.44 |
| 218 | 22.53 | 22.53 | 21.73 | 21.73 | 18.82 | 18.82 | 19.74 | 19.74 | 17.58 | 17.58 |
| 219 | 17.18 | 17.18 | 20.49 | 20.49 | 20.58 | 20.58 | 20.87 | 20.87 | 21.98 | 21.98 |
| 220 | 15.55 | 15.55 | 18.00 | 18.00 | 19.70 | 19.70 | 18.15 | 18.15 | 21.78 | 21.78 |
| 221 | 15.22 | 15.22 | 12.67 | 12.67 | 14.45 | 14.45 | 13.46 | 13.46 | 10.40 | 10.40 |
| 222 | 10.03 | 10.03 | 16.70 | 16.70 | 7.56 | 7.56 | 16.08 | 16.08 | 16.38 | 16.38 |
| 223 | 17.08 | 17.08 | 9.66 | 9.66 | 8.92 | 8.92 | 12.97 | 12.97 | 15.80 | 15.80 |
| 224 | 13.40 | 13.40 | 5.77 | 5.77 | 9.89 | 9.89 | 15.47 | 15.47 | 16.04 | 16.04 |
| 225 | -2.65 | -2.65 | 8.37 | 8.37 | 13.50 | 13.50 | 15.52 | 15.52 | 14.49 | 14.49 |
| 226 | 10.79 | 10.79 | 8.98 | 8.98 | 7.73 | 7.73 | 9.05 | 9.05 | 6.64 | 6.64 |
| 227 | 13.99 | 13.99 | -2.79 | -2.79 | 5.46 | 5.46 | 15.66 | 15.66 | 15.59 | 15.59 |
| 228 | 15.07 | 15.07 | 8.83 | 8.83 | 8.97 | 8.97 | 8.75 | 8.75 | 6.41 | 6.41 |
| 229 | 13.74 | 13.74 | 12.52 | 12.52 | 12.31 | 12.31 | -1.11 | -1.11 | -0.51 | -0.51 |
| 230 | 13.68 | 13.68 | 10.72 | 10.72 | 13.56 | 13.56 | -1.10 | -1.10 | 4.49 | 4.49 |
| 231 | 11.18 | 11.18 | 11.23 | 11.23 | 16.52 | 16.52 | 8.99 | 8.99 | -9.12 | -9.12 |
| 232 | 13.41 | 13.41 | 15.49 | 15.49 | 14.13 | 14.13 | 14.54 | 14.54 | 4.20 | 4.20 |
| 233 | 15.07 | 15.07 | 15.89 | 15.89 | 8.99 | 8.99 | 10.30 | 10.30 | -6.03 | -6.03 |
| 234 | 12.57 | 12.57 | 15.55 | 15.55 | 15.78 | 15.78 | 11.79 | 11.79 | 10.53 | 10.53 |
| 235 | 10.26 | 10.26 | 14.60 | 14.60 | 15.43 | 15.43 | 14.90 | 14.90 | 9.30 | 9.30 |
| 236 | 14.67 | 14.67 | 15.61 | 15.61 | 15.45 | 15.45 | 13.36 | 13.36 | 17.97 | 17.97 |
| 237 | 11.07 | 11.07 | 13.10 | 13.10 | 12.80 | 12.80 | 12.45 | 12.45 | 13.73 | 13.73 |
| 238 | 9.84 | 9.84 | 12.74 | 12.74 | 13.75 | 13.75 | 14.33 | 14.33 | 9.68 | 9.68 |
| 239 | 8.08 | 8.08 | 13.99 | 13.99 | 15.70 | 15.70 | 18.14 | 18.14 | 17.22 | 17.22 |
| 240 | 11.31 | 11.31 | 10.63 | 10.63 | 15.28 | 15.28 | 14.58 | 14.58 | 16.39 | 16.39 |
| 241 | 8.86 | 8.86 | 11.34 | 11.34 | 11.11 | 11.11 | 14.97 | 14.97 | 13.57 | 13.57 |
| 242 | 6.55 | 6.55 | 12.75 | 12.75 | 5.86 | 5.86 | 14.02 | 14.02 | 12.58 | 12.58 |
| 243 | 6.43 | 6.43 | 3.37 | 3.37 | 9.60 | 9.60 | 10.88 | 10.88 | 15.98 | 15.98 |
| 244 | -4.93 | -4.93 | 10.53 | 10.53 | 8.47 | 8.47 | 14.51 | 14.51 | 14.03 | 14.03 |
| 245 | -3.66 | -3.66 | 3.64 | 3.64 | 5.07 | 5.07 | 14.81 | 14.81 | 13.13 | 13.13 |
| 246 | 14.16 | 14.16 | 1.68 | 1.68 | 2.73 | 2.73 | 11.55 | 11.55 | 14.45 | 14.45 |
| 247 | 10.29 | 10.29 | 12.28 | 12.28 | 3.31 | 3.31 | 8.65 | 8.65 | 9.94 | 9.94 |
| 248 | 14.57 | 14.57 | 1.15 | 1.15 | -1.60 | -1.60 | 9.87 | 9.87 | -1.54 | -1.54 |
| 249 | 12.25 | 12.25 | 7.31 | 7.31 | 2.54 | 2.54 | 9.24 | 9.24 | 6.46 | 6.46 |
| 250 | 11.37 | 11.37 | 9.89 | 9.89 | 8.39 | 8.39 | 5.66 | 5.66 | 12.62 | 12.62 |

| Reflected Angle in ° | Incidence Angle in ° | | | | | | | | | |
|---|---|---|---|---|---|---|---|---|---|---|
| | 11 | 12 | 13 | 14 | 15 | 16 | 17 | 18 | 19 | 20 |
| 251 | 10.31 | 10.31 | 9.78 | 9.78 | 7.74 | 7.74 | 13.26 | 13.26 | 16.25 | 16.25 |
| 252 | 12.99 | 12.99 | 12.40 | 12.40 | 13.07 | 13.07 | 13.30 | 13.30 | 12.78 | 12.78 |
| 253 | 15.30 | 15.30 | 14.23 | 14.23 | 17.40 | 17.40 | 9.52 | 9.52 | 5.17 | 5.17 |
| 254 | 13.25 | 13.25 | 17.39 | 17.39 | 16.33 | 16.33 | 11.89 | 11.89 | 11.95 | 11.95 |
| 255 | 14.33 | 14.33 | 18.77 | 18.77 | 0.44 | 0.44 | 15.89 | 15.89 | 6.25 | 6.25 |
| 256 | 16.44 | 16.44 | 18.34 | 18.34 | 15.91 | 15.91 | 15.92 | 15.92 | 3.09 | 3.09 |
| 257 | 14.52 | 14.52 | 12.42 | 12.42 | 14.04 | 14.04 | 14.59 | 14.59 | 6.11 | 6.11 |
| 258 | 13.31 | 13.31 | 17.21 | 17.21 | 16.87 | 16.87 | 4.95 | 4.95 | 8.93 | 8.93 |
| 259 | 17.82 | 17.82 | 14.52 | 14.52 | 8.33 | 8.33 | 8.42 | 8.42 | 11.43 | 11.43 |
| 260 | 4.80 | 4.80 | 22.90 | 22.90 | 13.68 | 13.68 | 11.47 | 11.47 | 13.76 | 13.76 |
| 261 | 12.45 | 12.45 | 12.99 | 12.99 | 5.33 | 5.33 | 12.02 | 12.02 | 13.92 | 13.92 |
| 262 | 20.96 | 20.96 | 10.61 | 10.61 | 4.07 | 4.07 | 14.77 | 14.77 | 10.42 | 10.42 |
| 263 | 16.69 | 16.69 | 15.10 | 15.10 | 12.84 | 12.84 | 15.70 | 15.70 | 11.08 | 11.08 |
| 264 | 14.92 | 14.92 | 10.23 | 10.23 | 14.19 | 14.19 | 10.38 | 10.38 | 14.61 | 14.61 |
| 265 | 12.07 | 12.07 | 8.86 | 8.86 | 12.99 | 12.99 | 11.49 | 11.49 | 14.72 | 14.72 |
| 266 | 15.69 | 15.69 | 11.87 | 11.87 | 10.99 | 10.99 | 8.46 | 8.46 | 15.20 | 15.20 |
| 267 | 10.63 | 10.63 | 9.18 | 9.18 | 0.19 | 0.19 | 11.83 | 11.83 | 15.57 | 15.57 |
| 268 | 15.12 | 15.12 | 11.73 | 11.73 | 11.47 | 11.47 | 11.60 | 11.60 | 11.15 | 11.15 |
| 269 | 11.96 | 11.96 | 7.24 | 7.24 | 6.87 | 6.87 | 13.39 | 13.39 | 10.46 | 10.46 |
| 270 | 13.29 | 13.29 | 11.01 | 11.01 | 15.50 | 15.50 | 11.33 | 11.33 | 12.30 | 12.30 |
| 271 | 8.78 | 8.78 | 3.39 | 3.39 | 7.87 | 7.87 | 8.12 | 8.12 | 13.84 | 13.84 |
| 272 | 9.09 | 9.09 | 12.56 | 12.56 | 10.11 | 10.11 | 10.54 | 10.54 | 7.37 | 7.37 |
| 273 | 9.57 | 9.57 | 11.24 | 11.24 | 12.77 | 12.77 | 11.49 | 11.49 | 7.51 | 7.51 |
| 274 | 12.56 | 12.56 | 10.99 | 10.99 | 14.92 | 14.92 | 11.53 | 11.53 | 11.00 | 11.00 |
| 275 | 8.32 | 8.32 | 10.60 | 10.60 | 13.09 | 13.09 | 10.69 | 10.69 | 6.70 | 6.70 |
| 276 | 9.35 | 9.35 | 15.38 | 15.38 | 15.00 | 15.00 | 13.69 | 13.69 | 8.87 | 8.87 |
| 277 | 10.55 | 10.55 | 12.08 | 12.08 | 12.31 | 12.31 | 10.09 | 10.09 | 8.15 | 8.15 |
| 278 | 10.08 | 10.08 | 14.64 | 14.64 | 12.48 | 12.48 | 13.17 | 13.17 | -0.71 | -0.71 |
| 279 | 12.23 | 12.23 | 11.88 | 11.88 | 14.98 | 14.98 | 9.96 | 9.96 | 2.47 | 2.47 |
| 280 | 11.63 | 11.63 | 13.50 | 13.50 | 13.82 | 13.82 | 10.73 | 10.73 | -1.04 | -1.04 |
| 281 | 13.21 | 13.21 | 12.22 | 12.22 | 14.38 | 14.38 | 6.90 | 6.90 | 6.84 | 6.84 |
| 282 | 13.29 | 13.29 | 15.44 | 15.44 | 13.09 | 13.09 | 11.52 | 11.52 | 6.10 | 6.10 |
| 283 | 14.36 | 14.36 | 14.15 | 14.15 | 9.71 | 9.71 | 8.31 | 8.31 | 9.90 | 9.90 |
| 284 | 12.15 | 12.15 | 11.79 | 11.79 | 12.76 | 12.76 | 8.26 | 8.26 | 10.02 | 10.02 |
| 285 | 11.12 | 11.12 | 13.90 | 13.90 | 10.54 | 10.54 | 11.37 | 11.37 | 7.42 | 7.42 |
| 286 | 10.75 | 10.75 | 8.38 | 8.38 | 8.82 | 8.82 | 11.70 | 11.70 | 11.18 | 11.18 |
| 287 | 12.72 | 12.72 | 8.62 | 8.62 | 10.85 | 10.85 | 10.44 | 10.44 | 11.48 | 11.48 |
| 288 | 7.37 | 7.37 | 8.92 | 8.92 | 11.45 | 11.45 | 10.17 | 10.17 | 12.44 | 12.44 |
| 289 | 8.52 | 8.52 | 9.80 | 9.80 | 11.49 | 11.49 | 10.36 | 10.36 | 12.48 | 12.48 |
| 290 | 8.79 | 8.79 | 9.09 | 9.09 | 11.72 | 11.72 | 12.72 | 12.72 | 12.69 | 12.69 |
| 291 | 8.96 | 8.96 | 9.09 | 9.09 | 12.86 | 12.86 | 12.54 | 12.54 | 11.54 | 11.54 |
| 292 | 1.99 | 1.99 | 10.58 | 10.58 | 11.79 | 11.79 | 11.22 | 11.22 | 12.62 | 12.62 |
| 293 | 6.17 | 6.17 | 8.94 | 8.94 | 10.42 | 10.42 | 9.44 | 9.44 | 13.15 | 13.15 |
| 294 | 8.14 | 8.14 | 4.72 | 4.72 | 10.41 | 10.41 | 7.51 | 7.51 | 10.39 | 10.39 |
| 295 | 6.14 | 6.14 | 6.44 | 6.44 | 7.96 | 7.96 | 11.16 | 11.16 | 10.47 | 10.47 |
| 296 | -7.47 | -7.47 | 9.03 | 9.03 | 8.80 | 8.80 | 9.67 | 9.67 | 7.59 | 7.59 |
| 297 | 6.43 | 6.43 | -7.54 | -7.54 | 6.69 | 6.69 | 6.85 | 6.85 | 10.68 | 10.68 |
| 298 | 2.71 | 2.71 | 7.44 | 7.44 | 0.81 | 0.81 | 9.90 | 9.90 | 9.32 | 9.32 |
| 299 | 4.45 | 4.45 | -2.89 | -2.89 | 5.70 | 5.70 | 9.92 | 9.92 | 12.73 | 12.73 |
| 300 | 4.58 | 4.58 | 6.40 | 6.40 | 3.18 | 3.18 | 10.46 | 10.46 | 9.52 | 9.52 |

| Reflected Angle in ° | Incidence Angle in ° | | | | | | | | | |
|---|---|---|---|---|---|---|---|---|---|---|
| | 11 | 12 | 13 | 14 | 15 | 16 | 17 | 18 | 19 | 20 |
| 301 | 5.28 | 5.28 | 3.16 | 3.16 | 3.72 | 3.72 | 6.93 | 6.93 | 13.80 | 13.80 |
| 302 | 11.06 | 11.06 | 2.06 | 2.06 | 6.87 | 6.87 | 6.29 | 6.29 | 14.89 | 14.89 |
| 303 | 4.20 | 4.20 | 11.00 | 11.00 | 7.69 | 7.69 | 5.36 | 5.36 | 7.11 | 7.11 |
| 304 | 9.83 | 9.83 | 8.22 | 8.22 | 8.10 | 8.10 | 10.56 | 10.56 | 5.37 | 5.37 |
| 305 | 5.66 | 5.66 | 12.15 | 12.15 | 5.38 | 5.38 | 5.85 | 5.85 | 6.80 | 6.80 |
| 306 | 12.01 | 12.01 | 11.42 | 11.42 | 14.62 | 14.62 | 12.52 | 12.52 | 6.65 | 6.65 |
| 307 | 8.73 | 8.73 | 15.30 | 15.30 | 14.25 | 14.25 | 11.42 | 11.42 | 4.77 | 4.77 |
| 308 | 12.64 | 12.64 | 12.85 | 12.85 | 8.95 | 8.95 | 14.04 | 14.04 | 7.49 | 7.49 |
| 309 | 11.39 | 11.39 | 12.33 | 12.33 | 14.35 | 14.35 | 14.33 | 14.33 | 11.74 | 11.74 |
| 310 | 15.84 | 15.84 | 12.96 | 12.96 | 13.52 | 13.52 | 10.67 | 10.67 | 11.35 | 11.35 |
| 311 | 16.01 | 16.01 | 14.72 | 14.72 | 14.64 | 14.64 | 14.54 | 14.54 | 9.99 | 9.99 |
| 312 | 15.71 | 15.71 | 13.32 | 13.32 | 15.24 | 15.24 | 11.39 | 11.39 | 12.73 | 12.73 |
| 313 | 14.79 | 14.79 | 15.11 | 15.11 | 14.77 | 14.77 | 15.30 | 15.30 | 9.21 | 9.21 |
| 314 | 15.76 | 15.76 | 12.58 | 12.58 | 14.48 | 14.48 | 9.43 | 9.43 | 12.43 | 12.43 |
| 315 | 15.47 | 15.47 | 15.98 | 15.98 | 16.22 | 16.22 | 13.57 | 13.57 | 13.69 | 13.69 |
| 316 | 15.38 | 15.38 | 16.44 | 16.44 | 16.12 | 16.12 | 11.68 | 11.68 | 12.00 | 12.00 |
| 317 | 16.39 | 16.39 | 16.18 | 16.18 | 14.41 | 14.41 | 15.28 | 15.28 | 8.91 | 8.91 |
| 318 | 15.74 | 15.74 | 17.17 | 17.17 | 12.88 | 12.88 | 15.91 | 15.91 | 14.66 | 14.66 |
| 319 | 14.80 | 14.80 | 16.57 | 16.57 | 13.37 | 13.37 | 18.22 | 18.22 | 14.56 | 14.56 |
| 320 | 14.49 | 14.49 | 14.68 | 14.68 | 18.03 | 18.03 | 16.68 | 16.68 | 11.48 | 11.48 |
| 321 | 12.15 | 12.15 | 14.73 | 14.73 | 17.25 | 17.25 | 15.19 | 15.19 | 20.47 | 20.47 |
| 322 | 16.53 | 16.53 | 11.70 | 11.70 | 16.04 | 16.04 | 15.50 | 15.50 | 18.82 | 18.82 |
| 323 | 11.53 | 11.53 | 16.60 | 16.60 | 15.89 | 15.89 | 17.53 | 17.53 | 10.17 | 10.17 |
| 324 | 16.03 | 16.03 | 15.62 | 15.62 | 15.76 | 15.76 | 10.68 | 10.68 | 17.50 | 17.50 |
| 325 | 15.49 | 15.49 | 19.04 | 19.04 | 17.31 | 17.31 | 17.10 | 17.10 | 17.22 | 17.22 |
| 326 | 17.44 | 17.44 | 16.16 | 16.16 | 15.51 | 15.51 | 17.72 | 17.72 | 6.89 | 6.89 |
| 327 | 14.21 | 14.21 | 16.31 | 16.31 | 12.60 | 12.60 | 13.94 | 13.94 | 12.10 | 12.10 |
| 328 | 16.88 | 16.88 | 13.12 | 13.12 | 13.63 | 13.63 | 11.55 | 11.55 | 14.74 | 14.74 |
| 329 | 15.42 | 15.42 | 14.45 | 14.45 | 14.39 | 14.39 | 13.38 | 13.38 | 18.99 | 18.99 |
| 330 | 20.60 | 20.60 | 11.23 | 11.23 | 10.33 | 10.33 | 14.09 | 14.09 | 20.14 | 20.14 |
| 331 | 16.77 | 16.77 | 9.38 | 9.38 | 9.49 | 9.49 | 11.32 | 11.32 | 15.75 | 15.75 |
| 332 | 11.26 | 11.26 | 14.12 | 14.12 | 15.32 | 15.32 | 13.34 | 13.34 | 12.46 | 12.46 |
| 333 | 15.53 | 15.53 | 14.92 | 14.92 | 20.78 | 20.78 | 12.35 | 12.35 | 27.08 | 27.08 |
| 334 | 15.18 | 15.18 | 16.15 | 16.15 | 19.10 | 19.10 | 17.38 | 17.38 | 17.29 | 17.29 |
| 335 | 13.71 | 13.71 | 13.88 | 13.88 | 19.25 | 19.25 | 25.12 | 25.12 | 19.70 | 19.70 |
| 336 | 14.23 | 14.23 | 17.99 | 17.99 | 19.77 | 19.77 | 19.80 | 19.80 | 14.22 | 14.22 |
| 337 | 18.78 | 18.78 | 18.19 | 18.19 | 21.37 | 21.37 | 20.67 | 20.67 | 18.90 | 18.90 |
| 338 | 21.58 | 21.58 | 14.56 | 14.56 | 11.90 | 11.90 | 3.30 | 3.30 | 22.46 | 22.46 |
| 339 | 18.42 | 18.42 | 22.81 | 22.81 | 16.50 | 16.50 | 11.40 | 11.40 | 24.86 | 24.86 |
| 340 | 23.22 | 23.22 | 21.33 | 21.33 | 14.43 | 14.43 | 14.33 | 14.33 | 33.24 | 33.24 |
| 341 | 26.51 | 26.51 | 21.11 | 21.11 | 14.27 | 14.27 | 24.97 | 24.97 | 40.15 | 40.15 |
| 342 | 17.94 | 17.94 | 21.27 | 21.27 | 22.16 | 22.16 | 37.32 | 37.32 | 63.55 | 63.55 |
| 343 | 18.66 | 18.66 | 19.63 | 19.63 | 24.57 | 24.57 | 43.28 | 43.28 | 41.32 | 41.32 |
| 344 | 9.58 | 9.58 | 21.59 | 21.59 | 36.95 | 36.95 | 64.09 | 64.09 | 30.42 | 30.42 |
| 345 | 18.34 | 18.34 | 22.16 | 22.16 | 41.54 | 41.54 | 36.20 | 36.20 | 19.29 | 19.29 |
| 346 | 17.46 | 17.46 | 33.81 | 33.81 | 63.71 | 63.71 | 27.93 | 27.93 | 12.51 | 12.51 |
| 347 | 25.26 | 25.26 | 34.04 | 34.04 | 35.23 | 35.23 | 19.79 | 19.79 | 17.51 | 17.51 |
| 348 | 31.43 | 31.43 | 63.96 | 63.96 | 31.46 | 31.46 | 10.00 | 10.00 | 18.67 | 18.67 |
| 349 | 41.01 | 41.01 | 35.31 | 35.31 | 23.28 | 23.28 | 19.26 | 19.26 | 16.58 | 16.58 |
| 350 | 64.33 | 64.33 | 28.28 | 28.28 | 16.32 | 16.32 | 13.57 | 13.57 | 10.78 | 10.78 |

| Reflected Angle in ° | Incidence Angle in ° | | | | | | | | | |
|---|---|---|---|---|---|---|---|---|---|---|
| | 11 | 12 | 13 | 14 | 15 | 16 | 17 | 18 | 19 | 20 |
| 351 | 30.45 | 30.45 | 19.82 | 19.82 | 18.92 | 18.92 | 13.74 | 13.74 | 0.97 | 0.97 |
| 352 | 28.76 | 28.76 | 22.20 | 22.20 | 15.98 | 15.98 | 15.62 | 15.62 | 14.58 | 14.58 |
| 353 | 20.71 | 20.71 | 20.03 | 20.03 | 9.53 | 9.53 | 7.99 | 7.99 | 9.54 | 9.54 |
| 354 | 17.81 | 17.81 | 15.04 | 15.04 | 19.14 | 19.14 | 14.55 | 14.55 | 16.48 | 16.48 |
| 355 | 19.76 | 19.76 | 13.00 | 13.00 | 9.55 | 9.55 | 16.33 | 16.33 | 10.34 | 10.34 |
| 356 | 13.23 | 13.23 | 14.32 | 14.32 | 12.71 | 12.71 | 4.00 | 4.00 | 14.58 | 14.58 |
| 357 | 13.80 | 13.80 | 17.12 | 17.12 | 17.32 | 17.32 | 13.32 | 13.32 | 18.57 | 18.57 |
| 358 | 3.69 | 3.69 | 14.62 | 14.62 | 15.89 | 15.89 | 12.94 | 12.94 | 15.69 | 15.69 |
| 359 | 12.05 | 12.05 | 17.37 | 17.37 | 13.46 | 13.46 | 16.63 | 16.63 | 16.40 | 16.40 |
| 360 | 16.56 | 16.56 | 12.73 | 12.73 | 17.76 | 17.76 | 15.90 | 15.90 | 18.21 | 18.21 |

# APPENDIX F. MATLAB SOURCE CODE FOR DETECTION COVERAGE PLOT

```
% Chong Sze Sing (March 2014)
% Bistatic RCS Look-up Table
load('3GHz_full.mat')
biRCS3 = num;
load('9GHz_full.mat')
biRCS9 = num;

sen=10; % sensitivity

% For Tx 1
Xcoord1 = [];
Ycoord1 = [];
SNR1 = [];
SNRdBm1 = [];
Err_thetaR1 = [];
Err_time1 = [];
Err_L1 = [];
Tx1=45;
L1=18000;
%For Tx2
Xcoord2 = [];
Ycoord2 = [];
SNR2 = [];
SNRdBm2 = [];
Err_thetaR2 = [];
Err_time2 = [];
Err_L2 = [];
Tx2=135;
L2=18000;
%For Tx3
Xcoord3 = [];
Ycoord3 = [];
SNR3 = [];
SNRdBm3 = [];
Err_thetaR3 = [];
Err_time3 = [];
Err_L3 = [];
Tx3=225;
L3=18000;
%For Tx4
Xcoord4 = [];
Ycoord4 = [];
SNR4 = [];
SNRdBm4 = [];
Err_thetaR4 = [];
Err_time4 = [];
Err_L4 = [];
Tx4=315;
L4=18000;
```

```
%For Tx5
Xcoord5 = [];
Ycoord5 = [];
SNR5 = [];
SNRdBm5 = [];
Err_thetaR5 = [];
Err_time5 = [];
Err_L5 = [];
Tx5=0;
L5=18000;
%For Tx6
Xcoord6 = [];
Ycoord6 = [];
SNR6 = [];
SNRdBm6 = [];
Err_thetaR6 = [];
Err_time6 = [];
Err_L6 = [];
Tx6=90;
L6=18000;
%For Tx7
Xcoord7 = [];
Ycoord7 = [];
SNR7 = [];
SNRdBm7 = [];
Err_thetaR7 = [];
Err_time7 = [];
Err_L7 = [];
Tx7=180;
L7=18000;
%For Tx8
Xcoord8 = [];
Ycoord8 = [];
SNR8 = [];
SNRdBm8 = [];
Err_thetaR8 = [];
Err_time8 = [];
Err_L8 = [];
Tx8=270;
L8=18000;

% Bi-static Radar Equation
% Constants
k = 1.38e-23;    % Boltzmann
c = 3e8;         % Speed of light

% Variables
% Parameters are based Furuno Marine Radar FAR-28x7 series in both X-band
and S-band

% Bi-static Radar Equation
% Constants
k = 1.38e-23;    % Boltzmann
c = 3e8;         % Speed of light
```

```
Select = 1; %chose which radar to use
% Variables
% Parameters are based Furuno Marine Radar FAR-28x7 series in both X-band
% and S-band

%S-band Radar (1)
BeamAz_S = 1.8;    % in degrees
BeamEL_S = 25;     % in degrees
Scanrate_S = 45;   % in rpm for range of 24 nmi or higher
Pt_S = 30e3;          % Tx peak power output
Gt_S = 10^(28/10);  % Tx Antenna Gain given as 28dB
Gr_S = 2;          % Rx Antenna Gain
f_S = 3050e6;      % frequency
lambda_S = c/f_S;      % wavelength
Ft_S = 1;          % Prop Factor for Tx-Tgt path. See Advances in Bistatic
Radar - Chp 6.5.5.6
Fr_S = 1;          % Prop Factor for Rx-Tgt path
Ts_S = 290+290*(13.5-1);      % System Noise Temp of Rx of NF=6dB using
formula Te=(NF-1)290 and Ts=Te+290K
Bn_S = 500e6;      % Noise Bandwidth of ESM Rx Wideband Channalised (500
MHz)
Lt_S = 2;          % Ref to See Advances in Bistatic Radar - Chp 6.5.5.6
Lr_S = 2;
% this is calculation of pulse integration sqrt(N)
PRF_S = 2000;
TOT_S = BeamAz_S/(Scanrate_S*360);
N_S = TOT_S*PRF_S;

%X-band Radar (2)
BeamAz_X = 0.95;    % in degrees
BeamEL_X = 25;     % in degrees
Scanrate_X = 45;   % in rpm for range of 24 nmi or higher
Pt_X = 25e3;          % Tx peak power output
Gt_X = 10^(31/10);    % Tx Antenna Gain is given as 31 dB
Gr_X = 2;          % Rx Antenna Gain
f_X = 9410e6;      % frequency
lambda_X = c/f_X;      % wavelength
Ft_X = 1;          % Prop Factor for Tx-Tgt path. See Advances in Bistatic
Radar - Chp 6.5.5.6
Fr_X = 1;          % Prop Factor for Rx-Tgt path
Ts_X = 290+290*(6-1);      % System Noise Temp of Rx of NF=6dB using
formula Te=(NF-1)290 and Ts=Te+290K
Bn_X = 500e6;      % Noise Bandwidth of ESM Rx Wideband Channalised (500
MHz)
Lt_X = 2;          % Ref to See Advances in Bistatic Radar - Chp 6.5.5.6
Lr_X = 2;
% this is calculation of pulse integration sqrt(N)
PRF_X = 1500;
TOT_X = BeamAz_X/(Scanrate_X*360);
N_X = TOT_X*PRF_X;
```

```
if Select ==1
    BeamEL = BeamEL_S;   % in degrees
    BeamAz = BeamAz_S;    % in degrees
    Scanrate = Scanrate_S;  % in rpm for range of 24 nmi or higher
    Pt = Pt_S;          % Tx peak power output
    Gt = Gt_S;   % Tx Antenna Gain is given as 31 dB
    Gr = Gr_S;          % Rx Antenna Gain
    f = f_S;     % frequency
    lambda = lambda_S;     % wavelength
    Ft = Ft_S;          % Prop Factor for Tx-Tgt path. See Advances in
Bistatic Radar - Chp 6.5.5.6
    Fr = Fr_S;          % Prop Factor for Rx-Tgt path
    Ts = Ts_S;      % System Noise Temp of Rx of NF=6dB using formula
Te=(NF-1)290 and Ts=Te+290K
    Bn = Bn_S;     % Noise Bandwidth of ESM Rx Wideband Channalised (500
MHz)
    Lt = Lt_S;          % Ref to See Advances in Bistatic Radar - Chp
6.5.5.6
    Lr = Lr_S;
% this is calculation of pulse integration sqrt(N)
    PRF = PRF_S;
    TOT = TOT_S;
    N = N_S;
else
    BeamEL = BeamEL_X;   % in degrees
    BeamAz = BeamAz_X;    % in degrees
    Scanrate = Scanrate_X;  % in rpm for range of 24 nmi or higher
    Pt = Pt_X;          % Tx peak power output
    Gt = Gt_X;   % Tx Antenna Gain is given as 31 dB
    Gr = Gr_X;          % Rx Antenna Gain
    f = f_X;     % frequency
    lambda = lambda_X;     % wavelength
    Ft = Ft_X;          % Prop Factor for Tx-Tgt path. See Advances in
Bistatic Radar - Chp 6.5.5.6
    Fr = Fr_X;          % Prop Factor for Rx-Tgt path
    Ts = Ts_X;      % System Noise Temp of Rx of NF=6dB using formula
Te=(NF-1)290 and Ts=Te+290K
    Bn = Bn_X;     % Noise Bandwidth of ESM Rx Wideband Channalised (500
MHz)
    Lt = Lt_X;          % Ref to See Advances in Bistatic Radar - Chp
6.5.5.6
    Lr = Lr_X;
% this is calculation of pulse integration sqrt(N)
    PRF = PRF_X;
    TOT = TOT_X;
    N = N_X;
end
```

```
%%%%%%%%%%%%%%%%%%%%%% INPUT %%%%%%%%%%%%%%%%%%%%%%
% We only take in three measurments from the ESM - L, Rt+Rr and thetaR

%%%%%%%%%%%%%%%%%%%%%% Tx 1 %%%%%%%%%%%%%%%%%%%%%%%%%%%%
    for CombinR=18500:200:50000

        for thetaR=0:0.5:360

            RrAct=((CombinR)^2 -
L1^2)/(2*(CombinR+L1*sin(thetaR*pi/180)));
            RtAct=sqrt(RrAct^2+L1^2-2*RrAct*L1*cos(pi/2+thetaR*pi/180));

            Beta=round((180/pi)*acos((RrAct^2+RtAct^2-
L1^2)/(2*RrAct*RtAct)));
            % Assuming the low RCS ship is heading south towards the Rx
            % position. Then, Beta/2 is incident angle on one side and
            % scattered angle on the other side.
            Beta1=round(Beta/2);

            % Organise the RCS values by
            RCS=10^(biRCS3(90-Beta1+1,90+Beta1)/10);
            %RCS=10^(biRCS3(Beta1+1,Beta1+1)/10);

            K1 = Pt*Gt*Gr*(lambda^2)*RCS*(Ft^2)*(Fr^2);
            K2 = ((4*pi)^3)*k*Ts*Bn*Lt*Lr;
            K = K1/K2;      % Bi-static Radar Constant

            e=L1/(RrAct+RtAct); % eccentricity

            SNR = K/(RrAct^2*RtAct^2);   %
            SNRdBm = 10*log(SNR)+ sqrt(N);

            Xcoord = RrAct*sin((thetaR+Tx1)*pi/180);
            Ycoord = RrAct*cos((thetaR+Tx1)*pi/180);

                        % Error to measurement of Rt + Rr
            % Antenna scan rate of 45 rpm or 270 deg/s
            % With horizontal beamwidth of 1.8 deg, assuming that the
edge of the
            % beamwidth creates enough SNR to be received by the receiver
as
            % reflections from the tgt
            % From eqn 3.18
            % rms error

            Err_factor_time =
(1+e^2+2*e*sin(thetaR*pi/180))/(2*(1+e*sin(thetaR*pi/180))^2);
            Err_time=Err_factor_time*(BeamAz/2*pi/180)*RtAct; % r*theta
corresponding to half of the beamwidth of 1.8 deg
```

```
%Err_time3 = (0.55/Bn)*1/sqrt(Bn*SNR1)*c; % Ref to Alogrithms for
Ambiguity Function Processing (Eqn - 11b)
            %Err_time1 = Err_time3 + Err_time1;
            % Error to measurement of L
            % For a Class A Marine AIS, positional acciracy is up to
0.0001 mins where
            % 1 deg equals to 60nmi
            % Update rate is between 2 to 10 seconds
            % Assumming a opening speed of Tx at 12 knots and Rx at 12
knots

            Err_factor_L = (-
(e^2+1)*sin(thetaR*pi/180)+2*e)/(2*(1+e*sin(thetaR*pi/180))^2);
            Err_L = Err_factor_L*((0.0001*1824)+(10*1824*5/3600));% Net
opening speed of 10 knots + 5s update rate

            % Error to measurement of thetaR
            % Error due to thetaR
            % the error will be coming from the DF error from the ESM
system
            % which is up to +/-1.5 deg
            % I modified this equation as I have factor in the L in my
error so I
            % normalised it with L so as not to double count

            Err_factor_theta = (1-
e^2)*cos(thetaR*pi/180)/(2*(1+e*sin(thetaR*pi/180))^2);
            Err_thetaR = Err_factor_theta*(RtAct*1.5*pi/180);

            if SNRdBm >= sen
            Xcoord1 = [Xcoord1,Xcoord];
            Ycoord1 = [Ycoord1,Ycoord];
            SNR1 = [SNR1,SNR];
            SNRdBm1 = [SNRdBm1,SNRdBm];
            Err_time1 = [Err_time1,Err_time];
            Err_L1 = [Err_L1,Err_L];
            Err_thetaR1 = [Err_thetaR1,Err_thetaR];
            else
            end
        end
    end

    Err_Total1=zeros(size(Err_time1));
 % Find th emax of the three source of error and use that for that
 % coordinate position
 for aa=1:1:length(Err_time1)
    Err_Total1(aa) =
max(abs(Err_time1(aa)),abs(Err_L1(aa))+abs(Err_thetaR1(aa)));
 end
 for aa=1:1:length(Err_time1)
    Err_Total1(aa) = max(abs(Err_Total1(aa)),abs(Err_thetaR1(aa)));
 end
```

```
%%%%%%%%%%%%%%%%%%%%% Tx 2 %%%%%%%%%%%%%%%%%%%%%%%%%%%%

      for CombinR=18500:200:50000

        for thetaR=0:0.5:360

            RrAct=((CombinR)^2 -
L2^2)/(2*(CombinR+L2*sin(thetaR*pi/180)));
            RtAct=sqrt(RrAct^2+L2^2-2*RrAct*L2*cos(pi/2+thetaR*pi/180));

            Beta=round((180/pi)*acos((RrAct^2+RtAct^2-
L2^2)/(2*RrAct*RtAct)));
            % Assuming the low RCS ship is heading south towards the Rx
            % position. Then, Beta/2 is incident angle on one side and
            % scattered angle on the other side.
            Beta1=round(Beta/2);

            % Organise the RCS values by
            RCS=10^(biRCS3(90-Beta1+1,90+Beta1)/10);
            %RCS=10^(biRCS3(Beta1+1,Beta1+1)/10);

            K1 = Pt*Gt*Gr*(lambda^2)*RCS*(Ft^2)*(Fr^2);
            K2 = ((4*pi)^3)*k*Ts*Bn*Lt*Lr;
            K = K1/K2;      % Bi-static Radar Constant

            e=L2/(RrAct+RtAct); % eccentricity

            SNR = K/(RrAct^2*RtAct^2);
            SNRdBm = 10*log(SNR)+ sqrt(N);

            Xcoord = RrAct*sin((thetaR+Tx2)*pi/180);
            Ycoord = RrAct*cos((thetaR+Tx2)*pi/180);

            % Error to measurement of Rt + Rr
            % Antenna scan rate of 45 rpm or 270 deg/s
            % With horizontal beamwidth of 1.8 deg, assuming that the
edge of the
            % beamwidth creates enough SNR to be received by the receiver
as
            % reflections from the tgt
            % From eqn 3.18
            % rms error

            Err_factor_time =
(1+e^2+2*e*sin(thetaR*pi/180))/(2*(1+e*sin(thetaR*pi/180))^2);
            Err_time=Err_factor_time*(BeamAz/2*pi/180)*RtAct; % r*theta
corresponding to half of the beamwidth of 1.8 de
```

```
%Err_time3 = (0.55/Bn)*1/sqrt(Bn*SNR1)*c; % Ref to Alogrithms for
Ambiguity Function Processing (Eqn - 11b)
            %Err_time1 = Err_time3 + Err_time1;
            % Error to measurement of L
            % For a Class A Marine AIS, positional acciracy is up to
0.0001 mins where
            % 1 deg equals to 60nmi
            % Update rate is between 2 to 10 seconds
            % Assumming a opening speed of Tx at 12 knots and Rx at 12
knots

            Err_factor_L = (-
(e^2+1)*sin(thetaR*pi/180)+2*e)/(2*(1+e*sin(thetaR*pi/180))^2);
            Err_L = Err_factor_L*((0.0001*1824)+(10*1824*5/3600)); % Net
opening speed of 10 knots + 5s update rate

            % Error to measurement of thetaR
            % Error due to thetaR
            % the error will be coming from the DF error from the ESM
system
            % which is up to +/-1.5 deg
            % I modified this equation as I have factor in the L in my
error so I
            % normalised it with L so as not to double count

            Err_factor_theta = (1-
e^2)*cos(thetaR*pi/180)/(2*(1+e*sin(thetaR*pi/180))^2);
            Err_thetaR = Err_factor_theta*(RtAct*1.5*pi/180);
            if SNRdBm >= sen
            Xcoord2 = [Xcoord2,Xcoord];
            Ycoord2 = [Ycoord2,Ycoord];
            SNR2 = [SNR2,SNR];
            SNRdBm2 = [SNRdBm2,SNRdBm];
            Err_time2 = [Err_time2,Err_time];
            Err_L2 = [Err_L2,Err_L];
            Err_thetaR2 = [Err_thetaR2,Err_thetaR];
            else
            end
        end
      end

    Err_Total2=zeros(size(Err_time2));
 % Find th emax of the three source of error and use that for that
 % coordinate position
 for aa=1:1:length(Err_time2)
    Err_Total2(aa) = max(abs(Err_time2(aa)),abs(Err_L2(aa)));
 end
 for aa=1:1:length(Err_time2)
    Err_Total2(aa) = max(abs(Err_Total2(aa)),abs(Err_thetaR2(aa)));
 end
```

```
%%%%%%%%%%%%%%%%%%%%% Tx 3 %%%%%%%%%%%%%%%%%%%%%%%%%%%%

      for CombinR=18500:200:50000

        for thetaR=0:0.5:360

            RrAct=((CombinR)^2 -
L3^2)/(2*(CombinR+L3*sin(thetaR*pi/180)));
            RtAct=sqrt(RrAct^2+L3^2-2*RrAct*L3*cos(pi/2+thetaR*pi/180));

            Beta=round((180/pi)*acos((RrAct^2+RtAct^2-
L3^2)/(2*RrAct*RtAct)));
            % Assuming the low RCS ship is heading south towards the Rx
            % position. Then, Beta/2 is incident angle on one side and
            % scattered angle on the other side.
            Beta1=round(Beta/2);

            % Organise the RCS values by
            RCS=10^(biRCS3(90-Beta1+1,90+Beta1)/10);
            %RCS=10^(biRCS3(Beta1+1,Beta1+1)/10);

            K1 = Pt*Gt*Gr*(lambda^2)*RCS*(Ft^2)*(Fr^2);
            K2 = ((4*pi)^3)*k*Ts*Bn*Lt*Lr;
            K = K1/K2;      % Bi-static Radar Constant

            e=L3/(RrAct+RtAct); % eccentricity

            SNR = K/(RrAct^2*RtAct^2);
            SNRdBm = 10*log(SNR)+ sqrt(N);

            Xcoord = RrAct*sin((thetaR+Tx3)*pi/180);
            Ycoord = RrAct*cos((thetaR+Tx3)*pi/180);

            % Error to measurement of Rt + Rr
            % Antenna scan rate of 45 rpm or 270 deg/s
            % With horizontal beamwidth of 1.8 deg, assuming that the
edge of the
            % beamwidth creates enough SNR to be received by the receiver
as
            % reflections from the tgt
            % From eqn 3.18
            % rms error

            Err_factor_time =
(1+e^2+2*e*sin(thetaR*pi/180))/(2*(1+e*sin(thetaR*pi/180))^2);
            Err_time=Err_factor_time*(BeamAz/2*pi/180)*RtAct; % r*theta
corresponding to half of the beamwidth of 1.8 deg
```

```
%Err_time3 = (0.55/Bn)*1/sqrt(Bn*SNR1)*c; % Ref to Alogrithms for
Ambiguity Function Processing (Eqn - 11b)
            %Err_time1 = Err_time3 + Err_time1;
            % Error to measurement of L
            % For a Class A Marine AIS, positional acciracy is up to
0.0001 mins where
            % 1 deg equals to 60nmi
            % Update rate is between 2 to 10 seconds
            % Assumming a opening speed of Tx at 12 knots and Rx at 12
knots

            Err_factor_L = (-
(e^2+1)*sin(thetaR*pi/180)+2*e)/(2*(1+e*sin(thetaR*pi/180))^2);
            Err_L = Err_factor_L*((0.0001*1824)+(10*1824*5/3600)); % Net
opening speed of 10 knots + 5s update rate

            % Error to measurement of thetaR
            % Error due to thetaR
            % the error will be coming from the DF error from the ESM
system
            % which is up to +/-1.5 deg
            % I modified this equation as I have factor in the L in my
error so I
            % normalised it with L so as not to double count

            Err_factor_theta = (1-
e^2)*cos(thetaR*pi/180)/(2*(1+e*sin(thetaR*pi/180))^2);
            Err_thetaR = Err_factor_theta*(RtAct*1.5*pi/180);

            if SNRdBm >= sen
            Xcoord3 = [Xcoord3,Xcoord];
            Ycoord3 = [Ycoord3,Ycoord];
            SNR3 = [SNR3,SNR];
            SNRdBm3 = [SNRdBm3,SNRdBm];
            Err_time3 = [Err_time3,Err_time];
            Err_L3 = [Err_L3,Err_L];
            Err_thetaR3 = [Err_thetaR3,Err_thetaR];
            else
            end
        end
      end

    Err_Total3=zeros(size(Err_time3));
 % Find th emax of the three source of error and use that for that
 % coordinate position
 for aa=1:1:length(Err_time3)
    Err_Total3(aa) = max(abs(Err_time3(aa)),abs(Err_L3(aa)));
 end
 for aa=1:1:length(Err_time3)
    Err_Total3(aa) = max(abs(Err_Total3(aa)),abs(Err_thetaR3(aa)));
 end
```

```
%%%%%%%%%%%%%%%%%%%%% Tx 4 %%%%%%%%%%%%%%%%%%%%%%%%%%%%

      for CombinR=18500:200:45000

        for thetaR=0:0.5:360

            RrAct=((CombinR)^2 -
L4^2)/(2*(CombinR+L4*sin(thetaR*pi/180)));
            RtAct=sqrt(RrAct^2+L4^2-2*RrAct*L4*cos(pi/2+thetaR*pi/180));

            Beta=round((180/pi)*acos((RrAct^2+RtAct^2-
L4^2)/(2*RrAct*RtAct)));
            % Assuming the low RCS ship is heading south towards the Rx
            % position. Then, Beta/2 is incident angle on one side and
            % scattered angle on the other side.
            Beta1=round(Beta/2);

            % Organise the RCS values by
            RCS=10^(biRCS3(90-Beta1+1,90+Beta1)/10);
            %RCS=10^(biRCS3(Beta1+1,Beta1+1)/10);

            K1 = Pt*Gt*Gr*(lambda^2)*RCS*(Ft^2)*(Fr^2);
            K2 = ((4*pi)^3)*k*Ts*Bn*Lt*Lr;
            K = K1/K2;      % Bi-static Radar Constant

            e=L4/(RrAct+RtAct); % eccentricity

            SNR = K/(RrAct^2*RtAct^2);
            SNRdBm = 10*log(SNR)+ sqrt(N);

            Xcoord = RrAct*sin((thetaR+Tx4)*pi/180);
            Ycoord = RrAct*cos((thetaR+Tx4)*pi/180);

            % Error to measurement of Rt + Rr
            % Antenna scan rate of 45 rpm or 270 deg/s
            % With horizontal beamwidth of 1.8 deg, assuming that the
edge of the
            % beamwidth creates enough SNR to be received by the receiver
as
            % reflections from the tgt
            % From eqn 3.18
            % rms error

            Err_factor_time =
(1+e^2+2*e*sin(thetaR*pi/180))/(2*(1+e*sin(thetaR*pi/180))^2);
            Err_time=Err_factor_time*(BeamAz/2*pi/180)*RtAct; % r*theta
corresponding to half of the beamwidth of 1.8 deg
```

```
%Err_time3 = (0.55/Bn)*1/sqrt(Bn*SNR1)*c; % Ref to Alogrithms for
Ambiguity Function Processing (Eqn - 11b)
            %Err_time1 = Err_time3 + Err_time1;
            % Error to measurement of L
            % For a Class A Marine AIS, positional acciracy is up to
0.0001 mins where
            % 1 deg equals to 60nmi
            % Update rate is between 2 to 10 seconds
            % Assumming a opening speed of Tx at 12 knots and Rx at 12
knots

            Err_factor_L = (-
(e^2+1)*sin(thetaR*pi/180)+2*e)/(2*(1+e*sin(thetaR*pi/180))^2);
            Err_L = Err_factor_L*((0.0001*1824)+(10*1824*5/3600)); % Net
opening speed of 10 knots + 5s update rate

            % Error to measurement of thetaR
            % Error due to thetaR
            % the error will be coming from the DF error from the ESM
system
            % which is up to +/-1.5 deg
            % I modified this equation as I have factor in the L in my
error so I
            % normalised it with L so as not to double count

            Err_factor_theta = (1-
e^2)*cos(thetaR*pi/180)/(2*(1+e*sin(thetaR*pi/180))^2);
            Err_thetaR = Err_factor_theta*(RtAct*1.5*pi/180);

            if SNRdBm >= sen
            Xcoord4 = [Xcoord4,Xcoord];
            Ycoord4 = [Ycoord4,Ycoord];
            SNR4 = [SNR4,SNR];
            SNRdBm4 = [SNRdBm4,SNRdBm];
            Err_time4 = [Err_time4,Err_time];
            Err_L4 = [Err_L4,Err_L];
            Err_thetaR4 = [Err_thetaR4,Err_thetaR];
            else
            end
        end
      end

    Err_Total4=zeros(size(Err_time4));
 % Find th emax of the three source of error and use that for that
 % coordinate position
 for aa=1:1:length(Err_time4)
    Err_Total4(aa) = max(abs(Err_time4(aa)),abs(Err_L4(aa)));
 end
 for aa=1:1:length(Err_time4)
    Err_Total4(aa) = max(abs(Err_Total4(aa)),abs(Err_thetaR4(aa)));
 end
```

```
%%%%%%%%%%%%%%%%%%%%% Tx 5 %%%%%%%%%%%%%%%%%%%%%%%%%%%

  for CombinR=18500:200:50000

        for thetaR=0:0.5:360

            RrAct=((CombinR)^2 -
L5^2)/(2*(CombinR+L5*sin(thetaR*pi/180)));
            RtAct=sqrt(RrAct^2+L5^2-2*RrAct*L5*cos(pi/2+thetaR*pi/180));

            Beta=round((180/pi)*acos((RrAct^2+RtAct^2-
L5^2)/(2*RrAct*RtAct)));
            % Assuming the low RCS ship is heading south towards the Rx
            % position. Then, Beta/2 is incident angle on one side and
            % scattered angle on the other side.
            Beta1=round(Beta/2);
            % Organise the RCS values by
            RCS=10^(biRCS3(90-Beta1,90+Beta1)/10);

            K1 = Pt*Gt*Gr*(lambda^2)*RCS*(Ft^2)*(Fr^2);
            K2 = ((4*pi)^3)*k*Ts*Bn*Lt*Lr;
            K = K1/K2;      % Bi-static Radar Constant

            e=L5/(RrAct+RtAct); % eccentricity

            SNR = K/(RrAct^2*RtAct^2);
            SNRdBm = 10*log(SNR)+30;

            Xcoord = RrAct*sin((thetaR+Tx5)*pi/180);
            Ycoord = RrAct*cos((thetaR+Tx5)*pi/180);

            % Error to measurement of Rt + Rr
            % Antenna scan rate of 45 rpm or 270 deg/s
            % With horizontal beamwidth of 1.8 deg, assuming that the
edge of the
            % beamwidth creates enough SNR to be received by the receiver
as
            % reflections from the tgt
            % From eqn 3.18
            % rms error

            Err_factor_time =
(1+e^2+2*e*sin(thetaR*pi/180))/(2*(1+e*sin(thetaR*pi/180))^2);
            Err_time=Err_factor_time*(BeamEL/2*pi/180)*RtAct; % r*theta
corresponding to half of the beamwidth of 1.8 deg
```

```
%Err_time3 = (0.55/Bn)*1/sqrt(Bn*SNR1)*c; % Ref to Alogrithms for
Ambiguity Function Processing (Eqn - 11b)
            %Err_time1 = Err_time3 + Err_time1;
            % Error to measurement of L
            % For a Class A Marine AIS, positional acciracy is up to
0.0001 mins where
            % 1 deg equals to 60nmi
            % Update rate is between 2 to 10 seconds
            % Assumming a opening speed of Tx at 12 knots and Rx at 12
knots

            Err_factor_L = (-
(e^2+1)*sin(thetaR*pi/180)+2*e)/(2*(1+e*sin(thetaR*pi/180))^2);
            Err_L = Err_factor_L*((0.0001*1824)+(10*1824*5/3600)); % Net
opening speed of 10 knots + 5s update rate

            % Error to measurement of thetaR
            % Error due to thetaR
            % the error will be coming from the DF error from the ESM
system
            % which is up to +/-1.5 deg
            % I modified this equation as I have factor in the L in my
error so I
            % normalised it with L so as not to double count

            Err_factor_theta = (1-
e^2)*cos(thetaR*pi/180)/(2*(1+e*sin(thetaR*pi/180))^2);
            Err_thetaR = Err_factor_theta*(RtAct*1.5*pi/180);
            if SNRdBm >= sen
            Xcoord5 = [Xcoord5,Xcoord];
            Ycoord5 = [Ycoord5,Ycoord];
            SNR5 = [SNR5,SNR];
            SNRdBm5 = [SNRdBm5,SNRdBm];
            Err_time5 = [Err_time5,Err_time];
            Err_L5 = [Err_L5,Err_L];
            Err_thetaR5 = [Err_thetaR5,Err_thetaR];
            else
            end
        end
      end

    Err_Total5=zeros(size(Err_time5));
 % Find th emax of the three source of error and use that for that
 % coordinate position
 for aa=1:1:length(Err_time5)
    Err_Total5(aa) = max(abs(Err_time5(aa)),abs(Err_L5(aa)));
 end
 for aa=1:1:length(Err_time5)
    Err_Total5(aa) = max(abs(Err_Total5(aa)),abs(Err_thetaR5(aa)));
 end
```

```
%%%%%%%%%%%%%%%%%%%%% Tx 6 %%%%%%%%%%%%%%%%%%%%%%%%%%%

  for CombinR=18500:200:50000

        for thetaR=0:0.5:360

            RrAct=((CombinR)^2 -
L6^2)/(2*(CombinR+L6*sin(thetaR*pi/180)));
            RtAct=sqrt(RrAct^2+L6^2-2*RrAct*L6*cos(pi/2+thetaR*pi/180));

            Beta=round((180/pi)*acos((RrAct^2+RtAct^2-
L6^2)/(2*RrAct*RtAct)));
            % Assuming the low RCS ship is heading south towards the Rx
            % position. Then, Beta/2 is incident angle on one side and
            % scattered angle on the other side.
            Beta1=round(Beta/2);
            % Organise the RCS values by
            RCS=10^(biRCS3(90-Beta1,90+Beta1)/10);

            K1 = Pt*Gt*Gr*(lambda^2)*RCS*(Ft^2)*(Fr^2);
            K2 = ((4*pi)^3)*k*Ts*Bn*Lt*Lr;
            K = K1/K2;      % Bi-static Radar Constant

            e=L6/(RrAct+RtAct); % eccentricity

            SNR = K/(RrAct^2*RtAct^2);
            SNRdBm = 10*log(SNR)+30;

            Xcoord = RrAct*sin((thetaR+Tx6)*pi/180);
            Ycoord = RrAct*cos((thetaR+Tx6)*pi/180);

            % Error to measurement of Rt + Rr
            % Antenna scan rate of 45 rpm or 270 deg/s
            % With horizontal beamwidth of 1.8 deg, assuming that the
edge of the
            % beamwidth creates enough SNR to be received by the receiver
as
            % reflections from the tgt
            % From eqn 3.18
            % rms error

            Err_factor_time =
(1+e^2+2*e*sin(thetaR*pi/180))/(2*(1+e*sin(thetaR*pi/180))^2);
            Err_time=Err_factor_time*(BeamEL/2*pi/180)*RtAct; % r*theta
corresponding to half of the beamwidth of 1.8 deg
```

```
%Err_time3 = (0.55/Bn)*1/sqrt(Bn*SNR1)*c; % Ref to Alogrithms for
Ambiguity Function Processing (Eqn - 11b)
            %Err_time1 = Err_time3 + Err_time1;
            % Error to measurement of L
            % For a Class A Marine AIS, positional acciracy is up to
0.0001 mins where
            % 1 deg equals to 60nmi
            % Update rate is between 2 to 10 seconds
            % Assumming a opening speed of Tx at 12 knots and Rx at 12
knots

            Err_factor_L = (-
(e^2+1)*sin(thetaR*pi/180)+2*e)/(2*(1+e*sin(thetaR*pi/180))^2);
            Err_L = Err_factor_L*((0.0001*1824)+(10*1824*5/3600)); % Net
opening speed of 10 knots + 5s update rate

            % Error to measurement of thetaR
            % Error due to thetaR
            % the error will be coming from the DF error from the ESM
system
            % which is up to +/-1.5 deg
            % I modified this equation as I have factor in the L in my
error so I
            % normalised it with L so as not to double count

            Err_factor_theta = (1-
e^2)*cos(thetaR*pi/180)/(2*(1+e*sin(thetaR*pi/180))^2);
            Err_thetaR = Err_factor_theta*(RtAct*1.5*pi/180);

            if SNRdBm >= sen
            Xcoord6 = [Xcoord6,Xcoord];
            Ycoord6 = [Ycoord6,Ycoord];
            SNR6 = [SNR6,SNR];
            SNRdBm6 = [SNRdBm6,SNRdBm];
            Err_time6 = [Err_time6,Err_time];
            Err_L6 = [Err_L6,Err_L];
            Err_thetaR6 = [Err_thetaR6,Err_thetaR];
            else
            end
             end
      end

    Err_Total6=zeros(size(Err_time6));
 % Find th emax of the three source of error and use that for that
 % coordinate position
 for aa=1:1:length(Err_time6)
    Err_Total6(aa) = max(abs(Err_time6(aa)),abs(Err_L6(aa)));
 end
 for aa=1:1:length(Err_time6)
    Err_Total6(aa) = max(abs(Err_Total6(aa)),abs(Err_thetaR6(aa)));
 end
```

```
%%%%%%%%%%%%%%%%%%%%% Tx 7 %%%%%%%%%%%%%%%%%%%%%%%%%%%

  for CombinR=18500:200:50000

        for thetaR=0:0.5:360

            RrAct=((CombinR)^2 -
L7^2)/(2*(CombinR+L7*sin(thetaR*pi/180)));
            RtAct=sqrt(RrAct^2+L7^2-2*RrAct*L7*cos(pi/2+thetaR*pi/180));

            Beta=round((180/pi)*acos((RrAct^2+RtAct^2-
L7^2)/(2*RrAct*RtAct)));
            % Assuming the low RCS ship is heading south towards the Rx
            % position. Then, Beta/2 is incident angle on one side and
            % scattered angle on the other side.
            Beta1=round(Beta/2);
            % Organise the RCS values by
            RCS=10^(biRCS3(90-Beta1,90+Beta1)/10);

            K1 = Pt*Gt*Gr*(lambda^2)*RCS*(Ft^2)*(Fr^2);
            K2 = ((4*pi)^3)*k*Ts*Bn*Lt*Lr;
            K = K1/K2;      % Bi-static Radar Constant

            e=L7/(RrAct+RtAct); % eccentricity

            SNR = K/(RrAct^2*RtAct^2);
            SNRdBm = 10*log(SNR)+30;

            Xcoord = RrAct*sin((thetaR+Tx7)*pi/180);
            Ycoord = RrAct*cos((thetaR+Tx7)*pi/180);

            % Error to measurement of Rt + Rr
            % Antenna scan rate of 45 rpm or 270 deg/s
            % With horizontal beamwidth of 1.8 deg, assuming that the
edge of the
            % beamwidth creates enough SNR to be received by the receiver
as
            % reflections from the tgt
            % From eqn 3.18
            % rms error

            Err_factor_time =
(1+e^2+2*e*sin(thetaR*pi/180))/(2*(1+e*sin(thetaR*pi/180))^2);
            Err_time=Err_factor_time*(BeamEL/2*pi/180)*RtAct; % r*theta
corresponding to half of the beamwidth of 1.8 deg
```

```
%Err_time3 = (0.55/Bn)*1/sqrt(Bn*SNR1)*c; % Ref to Alogrithms for
Ambiguity Function Processing (Eqn - 11b)
            %Err_time1 = Err_time3 + Err_time1;
            % Error to measurement of L
            % For a Class A Marine AIS, positional acciracy is up to
0.0001 mins where
            % 1 deg equals to 60nmi
            % Update rate is between 2 to 10 seconds
            % Assumming a opening speed of Tx at 12 knots and Rx at 12
knots

            Err_factor_L = (-
(e^2+1)*sin(thetaR*pi/180)+2*e)/(2*(1+e*sin(thetaR*pi/180))^2);
            Err_L = Err_factor_L*((0.0001*1824)+(10*1824*5/3600)); % Net
opening speed of 10 knots + 5s update rate

            % Error to measurement of thetaR
            % Error due to thetaR
            % the error will be coming from the DF error from the ESM
system
            % which is up to +/-1.5 deg
            % I modified this equation as I have factor in the L in my
error so I
            % normalised it with L so as not to double count

            Err_factor_theta = (1-
e^2)*cos(thetaR*pi/180)/(2*(1+e*sin(thetaR*pi/180))^2);
            Err_thetaR = Err_factor_theta*(RtAct*1.5*pi/180);
            if SNRdBm >= sen
            Xcoord7 = [Xcoord7,Xcoord];
            Ycoord7 = [Ycoord7,Ycoord];
            SNR7 = [SNR7,SNR];
            SNRdBm7 = [SNRdBm7,SNRdBm];
            Err_time7 = [Err_time7,Err_time];
            Err_L7 = [Err_L7,Err_L];
            Err_thetaR7 = [Err_thetaR7,Err_thetaR];
            else
            end
        end
      end

    Err_Total7=zeros(size(Err_time7));
 % Find th emax of the three source of error and use that for that
 % coordinate position
 for aa=1:1:length(Err_time7)
    Err_Total7(aa) = max(abs(Err_time7(aa)),abs(Err_L7(aa)));
 end
 for aa=1:1:length(Err_time7)
    Err_Total7(aa) = max(abs(Err_Total7(aa)),abs(Err_thetaR7(aa)));
 end
```

```
%%%%%%%%%%%%%%%%%%%%% Tx 8 %%%%%%%%%%%%%%%%%%%%%%%%%%

  for CombinR=18500:200:50000

        for thetaR=0:0.5:360

            RrAct=((CombinR)^2 -
L8^2)/(2*(CombinR+L8*sin(thetaR*pi/180)));
            RtAct=sqrt(RrAct^2+L8^2-2*RrAct*L8*cos(pi/2+thetaR*pi/180));

            Beta=round((180/pi)*acos((RrAct^2+RtAct^2-
L8^2)/(2*RrAct*RtAct)));
            % Assuming the low RCS ship is heading south towards the Rx
            % position. Then, Beta/2 is incident angle on one side and
            % scattered angle on the other side.
            Beta1=round(Beta/2);
            % Organise the RCS values by
            RCS=10^(biRCS3(90-Beta1,90+Beta1)/10);

            K1 = Pt*Gt*Gr*(lambda^2)*RCS*(Ft^2)*(Fr^2);
            K2 = ((4*pi)^3)*k*Ts*Bn*Lt*Lr;
            K = K1/K2;      % Bi-static Radar Constant

            e=L8/(RrAct+RtAct); % eccentricity

            SNR = K/(RrAct^2*RtAct^2);
            SNRdBm = 10*log(SNR)+30;

            Xcoord = RrAct*sin((thetaR+Tx8)*pi/180);
            Ycoord = RrAct*cos((thetaR+Tx8)*pi/180);

            % Error to measurement of Rt + Rr
            % Antenna scan rate of 45 rpm or 270 deg/s
            % With horizontal beamwidth of 1.8 deg, assuming that the
edge of the
            % beamwidth creates enough SNR to be received by the receiver
as
            % reflections from the tgt
            % From eqn 3.18
            % rms error

            Err_factor_time =
(1+e^2+2*e*sin(thetaR*pi/180))/(2*(1+e*sin(thetaR*pi/180))^2);
            Err_time=Err_factor_time*(BeamEL/2*pi/180)*RtAct; % r*theta
corresponding to half of the beamwidth of 1.8 deg
```

```
%Err_time3 = (0.55/Bn)*1/sqrt(Bn*SNR1)*c; % Ref to Alogrithms for
Ambiguity Function Processing (Eqn - 11b)
            %Err_time1 = Err_time3 + Err_time1;
            % Error to measurement of L
            % For a Class A Marine AIS, positional acciracy is up to
0.0001 mins where
            % 1 deg equals to 60nmi
            % Update rate is between 2 to 10 seconds
            % Assumming a opening speed of Tx at 12 knots and Rx at 12
knots

            Err_factor_L = (-
(e^2+1)*sin(thetaR*pi/180)+2*e)/(2*(1+e*sin(thetaR*pi/180))^2);
            Err_L = Err_factor_L*((0.0001*1824)+(10*1824*5/3600)); % Net
opening speed of 10 knots + 5s update rate

            % Error to measurement of thetaR
            % Error due to thetaR
            % the error will be coming from the DF error from the ESM
system
            % which is up to +/-1.5 deg
            % I modified this equation as I have factor in the L in my
error so I
            % normalised it with L so as not to double count

            Err_factor_theta = (1-
e^2)*cos(thetaR*pi/180)/(2*(1+e*sin(thetaR*pi/180))^2);
            Err_thetaR = Err_factor_theta*(RtAct*1.5*pi/180);

            if SNRdBm >= sen
            Xcoord8 = [Xcoord8,Xcoord];
            Ycoord8 = [Ycoord8,Ycoord];
            SNR8 = [SNR8,SNR];
            SNRdBm8 = [SNRdBm8,SNRdBm];
            Err_time8 = [Err_time8,Err_time];
            Err_L8 = [Err_L8,Err_L];
            Err_thetaR8 = [Err_thetaR8,Err_thetaR];
            else
            end
        end
      end

    Err_Total8=zeros(size(Err_time8));
 % Find th emax of the three source of error and use that for that
 % coordinate position
 for aa=1:1:length(Err_time8)
    Err_Total8(aa) = max(abs(Err_time8(aa)),abs(Err_L8(aa)));
 end
 for aa=1:1:length(Err_time8)
    Err_Total68(aa) = max(abs(Err_Total8(aa)),abs(Err_thetaR8(aa)));
 end
```

```
%%%%%%%%%%%%%%%%%%%% Plots %%%%%%%%%%%%%%%%%%%%%%%%
X=horzcat(Xcoord1,Xcoord2,Xcoord3,Xcoord4,Xcoord5,Xcoord6,Xcoord7,Xcoord8
);
Y=horzcat(Ycoord1,Ycoord2,Ycoord3,Ycoord4,Ycoord5,Ycoord6,Ycoord7,Ycoord8
);
Z=horzcat(SNRdBm1,SNRdBm2,SNRdBm3,SNRdBm4,SNRdBm5,SNRdBm6,SNRdBm7,SNRdBm8
);
XX=horzcat(Err_thetaR1,Err_thetaR2,Err_thetaR3,Err_thetaR4,Err_thetaR5,Er
r_thetaR6,Err_thetaR7,Err_thetaR8);
YY=horzcat(Err_time1,Err_time2,Err_time3,Err_time4,Err_time5,Err_time6,Er
r_time7,Err_time8);
ZZ=horzcat(Err_L1,Err_L2,Err_L3,Err_L4,Err_L5,Err_L6,Err_L7,Err_L8);
AA=horzcat(Err_Total1,Err_Total2,Err_Total3,Err_Total4,Err_Total5,Err_Tot
al6,Err_Total7,Err_Total8);

    figure(1)
    load seamount
    scatter(X,Y,4,Z,'fill','o')
    colorbar('EastOutside')
    %title('Detection Coverage in Polar Plot(4 Tx)')
    xlabel('Distance in m','fontsize',14)
    ylabel('Distance in m','fontsize',14)
    hold on
    plot(0,0,'k*')
    text(40,0,'Rx','FontSize',15)
    plot(-12730,12730,'k*')
    text(-12730,12930,'Tx1','FontSize',15)
    plot(12730,12730,'k*')
    text(12730,12930,'Tx2','FontSize',15)
    plot(12730,-12730,'k*')
    text(12730,-12930,'Tx3','FontSize',15)
    plot(-12730,-12730,'k*')
    text(-12730,-12930,'Tx4','FontSize',15)
    plot(0,-18000,'k*')
    text(200,-18000,'Tx5','FontSize',15)
    plot(0,18000,'k*')
    text(200,18000,'Tx6','FontSize',15)
    plot(18000,0,'k*')
    text(18000,200,'Tx7','FontSize',15)
    plot(-18000,0,'k*')
    text(-18000,200,'Tx8','FontSize',15)
    hold off
```

THIS PAGE INTENTIONALLY LEFT BLANK

# APPENDIX G. MATLAB SOURCE CODE FOR UNCERTAINTY ELLIPSE

```
% Chong Sze Sing (March 2014)
% 8 Tx Uncertainty Ellipse

TargetX=4500;
TargetY=4500;

% Initializattion
%For Tx 1
Tx1=45;
L1=18000;
%For Tx2
Tx2=135;
L2=18000;
%For Tx3
Tx3=225;
L3=18000;
%For Tx4
Tx4=315;
L4=18000;
%For Tx5
Tx5=0;
L5=18000;
%For Tx6
Tx6=90;
L6=18000;
%For Tx7
Tx7=179;
L7=18000;
%For Tx8
Tx8=270;
L8=18000;

% Variables
% Parameters are based Furuno Marine Radar FAR-21x7 series in both X-
band
% and S-band
% Bi-static Radar Equation
% Constants
k = 1.38e-23;   % Boltzmann
c = 3e8;        % Speed of light
```

```
Select = 1; %chose which radar to use

%S-band Radar (1)
BeamAz_S = 1.8;    % in degrees
BeamEL_S = 25;     % in degrees
Scanrate_S = 45;   % in rpm for range of 24 nmi or higher
Pt_S = 25e3;          % Tx peak power output
Gt_S = 10^(28/10);  % Tx Antenna Gain given as 28dB
Gr_S = 2;          % Rx Antenna Gain
f_S = 3050e6;      % frequency
lambda_S = c/f_S;      % wavelength
Ft_S = 1;          % Prop Factor for Tx-Tgt path. See Advances in Bistatic
Radar - Chp 6.5.5.6
Fr_S = 1;          % Prop Factor for Rx-Tgt path
Ts_S = 290+290*(6-1);      % System Noise Temp of Rx of NF=6dB using
formula Te=(NF-1)290 and Ts=Te+290K
Bn_S = 100e6;      % Noise Bandwidth of ESM Rx Wideband Channalised (500
MHz)
Lt_S = 2;          % Ref to See Advances in Bistatic Radar - Chp 6.5.5.6
Lr_S = 2;
% this is calculation of pulse integration sqrt(N)
PRF_S = 2000;
TOT_S = BeamEL_S/(Scanrate_S*60);
N_S = TOT_S*PRF_S;


%X-band Radar (2)
BeamAz_X = 0.95;    % in degrees
BeamEL_X = 25;     % in degrees
Scanrate_X = 45;   % in rpm for range of 24 nmi or higher
Pt_X = 25e3;          % Tx peak power output
Gt_X = 10^(31/10);    % Tx Antenna Gain is given as 31 dB
Gr_X = 2;          % Rx Antenna Gain
f_X = 9410e6;      % frequency
lambda_X = c/f_X;      % wavelength
Ft_X = 1;          % Prop Factor for Tx-Tgt path. See Advances in Bistatic
Radar - Chp 6.5.5.6
Fr_X = 1;          % Prop Factor for Rx-Tgt path
Ts_X = 290+290*(6-1);      % System Noise Temp of Rx of NF=6dB using
formula Te=(NF-1)290 and Ts=Te+290K
Bn_X = 500e6;      % Noise Bandwidth of ESM Rx Wideband Channalised (500
MHz)
Lt_X = 2;          % Ref to See Advances in Bistatic Radar - Chp 6.5.5.6
Lr_X = 2;
% this is calculation of pulse integration sqrt(N)
PRF_X = 1500;
TOT_X = BeamEL_X/(Scanrate_X*360);
N_X = TOT_X*PRF_X;
```

```
if Select ==1
    BeamEL = BeamEL_S;   % in degrees
    BeamAz = BeamAz_S;    % in degrees
    Scanrate = Scanrate_S;  % in rpm for range of 24 nmi or higher
    Pt = Pt_S;          % Tx peak power output
    Gt = Gt_S;    % Tx Antenna Gain is given as 31 dB
    Gr = Gr_S;          % Rx Antenna Gain
    f = f_S;      % frequency
    lambda = lambda_S;     % wavelength
    Ft = Ft_S;          % Prop Factor for Tx-Tgt path. See Advances in
Bistatic Radar - Chp 6.5.5.6
    Fr = Fr_S;          % Prop Factor for Rx-Tgt path
    Ts = Ts_S;       % System Noise Temp of Rx of NF=6dB using formula
Te=(NF-1)290 and Ts=Te+290K
    Bn = Bn_S;     % Noise Bandwidth of ESM Rx Wideband Channalised (500
MHz)
    Lt = Lt_S;          % Ref to See Advances in Bistatic Radar - Chp
6.5.5.6
    Lr = Lr_S;
% this is calculation of pulse integration sqrt(N)
    PRF = PRF_S;
    TOT = TOT_S;
    N = N_S;
else
    BeamEL = BeamEL_X;   % in degrees
    BeamAz = BeamAz_X;    % in degrees
    Scanrate = Scanrate_X;  % in rpm for range of 24 nmi or higher
    Pt = Pt_X;          % Tx peak power output
    Gt = Gt_X;    % Tx Antenna Gain is given as 31 dB
    Gr = Gr_X;          % Rx Antenna Gain
    f = f_X;      % frequency
    lambda = lambda_X;     % wavelength
    Ft = Ft_X;          % Prop Factor for Tx-Tgt path. See Advances in
Bistatic Radar - Chp 6.5.5.6
    Fr = Fr_X;          % Prop Factor for Rx-Tgt path
    Ts = Ts_X;       % System Noise Temp of Rx of NF=6dB using formula
Te=(NF-1)290 and Ts=Te+290K
    Bn = Bn_X;     % Noise Bandwidth of ESM Rx Wideband Channalised (500
MHz)
    Lt = Lt_X;          % Ref to See Advances in Bistatic Radar - Chp
6.5.5.6
    Lr = Lr_X;
% this is calculation of pulse integration sqrt(N)
    PRF = PRF_X;
    TOT = TOT_X;
    N = N_X;
end
```

```
Rr=sqrt(TargetX^2+TargetY^2);
theta=atan(TargetX/TargetY); % Angle made with True North into
clockwise direction

%%%%%%%%%%%%% Tx1 Source %%%%%%%%%%%%%%%
% Eqn 5.1
syms a
syms A positive
A=solve(a^2-2*Rr*a-L1^2+2*Rr*L1*sin(theta));
RrRt=double(A);
Rt=abs(RrRt(1))-Rr;

e=L1/(Rr+Rt); % eccentricity
beta=(180/pi)*acos((Rr^2+Rt^2-L1^2)/(2*Rr*Rt)); % I am using beta to
add to the angle of

Err_factor_time = (1+e^2+2*e*sin(theta))/(2*(1+e*sin(theta)^2));
Err_time1=Err_factor_time*(BeamAz/2*pi/180)*Rt; % r*theta corresponding
to half of the beamwidth of 1.8 deg


Err_factor_L = abs((-(e^2+1)*sin(theta)+2*e)/(2*(1+e*sin(theta))^2));
Err_L1 = Err_factor_L*((0.0001*1824)+(10*1824*5/3600));% Net opening
speed of 10 knots + 5s update rate


Err_factor_theta = (1-e^2)*cos(theta)/(2*(1+e*sin(theta))^2);
Err_thetaR1 = Err_factor_theta*(Rt*1.5*pi/180);

% Decide which one is the major and minor axis
if  Err_time1 > Err_thetaR1
    Err_Max1=Err_time1;
    Err_Min1=Err_thetaR1;
    % this handles the four different quadrant and if err_time
dominates
    if theta>=0 && theta<=pi/4
        angle1=(-theta-pi/4);

    elseif theta>pi/4 && theta<=pi/2
        angle1=pi/2+(-theta-pi/4);

    elseif theta<0 && theta>=-pi/4
        angle1=(-theta+pi/4);

    else
        angle1=pi/2+(-theta+pi/4);

    end
```

```
else
    Err_Max1=Err_thetaR1;
    Err_Min1=Err_time1;
     % this handles the four different quadrant and if err_theta
dominates
    if theta>=0 && theta<=pi/4
        angle1=-theta;

    elseif theta>pi/4 && theta<=pi/2
        angle1=pi/2-theta;

    elseif theta<0 && theta>=-pi/4
        angle1=-theta;

    else
        angle1=pi/2-theta;

    end
end

% Decide what angle to put for each Tx contribuion

%%%%%%%%%%%%%% Tx2 Source %%%%%%%%%%%%%%%
% Eqn 5.1
syms a
syms A positive
A=solve(a^2-2*Rr*a-L2^2+2*Rr*L2*sin(theta));
RrRt=double(A);
Rt=abs(RrRt(1))-Rr;

e=L2/(Rr+Rt); % eccentricity
beta=(180/pi)*acos((Rr^2+Rt^2-L2^2)/(2*Rr*Rt)); % I am using beta to
add to the angle of

Err_factor_time = (1+e^2+2*e*sin(theta))/(2*(1+e*sin(theta)^2));
Err_time2=Err_factor_time*(BeamAz/2*pi/180)*Rt; % r*theta corresponding
to half of the beamwidth of 1.8 deg


Err_factor_L = abs((-(e^2+1)*sin(theta)+2*e)/(2*(1+e*sin(theta))^2));
Err_L2 = Err_factor_L*((0.0001*1824)+(10*1824*5/3600));% Net opening
speed of 10 knots + 5s update rate


Err_factor_theta = (1-e^2)*cos(theta)/(2*(1+e*sin(theta))^2);
Err_thetaR2 = Err_factor_theta*(Rt*1.5*pi/180);
```

```
% Decide which one is the major and minor axis
if  Err_time2 > Err_thetaR2
    Err_Max2=Err_time2;
    Err_Min2=Err_thetaR2;
    % this handles the four different quadrant and if err_time
dominates
    if theta>=0 && theta<=pi/4
        angle2=(-theta-pi/4);

    elseif theta>pi/4 && theta<=pi/2
        angle2=pi/2+(-theta-pi/4);

    elseif theta<0 && theta>=-pi/4
        angle2=(-theta+pi/4);

    else
        angle2=pi/2+(-theta+pi/4);

    end


else
    Err_Max2=Err_thetaR2;
    Err_Min2=Err_time2;
     % this handles the four different quadrant and if err_theta
dominates
    if theta>=0 && theta<=pi/4
        angle2=-theta;

    elseif theta>pi/4 && theta<=pi/2
        angle2=pi/2-theta;

    elseif theta<0 && theta>=-pi/4
        angle2=-theta;

    else
        angle2=pi/2-theta;

    end
end
% this function will always draw the majoraxis on the horizontal plane
and
% minoraxis in vertical plane
```

```
%%%%%%%%%%%%%% Tx3 Source %%%%%%%%%%%%%%%
% Eqn 5.1
syms a
syms A positive
A=solve(a^2-2*Rr*a-L3^2+2*Rr*L3*sin(theta));
RrRt=double(A);
Rt=abs(RrRt(1))-Rr;

e=L3/(Rr+Rt); % eccentricity
beta=(180/pi)*acos((Rr^2+Rt^2-L3^2)/(2*Rr*Rt)); % I am using beta to
add to the angle of

Err_factor_time = (1+e^2+2*e*sin(theta))/(2*(1+e*sin(theta)^2));
Err_time3=Err_factor_time*(BeamAz/2*pi/180)*Rt; % r*theta corresponding
to half of the beamwidth of 1.8 deg


Err_factor_L = abs((-(e^2+1)*sin(theta)+2*e)/(2*(1+e*sin(theta))^2));
Err_L3 = Err_factor_L*((0.0001*1824)+(10*1824*5/3600));% Net opening
speed of 10 knots + 5s update rate


Err_factor_theta = (1-e^2)*cos(theta)/(2*(1+e*sin(theta))^2);
Err_thetaR3 = Err_factor_theta*(Rt*1.5*pi/180);

% Decide which one is the major and minor axis
if  Err_time3 > Err_thetaR3
    Err_Max3=Err_time3;
    Err_Min3=Err_thetaR3;
    % this handles the four different quadrant and if err_time
dominates
    if theta>=0 && theta<=pi/4
        angle3=(-theta-pi/4);

    elseif theta>pi/4 && theta<=pi/2
        angle3=pi/2+(-theta-pi/4);

    elseif theta<0 && theta>=-pi/4
        angle3=(-theta+pi/4);

    else
        angle3=pi/2+(-theta+pi/4);

    end
```

```
else
    Err_Max3=Err_thetaR3;
    Err_Min3=Err_time3;
     % this handles the four different quadrant and if err_theta
dominates
    if theta>=0 && theta<=pi/4
        angle3=-theta;

    elseif theta>pi/4 && theta<=pi/2
        angle3=pi/2-theta;

    elseif theta<0 && theta>=-pi/4
        angle3=-theta;

    else
        angle3=pi/2-theta;

    end
end

%%%%%%%%%%%%% Tx4 Source %%%%%%%%%%%%%%%
% Eqn 5.1
syms a
syms A positive
A=solve(a^2-2*Rr*a-L4^2+2*Rr*L4*sin(theta));
RrRt=double(A);
Rt=abs(RrRt(1))-Rr;

e=L4/(Rr+Rt); % eccentricity
beta=(180/pi)*acos((Rr^2+Rt^2-L4^2)/(2*Rr*Rt)); % I am using beta to add
to the angle of

Err_factor_time = (1+e^2+2*e*sin(theta))/(2*(1+e*sin(theta)^2));
Err_time4=Err_factor_time*(BeamAz/2*pi/180)*Rt; % r*theta corresponding
to half of the beamwidth of 1.8 deg


Err_factor_L = abs((-(e^2+1)*sin(theta)+2*e)/(2*(1+e*sin(theta))^2));
Err_L4 = Err_factor_L*((0.0001*1824)+(10*1824*5/3600));% Net opening
speed of 10 knots + 5s update rate


Err_factor_theta = (1-e^2)*cos(theta)/(2*(1+e*sin(theta))^2);
Err_thetaR4 = Err_factor_theta*(Rt*1.5*pi/180);
```

```
% Decide which one is the major and minor axis
if  Err_time4 > Err_thetaR4
    Err_Max4=Err_time4;
    Err_Min4=Err_thetaR4;
    % this handles the four different quadrant and if err_time
dominates
    if theta>=0 && theta<=pi/4
        angle4=(-theta-pi/4);

    elseif theta>pi/4 && theta<=pi/2
        angle4=pi/2+(-theta-pi/4);

    elseif theta<0 && theta>=-pi/4
        angle4=(-theta+pi/4);

    else
        angle4=pi/2+(-theta+pi/4);

    end


else
    Err_Max4=Err_thetaR4;
    Err_Min4=Err_time4;
     % this handles the four different quadrant and if err_theta
dominates
    if theta>=0 && theta<=pi/4
        angle4=-theta;

    elseif theta>pi/4 && theta<=pi/2
        angle4=pi/2-theta;

    elseif theta<0 && theta>=-pi/4
        angle4=-theta;

    else
        angle4=pi/2-theta;

    end
end

%%%%%%%%%%%%%% Tx5 Source %%%%%%%%%%%%%%%
% Eqn 5.1
syms a
syms A positive
A=solve(a^2-2*Rr*a-L5^2+2*Rr*L5*sin(theta));
RrRt=double(A);
Rt=abs(RrRt(1))-Rr;
```

```
e=L5/(Rr+Rt); % eccentricity
beta=(180/pi)*acos((Rr^2+Rt^2-L5^2)/(2*Rr*Rt)); % I am using beta to
add to the angle of
Err_factor_time = (1+e^2+2*e*sin(theta))/(2*(1+e*sin(theta)^2));
Err_time5=Err_factor_time*(BeamAz/2*pi/180)*Rt; % r*theta
corresponding to half of the beamwidth of 1.8 deg

Err_factor_L = abs((-(e^2+1)*sin(theta)+2*e)/(2*(1+e*sin(theta))^2));
Err_L5 = Err_factor_L*((0.0001*1824)+(10*1824*5/3600));% Net opening
speed of 10 knots + 5s update rate

Err_factor_theta = (1-e^2)*cos(theta)/(2*(1+e*sin(theta))^2);
Err_thetaR5 = Err_factor_theta*(Rt*1.5*pi/180);

% Decide which one is the major and minor axis
if  Err_time5 > Err_thetaR5
    Err_Max5=Err_time5;
    Err_Min5=Err_thetaR5;
    % this handles the four different quadrant and if err_time
dominates
    if theta>=0 && theta<=pi/4
        angle5=(-theta-pi/4);

    elseif theta>pi/4 && theta<=pi/2
        angle5=pi/2+(-theta-pi/4);

    elseif theta<0 && theta>=-pi/4
        angle5=(-theta+pi/4);

    else
        angle5=pi/2+(-theta+pi/4);
    end
else
    Err_Max5=Err_thetaR5;
    Err_Min5=Err_time5;
     % this handles the four different quadrant and if err_theta
dominates
    if theta>=0 && theta<=pi/4
        angle5=-theta;

    elseif theta>pi/4 && theta<=pi/2
        angle5=pi/2-theta;

    elseif theta<0 && theta>=-pi/4
        angle5=-theta;
    else
        angle5=pi/2-theta;

    end
end
```

```
%%%%%%%%%%%%%% Tx6 Source %%%%%%%%%%%%%%%
% Eqn 5.1
syms a
syms A positive
A=solve(a^2-2*Rr*a-L6^2+2*Rr*L6*sin(theta));
RrRt=double(A);
Rt=abs(RrRt(1))-Rr;

e=L6/(Rr+Rt); % eccentricity
beta=(180/pi)*acos((Rr^2+Rt^2-L6^2)/(2*Rr*Rt)); % I am using beta to
add to the angle of

Err_factor_time = (1+e^2+2*e*sin(theta))/(2*(1+e*sin(theta)^2));
Err_time6=Err_factor_time*(BeamAz/2*pi/180)*Rt; % r*theta
corresponding to half of the beamwidth of 1.8 deg


Err_factor_L = abs((-(e^2+1)*sin(theta)+2*e)/(2*(1+e*sin(theta))^2));
Err_L6 = Err_factor_L*((0.0001*1824)+(10*1824*5/3600));% Net opening
speed of 10 knots + 5s update rate


Err_factor_theta = (1-e^2)*cos(theta)/(2*(1+e*sin(theta))^2);
Err_thetaR6 = Err_factor_theta*(Rt*1.5*pi/180);

% Decide which one is the major and minor axis
if  Err_time6 > Err_thetaR6
    Err_Max6=Err_time6;
    Err_Min6=Err_thetaR6;
    % this handles the four different quadrant and if err_time
dominates
    if theta>=0 && theta<=pi/4
        angle6=(-theta-pi/4);

    elseif theta>pi/4 && theta<=pi/2
        angle6=pi/2+(-theta-pi/4);

    elseif theta<0 && theta>=-pi/4
        angle6=(-theta+pi/4);

    else
        angle6=pi/2+(-theta+pi/4);

    end
```

```
else
    Err_Max6=Err_thetaR6;
    Err_Min6=Err_time6;
     % this handles the four different quadrant and if err_theta
dominates
    if theta>=0 && theta<=pi/4
        angle6=-theta;

    elseif theta>pi/4 && theta<=pi/2
        angle6=pi/2-theta;

    elseif theta<0 && theta>=-pi/4
        angle6=-theta;

    else
        angle6=pi/2-theta;

    end
end

%%%%%%%%%%%%% Tx7 Source %%%%%%%%%%%%%%%
% Eqn 5.1
syms a
syms A positive
A=solve(a^2-2*Rr*a-L7^2+2*Rr*L7*sin(theta));
RrRt=double(A);
Rt=abs(RrRt(1))-Rr;

e=L7/(Rr+Rt); % eccentricity
beta=(180/pi)*acos((Rr^2+Rt^2-L7^2)/(2*Rr*Rt)); % I am using beta to
add to the angle of

Err_factor_time = (1+e^2+2*e*sin(theta))/(2*(1+e*sin(theta)^2));
Err_time7=Err_factor_time*(BeamAz/2*pi/180)*Rt; % r*theta
corresponding to half of the beamwidth of 1.8 deg


Err_factor_L = abs((-(e^2+1)*sin(theta)+2*e)/(2*(1+e*sin(theta))^2));
Err_L7 = Err_factor_L*((0.0001*1824)+(10*1824*5/3600));% Net opening
speed of 10 knots + 5s update rate


Err_factor_theta = (1-e^2)*cos(theta)/(2*(1+e*sin(theta))^2);
Err_thetaR7 = Err_factor_theta*(Rt*1.5*pi/180);
```

```
% Decide which one is the major and minor axis
if  Err_time7 > Err_thetaR7
    Err_Max7=Err_time7;
    Err_Min7=Err_thetaR7;
    % this handles the four different quadrant and if err_time
dominates
    if theta>=0 && theta<=pi/4
        angle7=(-theta-pi/4);

    elseif theta>pi/4 && theta<=pi/2
        angle7=pi/2+(-theta-pi/4);

    elseif theta<0 && theta>=-pi/4
        angle7=(-theta+pi/4);

    else
        angle7=pi/2+(-theta+pi/4);

    end


else
    Err_Max7=Err_thetaR7;
    Err_Min7=Err_time7;
     % this handles the four different quadrant and if err_theta
dominates
    if theta>=0 && theta<=pi/4
        angle7=-theta;

    elseif theta>pi/4 && theta<=pi/2
        angle7=pi/2-theta;

    elseif theta<0 && theta>=-pi/4
        angle7=-theta;

    else
        angle7=pi/2-theta;

    end
end

%%%%%%%%%%%%% Tx8 Source %%%%%%%%%%%%%%%
% Eqn 5.1
syms a
syms A positive
A=solve(a^2-2*Rr*a-L8^2+2*Rr*L8*sin(theta));
RrRt=double(A);
Rt=abs(RrRt(1))-Rr;
```

```
e=L8/(Rr+Rt); % eccentricity
beta=(180/pi)*acos((Rr^2+Rt^2-L8^2)/(2*Rr*Rt)); % I am using beta to add
to the angle of

Err_factor_time = (1+e^2+2*e*sin(theta))/(2*(1+e*sin(theta)^2));
Err_time8=Err_factor_time*(BeamAz/2*pi/180)*Rt; % r*theta corresponding
to half of the beamwidth of 1.8 deg

Err_factor_L = abs((-(e^2+1)*sin(theta)+2*e)/(2*(1+e*sin(theta))^2));
Err_L8 = Err_factor_L*((0.0001*1824)+(10*1824*5/3600));% Net opening
speed of 10 knots + 5s update rate

Err_factor_theta = (1-e^2)*cos(theta)/(2*(1+e*sin(theta))^2);
Err_thetaR8 = Err_factor_theta*(Rt*1.5*pi/180);

% Decide which one is the major and minor axis
if  Err_time8 > Err_thetaR8
    Err_Max8=Err_time8;
    Err_Min8=Err_thetaR8;
    % this handles the four different quadrant and if err_time dominates
    if theta>=0 && theta<=pi/4
        angle8=(-theta-pi/4);
    elseif theta>pi/4 && theta<=pi/2
        angle8=pi/2+(-theta-pi/4);

    elseif theta<0 && theta>=-pi/4
        angle8=(-theta+pi/4);
    else
        angle8=pi/2+(-theta+pi/4);
    end
else
    Err_Max8=Err_thetaR8;
    Err_Min8=Err_time8;
     % this handles the four different quadrant and if err_theta
dominates
    if theta>=0 && theta<=pi/4
        angle8=-theta;

    elseif theta>pi/4 && theta<=pi/2
        angle8=pi/2-theta;

    elseif theta<0 && theta>=-pi/4
        angle8=-theta;

    else
        angle8=pi/2-theta;

    end
end
```

```
%%%%%%%%  Plotting  %%%%%%%%%%%%%%%%%%%

pdeellip(TargetX,TargetY,Err_Max1,Err_Min1,angle1-(Tx1*pi/180),'Tx1');
pdeellip(TargetX,TargetY,Err_Max2,Err_Min2,angle2-(Tx2*pi/180),'Tx2');
pdeellip(TargetX,TargetY,Err_Max3,Err_Min3,angle3-(Tx3*pi/180),'Tx3');
pdeellip(TargetX,TargetY,Err_Max4,Err_Min4,angle4-(Tx4*pi/180),'Tx4');
pdeellip(TargetX,TargetY,Err_Max5,Err_Min5,angle5-(Tx5*pi/180),'Tx5');
pdeellip(TargetX,TargetY,Err_Max6,Err_Min6,angle6-(Tx6*pi/180),'Tx6');
pdeellip(TargetX,TargetY,Err_Max7,Err_Min7,angle7-(Tx7*pi/180),'Tx7');
pdeellip(TargetX,TargetY,Err_Max8,Err_Min8,angle8-(Tx8*pi/180),'Tx8');

hold on
axis square
grid on
plot(0,0,'k*')
text(40,0,'Rx','FontSize',14)
plot(-12730,12730,'k*')
text(-12730,12930,'Tx1','FontSize',15)
plot(12730,12730,'k*')
text(12730,12930,'Tx2','FontSize',15)
plot(12730,-12730,'k*')
text(12730,-12930,'Tx3','FontSize',15)
plot(-12730,-12730,'k*')
text(-12730,-12930,'Tx4','FontSize',15)
plot(0,-18000,'k*')
text(200,-18000,'Tx5','FontSize',15)
plot(0,18000,'k*')
text(200,18000,'Tx6','FontSize',15)
plot(18000,0,'k*')
text(18000,200,'Tx7','FontSize',15)
plot(-18000,0,'k*')
text(-18000,200,'Tx8','FontSize',15)
plot(4500,4500,'k*')
text(4600,4500,'Target','FontSize',15)
hold off
```

THIS PAGE INTENTIONALLY LEFT BLANK

# LIST OF REFERENCES


[1] N. J. Willis, *Bistatic Radar*. Norwood, MA: Artech House, Technology Service Corporation, p. 1, 1995.

[2] D. C. Jenn, *Radar and Laser Cross Section Engineering*, 2nd ed. Reston, VA: AIAA Education Series, pp. 32, 41–42, 2005.

[3] B. Lovell (Sir), "The cavity magnetron in World War II: Was the secrecy justified?" *The Royal Society Journal of the History of Science*, vol. 3, no. 58, p. 284, Sep 2004.

[4] N. J. Wills, H. D. Griffiths, and D. K. Barton, *Advances in Bistatic Radar*. Raleigh, NC: SciTech Publishing, 2007.

[5] C. Kabakchiev, I. Garvanov, V. Behar, A. Kabakchiev, D. Kabakcueva, "Forward scatter radar detection and estimation of marine targets," in *19th International Radar Symposium*, Warsaw, Poland, pp. 533–538, 2012.

[6] Ø. Overrein, J. Navarro, V. Sahajpal, R. Stemland, H. Røkkum, K. E. Olsen, S. Johnsrud, P. Sørnes, I. Tansem, T. Johnsen, "ISAR processing results from forward scatter radar measurements of ships," in *IEEE Radar Conference*, Mohawk Valley, New York, pp. 560–564, 2006.

[7] H. D. Griffiths and C. J. Baker, "Passive coherent location radar systems. Part 1: Performance prediction," in *IEEE Proceedings of Radar, Sonar and Navigation*, vol. 152, pp. 153–159, Jun 2005.

[8] S. Doughty, K. Woodbridge, and C. Baker, "Characterization of a multistatic radar system," in *Proceedings of the 3rd European Radar Conference*, Manchester, United Kingdom, pp. 5–8, 2006.

[9] P. Stinco, Maria S. Greco, F. Gini, A. Farina, "Cramér-Rao bounds and TX-RX selection in a multistatic radar scenario," in *IEEE Radar Conference*, Crystal City, Washington, DC, pp. 1371–1376, 2010.

[10] T. Derham, S. Doughty, C. Baker, K. T. Tsao, M. Slamani, P. Varshney, D. Weiner, H. Schwarzlander, "Ambiguity function for a bistatic radar," in *IEEE Trans. Aerosp. Electron. Syst.*, vol. 33, no. 3, pp. 1041–1051, Jul 1997.

[11] K. Woodbridge, "Ambiguity functions for spatially coherent and incoherent multistatic radar," *IEEE Trans. Aerosp. Electron. Syst.*, vol. 46, no. 1, pp. 230–244, Jan 2010.

[12] J. Friedman, T. Schmid, Z. Charbiwala, Mani B. Srivastava, Young H. Cho, "Multistatic pulse-wave angle-of-arrival-assisted relative interferometric RADAR," *IEEE Radar Conference*, Pasadena, California, May 2009.

[13] M. Skolnik, *Radar Handbook*, 3rd ed. New York: McGraw-Hill Companies, p. 1109, 2008.

[14] P. E. Pace, *Detecting and Classifying Low Probability of Intercept Radar*, 2nd ed. Norwood, MA: Artech House, p. 31, 2009.

[15] SOLAS Chapter V- Safety of Navigation, International Maritime Organisation, Jul 02.

[16] U.S. Energy Information Administration. (2012, August 22). "World oil transit chokepoint." [Online]. Accessed Feb. 8, 2014. Available: http://www.eia.gov /countries/analysisbriefs/World_Oil_Transit_Chokepoints/wotc.pdf

[17] R. M. Kamaruzaman, "Navigational safety in the strait of Malacca," *Singapore Journal of International and Comparative Law*, vol. 2, pp. 468–485, 1998.

[18] *Wikipedia*. "Formidable-class Frigate." [Online]. Accessed Feb. 21, 2014. Available: http://en.wikipedia.org/wiki/Formidable-class_frigate

[19] B. R. Mahafza and A. Z. Elsherbeni, *MATLAB Simulation for Radar Systems Design*. New York: Chapman & Hall/CRC, p. 30, 2004.

[20] S. Stein, "Algorithms for ambiguity function processing*," IEEE Trans. Acoust., Speech, Signal Process.*, vol. 29, no. 3, pp. 588–599, Jun 1981.

[21] Robey, F. C., Coutts, S., Weikle, D., McHarg, J.C., Cuomo, K., "MIMO radar theory and its experimental results," *Signals, Systems and Computer* – 38th *Asilomar Conference Record*, vol. 1, pp. 300–304, Nov 2004.

# INITIAL DISTRIBUTION LIST

1. Defense Technical Information Center
   Ft. Belvoir, Virginia

2. Dudley Knox Library
   Naval Postgraduate School
   Monterey, California